

## Responses to anonymous Referee #1

1. The Lyu et al. manuscript reports on a combined measurement-modeling analysis of a sustained ozone ( $O_3$ ) pollution event over the North China Plain. Continuous online measurements of  $O_3$ , NO, and  $NO_2$  were made in the city of Ji'nan, from the Shandong University campus. For a subset of the measurement period, samples were collected for offline analysis of oxygenated/volatile organic compounds (O/VOCs). Additional chemical and meteorological data were obtained from nearby monitoring stations. Positive matrix factorization (PMF) was used to identify sources of  $O_3$  precursors, using the chemical data as input parameters (VOCs, CO, NO, and  $NO_2$ ). In addition, the WRF-CMAQ chemical transport model was used to evaluate processes contributing to  $O_3$  formation and depletion, and an MCM-based box model was used to evaluate localized  $O_3$  chemistry. HYSPLIT back trajectory analysis was also performed to identify origins of air masses. Collectively, the research presented represents a significant effort to identify the primary drivers of the sustained  $O_3$  event. No major weaknesses are identified in the approach, the quality of the data, or the simulation results. The major weaknesses are in the presentation of the results and the synthesis of the findings.

We appreciate the referee's time and positive comments. The presentation of the results and the synthesis of the findings in the paper have been improved according to the referee's comments.

2. The introduction starts with a list of publications that have addressed  $O_3$  formation over the North China Plain (NCP). As written, it isn't clear whether there are major discrepancies between studies and/or whether there are gaps in understanding/model representation that are unaddressed by existing studies.

Many thanks for the good comment. The introduction has been reorganized and the knowledge gaps are more clearly presented. In the revised manuscript, the first paragraph in the introduction focuses on the severity and aggravation of  $O_3$  pollution in the NCP. Six publications are cited to illustrate this point, and we summarize the  $O_3$  pollution in the NCP with the sentence “Overall, the NCP suffers from severe  $O_3$  pollution, which is even aggravating.” The second and third paragraphs introduce the chemical and meteorological processes influencing  $O_3$  pollution. The knowledge gaps are summarized in the last paragraph as follows.

Despite many previous studies, the evolutions of the synoptic and photochemical processes in O<sub>3</sub> pollution events, and their contributions to the non-attainment of O<sub>3</sub> have been seldom looked into in the NCP. Besides, the local and regional contributions to the elevated O<sub>3</sub> in the NCP are not unambiguously quantified, limited by the deficiencies in model representation of either physical or local chemical processes. The situation was even much worse for Ji'nan, the capital of Shandong province. As early as 2000s, studies (Shan et al., 2008; Yin et al., 2009) reported the maximum hourly O<sub>3</sub> of 143.8 ppbv and 147.8 ppbv in June 2004 and 2005, respectively. Even higher O<sub>3</sub> (198 ppbv) was observed at a rural site downwind of Ji'nan in June 2013 (Zong et al., 2018). However, almost no study was carried out to explore the mechanisms responsible for high O<sub>3</sub> there, though it has been confirmed that air pollution in the NCP cities like Ji'nan influenced air quality in Beijing (Lin et al., 2008; Wang et al., 2010).

For details, please refer to lines 116 – 127, pages 4 – 5.

3. Further, it isn't clear (based on the abstract or implications) how the current work advances the current state of the science (understanding, prediction capabilities, etc.). As written, the implications section highlights that this work confirms O<sub>3</sub> levels are high in the NCP and the NCP may serve as a source region, which do not represent a substantial contribution. However, elucidation of the shifts in regime (from VOC-limited to transition) during the O<sub>3</sub> episodes appears to be a new finding, and therefore should be highlighted and expanded upon.

The valuable comment and suggestion are highly appreciated. Although Ding et al (2009) indicated the transport of O<sub>3</sub> from the NCP to the free troposphere and the downwind areas, their study was based on the aircraft measurement in northeast China and the simulation of the lifting processes of ground-level air masses. To our knowledge, no other study defined the NCP to be a source region of O<sub>3</sub>. The present study confirmed that the NCP was an O<sub>3</sub> source, through the ground-level measurement and simulation of in-situ photochemistry. Therefore, we still think that this finding advanced our understanding on the role of the NCP in O<sub>3</sub> pollution in the downwind regions and even whole China. We clarify the differences between this study and Ding et al (2009) in the implications, though the studies corroborated each other in term of the finding that the NCP is a source region of O<sub>3</sub>.

Another important finding in this study was that the NCP served as an O<sub>3</sub> source. This was ever proposed by Ding et al. (2009), based on the aircraft measurement and simulation of atmospheric

dynamics. We confirmed it through the ground-level observation and the simulation of in-situ photochemistry.

For details, please refer to lines 663 – 667, pages 27-28.

In addition, we accept the excellent suggestion on highlighting the change of O<sub>3</sub> formation mechanisms from VOC-limited regime to the transitional regime.

The finding that O<sub>3</sub> formation shifted from VOC-limited regime on relatively low O<sub>3</sub> days to the **transitional regime** on **O<sub>3</sub> non-attainment** days may elucidate the cause of the increase in O<sub>3</sub>, because O<sub>3</sub> productions in the **transitional regime** are even higher, despite decreases in NO<sub>x</sub> emissions. **It is unrealistic to expect a continuously linear reduction in NO<sub>x</sub> emissions in the NCP, after the substantial decreases of NO<sub>x</sub> emissions from power plants and industries in recent years. In other words, restraining on VOC emissions is urgent for O<sub>3</sub> abatement in the NCP.**

For details, please refer to lines 657 – 663, page 27.

Revisions have also been made in the abstract to highlight the two findings.

The NCP has been confirmed as a source region of tropospheric O<sub>3</sub>, where the widespread shift of regimes controlling O<sub>3</sub> formation like the case presented in this study can be expected, due to the substantial reductions of NO<sub>x</sub> emissions in recent years.

For details, please refer to lines 33 – 35, page 2.

4. Further, though significant effort was clearly made and the quality of the work is high, the results are relatively unorganized and presented as speculative. Regarding the latter, the word “might” is used 30 times in the paper; in many places it seems the authors have sufficient information to make more conclusive statements and the contribution of the work is minimized by presenting it as speculative. Regarding organization, in several places within the results and discussion, individual paragraphs are more than one page long (lines 335-378, 733-762, 795-832).

Thanks for the comments. All the conclusions and inferences have been checked throughout the paper and the wordings have been changed to be more definite wherever it is possible based on our confidence on the conclusions and the inferences. Besides, the whole paper has been reorganized to improve the readability. The long paragraphs pointed out by the referee have been

significantly shortened, while the contents are not changed much. For details, please refer to lines 327 – 344, 587 – 605 and 628 – 648.

5. Additionally, there is a lot of repetition in the results and the modeling doesn't clearly build on the measurements (or vice versa). Each section is almost presented as a separate study of processes. Because of these weaknesses, it is difficult to assess the overall importance of the paper and the likely contribution to the field. It is recommended that the paper undergo significant revision before publication in ACP. Specific comments are provided below.

We thank for the comments. The repetitions in the manuscript have been double checked and avoided. For example, the contribution of BVOCs to OH reactivity was discussed in lines 330 – 334 and lines 362 – 367 in the original manuscript, which is now only presented in lines 315 – 318 in the revised manuscript. The low O<sub>3</sub> on July 30 and August 1 were elaborated in the original manuscript in both section 3.1 and section 3.2. However, we only discuss it in section 3.1, with reference to the discussion in section 3.2 – “The low O<sub>3</sub> values on July 30 and August 1 were mainly attributable to the weak solar radiation and low temperature as discussed above.” (lines 419-420, page 16). More revisions on the repetition have been made throughout the manuscript.

In fact, the modeling and measurement were built on each other and the results supported each other. In the revised manuscript, the relationships between them are clarified.

The observations indicated the likely different regimes controlling local O<sub>3</sub> formation and the potential impacts of regional transport. To understand the atmospheric chemistry and dynamics, as well as their roles in this O<sub>3</sub> pollution event, the WRF-CMAQ was applied.

For details, please refer to lines 442 – 444, page 18.

The IPR analyses showed that chemical reactions served as an important source of O<sub>3</sub> on episode days in Ji'nan, particularly during 09:00-15:00 LT when O<sub>3</sub> was at high levels. This process was further studied through the simulation of the in-situ photochemistry by PBM-MCM. It should be noted that the simulations were based on the observed concentrations of O<sub>3</sub> precursors, which could be influenced by both local and regional air. It required cautions to extend the results to all the situations in Ji'nan, because the regional effect was not always consistent.

For details, please refer to lines 493 – 498, page 21.

Despite these discrepancies, overall the observed O<sub>3</sub> at the sampling site was well reproduced. In addition, the spatial distribution of the simulated O<sub>3</sub> was highly consistent with the observed O<sub>3</sub> distribution, as shown in Figure S10.

For details, please refer to Text S1 and Figure S10.

Noticeably, the change of regimes controlling O<sub>3</sub> formation is consistent with that predicted by the  $\frac{OH\text{ reactivity}_{VOCs\#}}{OH\text{ reactivity}_{NOx}}$  ratio and the ratio of the reaction rates between “HO<sub>2</sub>+RO<sub>2</sub>” and “OH+NO<sub>2</sub>”.

For details, please refer to lines 625 – 627, page 26.

The connections between the sections are also rewritten to make the whole paper more coherent. For details, please refer to lines 368 – 369, lines 442 – 444, lines 493 – 495 and lines 587 – 589.

Specific comments:

1. Technical and Editorial: Abstract, line 23: It would be useful to see the fractional contribution to O<sub>3</sub>, as well as the given production rates.

Thanks for the suggestion. The process analysis module in CMAQ did not calculate the contributions of different processes to O<sub>3</sub> (ppbv), but the contributions to the total variation rate of O<sub>3</sub> (ppbv/h). During 9:00 – 15:00 on O<sub>3</sub> episode days, the regional transport and chemical reactions elevated O<sub>3</sub> by 18.7 and 14.0 ppbv/h, respectively, which were most offset by dry deposition (-25.6 ppbv/h) and cloud processes (-0.1 ppbv/h). If the percentage contributions to the total variation rate of O<sub>3</sub> were calculated, they were 268%, 200%, -366% and -1% by regional transport, chemical reactions, dry deposition and cloud processes, respectively. To avoid confusion, we do not provide these seemingly strange percentages.

2. Abstract, lines 34-37: On line 34, the use of “great” implies something that is positive; suggestions to replace with “major” or “large” or something similar. On line 23, a local photochemical production rate of 14 ppbv/hr is reported for Aug. 9-10 (I believe that is the associated time period) and on line 32, a simulated local photochemical production rate (maximum) of 21.3 ppbv/hr is reported. With these large production rates, the ~1 ppbv/hr decrease in O<sub>3</sub> formation with a hypothetical 10% decrease in diesel and gasoline exhaust seems

insignificant. Even during non-episode periods, a simulated local maximum production rate of 16.9 ppbv/hr is reported. Thus the suggestion that constraining vehicle emissions is the most effective strategy to control O<sub>3</sub> production is not well supported by the numbers presented, and needs further explanation and/or clarification.

Thanks for the valuable suggestion and comment. The word “great” has been replaced with “large”. With regard to the seemingly low sensitivity of O<sub>3</sub> production to gasoline and diesel exhaust, it was because that the gasoline and diesel exhausts were assumed to be reduced by 10%. As shown in Figure S14 (Figure S12 in the original Supplement), the source of gasoline exhaust, diesel exhaust, BVOC, LPG usage, solvent usage and petrochemical industry accounted for 4.7, 5.8, 3.3, 1.4, 2.1 and 2.4 ppbv/hr of the maximum O<sub>3</sub> production, respectively. These O<sub>3</sub> productions added up to 19.6 ppbv/hr, comparable to the 21.3 ppbv/hr during O<sub>3</sub> episodes. The difference was explained by the O<sub>3</sub> production attributable to carbonyls, which were not included in the source apportionment. The statement that constraining vehicle emissions was the most effective strategy to control O<sub>3</sub> was supported by the highest O<sub>3</sub> reduction per 10% decrease in source emission for gasoline exhaust (0.47 ppbv/10% reduction in source emission) and diesel exhaust (0.58 ppbv/10% reduction in source emission). On one hand, we would like to inform the readers that the seemingly insignificant O<sub>3</sub> decrease resulted from 10% emission reduction of gasoline and diesel exhausts was due to the fact that many sources contributed to O<sub>3</sub> production and high reduction percentages were required if actions were only taken against one or two sources. On the other hand, the contributions of vehicle exhausts to O<sub>3</sub> production might be underestimated, without the inclusion of the primarily emitted carbonyls from vehicles. Clarifications have been added in the main text of the revised manuscript as follows, but we do not want to repeat them in the abstract.

In fact, the sensitivity of O<sub>3</sub> production rate to the vehicle exhausts might be somewhat underestimated, due to the exclusion of carbonyls in the source apportionment. However, the reductions of O<sub>3</sub> production rate by cutting 10% of vehicle exhausts were still insignificant, compared to the overall maximum O<sub>3</sub> production rate of 21.3 ppbv/hr during O<sub>3</sub> episodes. This indicated that by only restraining emissions from one to two sources, high percentages of emission reductions were required to sufficiently reduce the O<sub>3</sub> production rate. Otherwise, the combined efforts should be made to control the emissions of O<sub>3</sub> precursors from the diverse

sources. In particular, it is essential to get rid of the transitional regime featuring high O<sub>3</sub> production rates and low sensitivities of O<sub>3</sub> production to the precursors.

For details, please refer to lines 640 – 648, page 27.

3. Line 45: Suggestion to remove “of researchers”.

Accepted with thanks.

4. Line 52: May to August of which year?

Thanks for the question. The sampling year (2013) is specified (see lines 47-48).

5. Line 80: Can the authors please clarify what is meant by “air profiles”? Chemical composition?

Exactly. To avoid confusion. The term “air profiles” has been changed to “chemical composition of air pollutants”. For details, please refer to line 68, page 3.

6. Lines 92-95: The authors state that sources with a large fraction of alkenes, aromatics and carbonyls are significant contributors to photochemical O<sub>3</sub> production. As an example, they cite a paper by Ling and Guo that shows O<sub>3</sub> was most sensitive to xylenes from solvent usage, but this alone does not require a major contribution of xylenes from solvents.

Thanks for the comment. To better support the statement “Therefore, the sources with a bulk emission of these VOCs generally make considerable contributions to the photochemical production of ground-level O<sub>3</sub>”, we cite another study and the sentence has been revised as follows.

For example, Cheng et al. (2010) pointed out that carbonyls increased the peak O<sub>3</sub> production rates at a rural site and a suburban site in South China by 64% and 47%, respectively.

For details, please refer to lines 89 – 91, page 4.

7. Lines 122-123: This sentence starting with “contradictory” is confusing as written. What is contradictory?

Since this paragraph has been revised substantially, the sentence starting with “contradictory” has been deleted.

8. Line 183: Where is the “widely used” weather station in relation to the measurement site?

We thank for the question. The automatic weather station was deployed at the same site where we collected samples. The Model CAWS600-B weather stations produced by China Huayun group are used in ~2/3 of more than 1500 meteorological stations across China. Therefore, we defined it as a “widely used” weather station.

In addition, the meteorological parameters, including wind speed, wind direction, pressure, temperature and relative humidity, were monitored at the sampling site by a widely used weather station (China Huayun group, Model CAWS600-B).

For details, please refer to lines 194 – 196, page 7.

9. Lines 344-346: The authors discuss the potential interferences and overestimation of NO<sub>2</sub>, particularly on episode days. Do the authors mean that the OH reactivity during episodes might be overestimated? Or lower than during non-episodes as stated? Is there a way to approximate or bound the potential overestimation?

Thanks for the questions. Yes, the chemiluminescence NO-NO<sub>2</sub>-NO<sub>x</sub> analyzer generally overestimates NO<sub>2</sub> due to the reason discussed in section 2.2.1.

Studies indicated that NO<sub>2</sub> monitored with chemiluminescence was generally overestimated due to the conversion of the total odd nitrogen (NO<sub>y</sub>) to NO by molybdenum oxide catalysts (McClenny et al., 2002; Dunlea et al., 2007; Xu et al., 2013). The positive bias was more significant in more aged air masses, resulting from higher levels of NO<sub>z</sub> (NO<sub>z</sub> = NO<sub>y</sub> - NO<sub>x</sub>) (Dunlea et al., 2007).

For details, please refer to lines 165 – 169, pages 6-7.

Since OH reacts with NO<sub>2</sub> at a much higher rate than with NO<sub>z</sub>, the overestimate of NO<sub>2</sub> leads to overestimate of OH reactivity. NO<sub>z</sub> is often expected to be higher on O<sub>3</sub> episode days, because the sources of most NO<sub>z</sub> species are dominated by secondary formation. Therefore, we speculated that the OH reactivity was overestimated in this study and more overestimated on O<sub>3</sub> episode days than during non-episodes. Here, we adopted 30% and 10% as the upper limits of NO<sub>2</sub> overestimate during episodes and non-episodes, respectively. The rationality is given in the manuscript as follows.



The average overestimation of NO<sub>2</sub> was 22% in Mexico City, which even increased to 50% in the afternoon (Dunlea et al., 2007). Xu et al. (2013) suggested that the chemiluminescence monitors overestimated NO<sub>2</sub> by less than 10% in urban areas with fresh emission of NO<sub>x</sub>, **but the positive bias went up to 30-50% at the suburban sites.** As described in section 2.1, our sampling site was located in the urban area of Ji'nan and was only ~50 m to a main road. Therefore, we infer that NO<sub>2</sub> might not be significantly overestimated in this study. **However, the larger overestimations could be expected during O<sub>3</sub> episodes, because the stronger photochemical reactions enhanced the productions of many NO<sub>z</sub> species. We adopted 30% (minimum bias in suburban area) and 10% (maximum bias in urban area) as the maximum fraction of NO<sub>2</sub> overestimation during episodes and non-episodes at this urban site, respectively. The influences of the NO<sub>2</sub> measurement interferences on the results were discussed where necessary.**

For details, please refer to lines 169 – 180, page 7.

The OH reactivity of NO<sub>x</sub> was  $4.7 \pm 0.8 \text{ s}^{-1}$  and  $6.9 \pm 1.9 \text{ s}^{-1}$  during episodes and non-episodes, respectively. Taking 30% and 10% overestimate of NO<sub>2</sub> during episodes and non-episodes into account, we found that the OH reactivity of NO<sub>x</sub> during episodes ( $4.0 \pm 0.7 \text{ s}^{-1}$ ) was indeed lower ( $p < 0.05$ ) than during non-episodes ( $6.6 \pm 1.9 \text{ s}^{-1}$ ). It should be noted that the OH reactivity of VOCs was not influenced by the overestimate of NO<sub>2</sub>, which therefore was still comparable between episodes and non-episodes. Since NO accounted for a considerable part of OH reactivity of NO<sub>x</sub>, the maximum of 30% and 10% overestimate of NO<sub>2</sub> only led to  $17.5 \pm 1.1\%$  and  $5.4 \pm 0.7\%$  overestimate of OH reactivity of NO<sub>x</sub> during O<sub>3</sub> episodes and non-episodes, respectively. Discussions are given in the manuscript as follows.

**Taking the positive biases of NO<sub>2</sub> measurement into account (section 2.2.1), we found that the OH reactivity of NO<sub>x</sub> was overestimated by the maximum of  $17.5 \pm 1.1\%$  and  $5.4 \pm 0.7\%$  during O<sub>3</sub> episodes and non-episodes, respectively. In the case of maximum overestimations, the actual OH reactivity of NO<sub>x</sub> during episodes ( $4.0 \pm 0.7 \text{ s}^{-1}$ ) might be lower ( $p < 0.05$ ) than that during non-episodes ( $6.6 \pm 1.9 \text{ s}^{-1}$ ).**

For details, please refer to lines 331 – 335, page 12.

10. Line 350: “More importantly” than what? High pressures?

Sorry for the confusion. The sentence has been revised to be more concise, and the term “More importantly” was deleted.

The high OH reactivity during non-episodes mainly occurred on July 30 and August 1, due to the high pressure, weak solar radiation and low temperature.

For details, please refer to lines 335 – 337, page 12.

11. Section 3.3: The authors spend a significant time discussing the quality of the O<sub>3</sub> modeling. Since matching observations is not the primary goal of the modeling component, much of that discussion could be moved to the supplement.

The good suggestion is accepted with thanks.

Discussions on the discrepancies and the detailed model validation are provided in Text S1, Figures S9-S11 and Table S4.

For details, please refer to lines 448-449, page 18, and Text S1, Figures S9-S11 and Table S4.

## Responses to anonymous Referee #2

General Comments This paper presented a comprehensive diagnostic study of the Ozone-NO<sub>x</sub>-VOCs sensitivity in urban Ji'nan. The analysis is trying to synthesize the analysis tools from both observational constrained box model and regional model. This study is on the good way for the exploration of the ozone chemistry in urban China. Nevertheless, there are still trivial problems on the issues like site representation, measurement quality of key parameters like NO, ways to compare box model and regional model, the use and interpretation of PMF on VOCs source apportionment, etc which I provided detailed comments as follows. I suggest publication after addressing the following comments.

We sincerely thank for the positive and valuable comments. Revisions have been made accordingly, and the responses are given below item by item.

Specific Comments 1. Introduction: the review of the current O<sub>3</sub> studies in the part of the introduction was not as comprehensive as it normally required. Recently, there were several papers about the Ozone-NO<sub>x</sub>-VOCs sensitivity issues in Chinese megacities been published. It may be useful to include as a comparison.

We thank for the good comment. The review of the current O<sub>3</sub> studies, particularly on the O<sub>3</sub>-VOC-NO<sub>x</sub> sensitivity in the introduction has been updated.

Xue et al. (2014) indicated that the summer O<sub>3</sub> formation was limited by NO<sub>x</sub> in Lanzhou, consistent with Liu et al. (2010) who identified the NO<sub>x</sub>-limited regime in most areas of northwest China. In the southwest, O<sub>3</sub> formation was diagnosed as VOC-limited in Chengdu, but NO<sub>x</sub>-limited in Pengzhou due to the large quantities of emissions from petrochemical industry (Tan et al., 2018a). Lyu et al. (2016) reported the VOC-limited regime in Wuhan, central China. The VOC-limited regime has also been repeatedly confirmed for O<sub>3</sub> formation in Shanghai (Xue et al., 2014; Xing et al., 2017) and Nanjing (Ding et al., 2013), eastern China. In the Pearl River Delta of southern China, it was found that O<sub>3</sub> formation was generally limited by VOCs in the southwest, while limited by NO<sub>x</sub> in the northeast (Ye et al., 2016). In the NCP, both Han et al. (2018) and Xing et al. (2018) summarized that VOCs limited O<sub>3</sub> formation in most urban areas. However, in the suburban and rural areas, O<sub>3</sub> formation was generally in the transitional regime, *e.g.* Yucheng (Zong et al., 2018), or limited by NO<sub>x</sub>, *e.g.* Wangdu (Tan et al., 2018b). From a historical perspective, Jin et al. (2017) pointed out that the sensitivity of O<sub>3</sub> formation to VOCs increased in most Chinese cities, however decreased in some megacities (such as Beijing and Shanghai) due to the stringent control of NO<sub>x</sub> emissions in recent years. Different VOCs play non-equivalent roles in O<sub>3</sub> formation.

For details, please refer to lines 70 – 86, page 3.

2. Methodology: as shown by previous studies (*e.g.* Lu et al., JGR, 2010, 115, D07303; Cardelino and Chameides, AE, 2000, 34, 2325), the measurement quality of NO is of crucial importance for the diagnosis of the Ozone-NO<sub>x</sub>-VOCs sensitivity, sometimes this may lead to totally different results. The important point is that the detection limit of NO shall be on the level of 100 ppt so that sub-ppb NO can be accurately captured. The use of Mo-converter for the NO<sub>2</sub>

measurement is another weakness of the current paper. The interference is really variable case by case.

The excellent and professional comment is highly appreciated. We agree that the accurate diagnosis of O<sub>3</sub>-VOC-NO<sub>x</sub> sensitivity strongly depends upon the measurement quality of NO and NO<sub>2</sub>. In this study, the NO<sub>x</sub> analyzer used had the detection limit of 0.4 ppbv for NO, higher than the 50 pptv achievable by Lu et al. (2010) and Cardelino and Chameides (2000). However, the lowest mixing ratio of NO during the sampling period was recorded as 2.4 ppbv, which was also much higher than the lowest mixing ratios (lower than 50 pptv in many afternoons) reported by Lu et al. (2010) and Cardelino and Chameides (2000). Moreover, the lowest value of 2.4 ppbv was 6 times (600% of) the lower detection limit of the instrument. Taking the measurement accuracy of <15% into consideration, we believe that the NO measurement was basically reliable in this study. The reliability of NO measurement is justified in the revised manuscript.

The lowest NO observed during the sampling period was 2.4 ppbv, 6 times (600% of) the lower detection of the NO<sub>x</sub> analyzer (0.4 ppbv). Taking the measurement accuracy of <15% into consideration, we believe that the NO measurements were basically reliable.

For details, please refer to lines 160 – 163, page 6.

The potential biases of NO<sub>2</sub> measurements and its influences on the results, including the O<sub>3</sub>-VOC-NO<sub>x</sub> sensitivity, have been fully discussed in the manuscript.

Studies indicated that NO<sub>2</sub> monitored with chemiluminescence was generally overestimated due to the conversion of the total odd nitrogen (NO<sub>y</sub>) to NO by molybdenum oxide catalysts (McClenny et al., 2002; Dunlea et al., 2007; Xu et al., 2013). The positive bias was more significant in more aged air masses, resulting from higher levels of NO<sub>z</sub> (NO<sub>z</sub> = NO<sub>y</sub> - NO<sub>x</sub>) (Dunlea et al., 2007). The average overestimation of NO<sub>2</sub> was 22% in Mexico City, which even increased to 50% in the afternoon (Dunlea et al., 2007). Xu et al. (2013) suggested that the chemiluminescence monitors overestimated NO<sub>2</sub> by less than 10% in urban areas with fresh emission of NO<sub>x</sub>, but the positive bias went up to 30-50% at the suburban sites. As described in section 2.1, our sampling site was located in the urban area of Ji'nan and was only ~50 m to a main road. Therefore, we infer that NO<sub>2</sub> might not be significantly overestimated in this study. However, the larger overestimations could be expected during O<sub>3</sub> episodes, because the stronger photochemical reactions enhanced the productions of many NO<sub>z</sub> species. We adopted 30% (minimum bias in suburban area) and 10% (maximum bias in urban area) as the maximum fraction of NO<sub>2</sub> overestimation during episodes and non-episodes at this urban site, respectively. The influences of the NO<sub>2</sub> measurement interferences on the results were discussed where necessary.

For details, please refer to lines 165 – 180, pages 6 – 7.

Taking the positive biases of NO<sub>2</sub> measurement into account (section 2.2.1), we found that the OH reactivity of NO<sub>x</sub> was overestimated by the maximum of 17.5±1.1% and 5.4±0.7% during O<sub>3</sub> episodes and non-episodes, respectively. In the case of maximum overestimations, the actual OH

reactivity of  $\text{NO}_x$  during episodes ( $4.0 \pm 0.7 \text{ s}^{-1}$ ) might be lower ( $p < 0.05$ ) than that during non-episodes ( $6.6 \pm 1.9 \text{ s}^{-1}$ ).

For details, please refer to lines 331 – 335, page 12.

In reality, the sensitivity of  $\text{O}_3$  formation to  $\text{NO}_x$  might be underemphasized due to the positive biases of  $\text{NO}_2$  measurement (Lu et al., 2010). This effect was expected to be more significant during episodes when the overestimates of  $\text{NO}_2$  were higher. However,  $\text{O}_3$  formation was not likely only limited by  $\text{NO}_x$  even during  $\text{O}_3$  episodes, which should be still sensitive to VOCs, as  $\text{NO}_2$  could not be much overestimated in the urban areas (see section 2.2.1).

For details, please refer to lines 618 – 622, page 26.

3. Methodology: as described the sampling site is very close ( $\sim 50 \text{ m}$ ) to a main road which would be a problem for a regional (city scale) perspective.

Thanks for the comment. Though the sampling site was very close to a main road, we still believe that the observations at this site to some extent represented the regional  $\text{O}_3$  pollution characteristics, in view of the comparable  $\text{O}_3$  at this site to those observed at the air quality monitoring stations in the NCP, and the strong influences of regional transport on  $\text{O}_3$  variations at this site. Justifications have been added in the revised manuscript.

The high  $\text{O}_3$  at almost all the AQMSs in the NCP (Figure 1 (a)) indicated a regional  $\text{O}_3$  pollution event in this period. The regional-wide homogeneity was to some extent represented by the observations at the sampling site, in view of the comparable  $\text{O}_3$  levels. This was confirmed by the strong influences of regional transport on  $\text{O}_3$  variations at the site, as discussed in section 3.3.

For details, please refer to lines 144 – 148, pages 5-6.

At the same time,  $\text{O}_3$  was also elevated by transport at an average rate of  $18.7 \pm 4.0 \text{ ppbv/hr}$ , as a combined effect of vertical transport ( $-40.8 \pm 20.2 \text{ ppbv/hr}$ ) and horizontal transport ( $59.5 \pm 19.8 \text{ ppbv/hr}$ ).

For details, please refer to lines 466 – 469, page 19.

4. Section 3.3, Figure 7: it is shown the ozone in Ji'an were actually come from the vertical and horizontal transport processes while removed through chemical reactions for most of time. Even during the  $\text{O}_3$  pollution episodes, the chemical production of  $\text{O}_3$  were much smaller than that from vertical transport. The diagnosed results again showed that this site is not ideal for the study of the Ozone- $\text{NO}_x$ -VOCs sensitivity and significantly reduced the value of current study.

Thanks for the comment. It is true that regional transport made considerable contributions to  $\text{O}_3$  variation rate in Ji'an, though the regional  $\text{O}_3$  was still originated from the NCP. However, during 9:00 – 15:00 on  $\text{O}_3$  episode days, the contributions of chemical reactions ( $14.0 \pm 2.3 \text{ ppbv/hr}$ ) and transport ( $18.7 \pm 4.0 \text{ ppbv/hr}$ ) to  $\text{O}_3$  variation rate were comparable.

During  $\text{O}_3$  episodes, chemical reactions made positive contributions to  $\text{O}_3$  production between 09:00 LT and 15:00 LT, with the average hourly  $\text{O}_3$  production rate of  $14.0 \pm 2.3 \text{ ppbv/hr}$ . At the same time,  $\text{O}_3$  was also elevated by transport at an average rate of  $18.7 \pm 4.0 \text{ ppbv/hr}$ , as a

combined effect of vertical transport ( $-40.8 \pm 20.2$  ppbv/hr) and horizontal transport ( $59.5 \pm 19.8$  ppbv/hr).

For details, please refer to lines 465 – 469, page 19.

Besides, the  $O_3$ - $NO_x$ -VOC sensitivity identified in this study was not necessary to represent the completely local or completely regional photochemistry. In fact, the observation based model simulated the in-situ photochemistry, where the observed concentrations of  $O_3$  precursors could be influenced by both local and regional air. It requires caution to extend the results to all the situations, but it is also hard to negate the possible representativeness of the results. Therefore, we emphasize the in-situ photochemical modeling and acknowledge the limitation of the results in the revised manuscript as follows.

This process was further studied through the simulation of the in-situ photochemistry by PBM-MCM. It should be noted that the simulations were based on the observed concentrations of  $O_3$  precursors, which could be influenced by both local and regional air. It required cautions to extend the results to all the situations in Ji'nan, because the regional effect was not always consistent.

For details, please refer to lines 494 – 498, page 21.

5. Figure 8 and Figure 9, et al.: there is a general problem related to the PMF analysis of the observed VOCs samples. As the observed VOCs concentration were quite different from the emitted values, the PMF analysis is not applicable for the observed VOCs concentrations. To consider the VOCs consumption after emission through an estimation of the photochemical age is also not very helpful. The photochemical ages from different sources would be quite different for this site and also for different compounds. I suggest to remove this part and the following related discussions.

Many thanks for the comment. We agree that the ambient concentrations of VOCs were most likely different from those immediately emitted from the sources, because the VOCs were subject to complicated atmospheric processes (such as dispersion, deposition and chemical reactions). Also due to this, the source apportionment of VOCs using PMF sometimes did not represent the real source emission characteristics and contributions to VOCs. However, as one of the most commonly used receptor models, PMF has been extensively employed to resolve the sources of VOCs with the ambient concentrations as input. We think that this application had some rationalities, if the source apportionment results were explained with caution. What we would like to emphasize is that PMF identified the source contributions to the steady – state concentrations of VOCs in the atmosphere. In fact, the observation – based model to simulate  $O_3$  was also constrained by the steady – state concentrations of VOCs and the other  $O_3$  precursors. That was why PMF was applied in combination with the PBM-MCM model (an observation – based model) in this study. Explanations to the source apportionment results are added as follows.

Since the source apportionment was performed for the ambient  $O_3$  precursors which were already subject to atmospheric processes, such as dispersion, deposition and chemical reactions,

the results represented the source contributions to the steady – state concentrations of O<sub>3</sub> precursors and the corresponding O<sub>3</sub> productions.

For details, please refer to lines 552 – 555, page 23.

On one hand, the source apportionment of VOCs was not the main objective of this study. On the other hand, we agree that uncertainties existed in the results due to the reasons raised by the referee and the limited number of samples. Therefore, the source apportionment has been moved to the Supplement. For details, please refer to Text S2.

6. Figure 9: the ozone production rates from the box model and that from the regional model are not directly comparable. The box model results assumed a well-mixed condition of the PBL. And it is better compared with the PBL averaged value of the ozone production rates from the regional model.

Thanks for the comment. It is true that the box model simulations assumed the well-mix of air pollutants within the boundary layer. However, the model was constrained by the concentrations of O<sub>3</sub> precursors near the surface (~ 22 m a.g.l.) in this study. Therefore, we believe that the results from the box model should be compared with those simulated on the ground-level layer by the regional model. The justifications are provided in the revised manuscript.

Since the field observations were conducted near the surface (~ 22 m a.g.l.), and the box model introduced below was constrained by the observations, the modeling results on the ground-level layer were extracted from WRF-CMAQ for analyses in this study.

For details, please refer to lines 260 – 263, page 10.

7. Figure 10: the solid lines #1 - #6 from different retrieved sources were not so meaningful as discussed above.

Thanks for the comment. We keep the solid lines #1 - #6 in Figure 8 (Figure 10 in the original manuscript) and the corresponding discussions in the main text due to the reasons illustrated in the response to comment #5.

For details, please refer to the response to comment #5.

# 1 Causes of a continuous summertime O<sub>3</sub> pollution event in Ji'nan, a central 2 city in the North China Plain

3 Xiaopu Lyu<sup>1</sup>, Nan Wang<sup>2</sup>, Hai Guo<sup>1\*</sup>, Likun Xue<sup>3</sup>, Fei Jiang<sup>4</sup>, Yangzong Zeren<sup>1</sup>, Hairong Cheng  
4 <sup>5</sup>, Zhe Cai<sup>4</sup>, Lihui Han<sup>6</sup>, Ying Zhou<sup>6</sup>

5 <sup>1</sup> Department of Civil and Environmental Engineering, The Hong Kong Polytechnic University,  
6 Hong Kong, China

7 <sup>2</sup> Division of Environmental Meteorology, Institute of Tropical and Marine Meteorology,  
8 China Meteorology Administration, Guangzhou, China

9 <sup>3</sup> Environment Research Institute, Shandong University, Ji'nan, China

10 <sup>4</sup> Jiangsu Provincial Key Laboratory of Geographic Information Science and Technology,  
11 International Institute for Earth System Science, Nanjing University, Nanjing, China

12 <sup>5</sup> Department of Environmental Engineering, School of Resource and Environmental Sciences,  
13 Wuhan University, Wuhan, China

14 <sup>6</sup> Department of Environmental Science, College of Environmental and Energy Engineering,  
15 Beijing University of Technology, Beijing, China

16 \* Corresponding author: [ceguohai@polyu.edu.hk](mailto:ceguohai@polyu.edu.hk)

17

18 **Abstract:** In summer 2017, measurements of ozone (O<sub>3</sub>) and its precursors were carried out at an  
19 urban site in Ji'nan, a central city in the North China Plain (NCP). A continuous O<sub>3</sub> pollution  
20 event was captured during August 4-11, with the maximum hourly O<sub>3</sub> reaching 154.1 ppbv.  
21 Model simulation indicated that local photochemical formation and regional transport  
22 contributed  $14.0 \pm 2.3$  and  $18.7 \pm 4.0$  ppbv/hr to O<sub>3</sub> increase during 09:00-15:00 local time (LT) **in**  
23 **this event**, respectively. For local O<sub>3</sub> formation, the calculated OH reactivity of volatile organic  
24 compounds (VOCs) and carbon monoxide (CO) was comparable between O<sub>3</sub> episodes and non-  
25 episodes ( $p > 0.05$ ), so was the OH reactivity of nitrogen oxides (NO<sub>x</sub>). However, the ratio of OH  
26 reactivity of VOCs and CO to that of NO<sub>x</sub> increased from  $2.0 \pm 0.4$  s<sup>-1</sup>/s<sup>-1</sup> during non-episodes to  
27  $3.7 \pm 0.7$  s<sup>-1</sup>/s<sup>-1</sup> during O<sub>3</sub> episodes, which resulted in the change of O<sub>3</sub> formation mechanism from



28 the VOC-limited regime before the O<sub>3</sub> pollution event to the transitional regime during the event.  
29 Correspondingly, the simulated local O<sub>3</sub> production rate during the event (maximum: 21.3  
30 ppbv/hr) was markedly higher than that before the event ( $p < 0.05$ ) (maximum: 16.9 ppbv/hr).  
31 Given that gasoline and diesel exhaust made large contributions to O<sub>3</sub> precursors and O<sub>3</sub>  
32 production rate, constraint on vehicular emissions is the most effective strategy to control O<sub>3</sub>  
33 pollution in Ji'nan. The NCP has been confirmed as a source region of tropospheric O<sub>3</sub>, where  
34 the widespread shift of regimes controlling O<sub>3</sub> formation like the case presented in this study can  
35 be expected, due to the substantial reductions of NO<sub>x</sub> emissions in recent years.

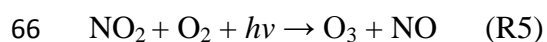
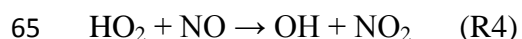
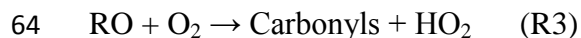
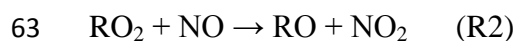
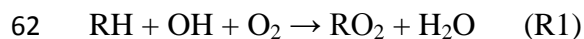
36 **Keywords:** Ozone, local formation, regional transport, volatile organic compound, North China  
37 Plain

## 38 1 Introduction

39 Air pollution in the North China Plain (NCP), the largest alluvial plain of China consisting of  
40 Beijing, Tianjin and many cities in Hebei, Shandong, and Henan provinces, has attracted much  
41 attention in recent years. While the annual average concentration of PM<sub>2.5</sub> (particulate matters  
42 with aerodynamic diameter less than or equal to 2.5 μm) has been reduced under concerted  
43 efforts on emission restrictions (Zhang et al., 2015; Lang et al., 2017), the tropospheric ozone  
44 (O<sub>3</sub>) pollution, which is less visible than haze but may be equivalently harmful to human health,  
45 is still severe. At a regional receptor site of the NCP in a mountainous area north of Beijing,  
46 Wang et al. (2006) reported the maximum hourly O<sub>3</sub> of 286 ppbv. A year-round observation of  
47 O<sub>3</sub> at 10 urban sites in Beijing also revealed high O<sub>3</sub> concentrations through May to August of  
48 2013 (Wang et al., 2015a). Hourly O<sub>3</sub> mixing ratios of up to 120 ppbv were reported on Mt. Tai,  
49 the highest mountain in the NCP (1534 m a.s.l.) (Gao et al., 2005). This indicates the significant  
50 photochemical O<sub>3</sub> pollution over the entire NCP. Moreover, O<sub>3</sub> has been increasing in the NCP  
51 during the last decades (Zhang et al., 2014; Zhang et al., 2015). The increase rate of O<sub>3</sub> at an  
52 urban site in Beijing from 2005 to 2011 was quantified as 2.6 ppbv/year (Zhang et al., 2014),  
53 comparable to that (1.7-2.1 ppbv/year) at Mt. Tai in the summer between 2003 and 2015 (Sun et  
54 al., 2016). Overall, the NCP suffers from severe O<sub>3</sub> pollution, which is even aggravating.

55 Apart from the intrusion of stratospheric O<sub>3</sub> in some places with high elevations (Cooper et al.,  
56 2005; Lin et al., 2015), photochemical formation is the main source of the ground-level O<sub>3</sub>.  
57 Volatile organic compounds (VOCs), carbon monoxide (CO) and nitrogen oxides (NO<sub>x</sub>) are key

58 precursors of tropospheric O<sub>3</sub> (Crutzen, 1973; Chameides and Walker, 1973; Carter, 1994; Carter  
59 et al., 1995). The general chemical reactions R(1) - R(5) show the production of O<sub>3</sub> from the OH  
60 initiated oxidation of hydrocarbons (RH) (Jenkin et al., 1997; Atkinson, 2000; Jenkin and  
61 Clemitshaw, 2000).



67 The production of O<sub>3</sub> is generally limited by VOCs or NO<sub>x</sub> or co-limited by both VOCs and NO<sub>x</sub>,  
68 depending upon the **chemical composition of air pollutants**, particularly the relative OH  
69 reactivity of VOCs and NO<sub>x</sub> (OH reactivity is the sum of the products of O<sub>3</sub> precursors  
70 concentrations and the reaction rate constants between O<sub>3</sub> precursors and OH). **Xue et al. (2014)**  
71 **indicated that the summer O<sub>3</sub> formation was limited by NO<sub>x</sub> in Lanzhou, consistent with Liu et al.**  
72 **(2010) who identified the NO<sub>x</sub>-limited regime in most areas of northwest China. In the southwest,**  
73 **O<sub>3</sub> formation was diagnosed as VOC-limited in Chengdu, but NO<sub>x</sub>-limited in Pengzhou due to**  
74 **the large quantities of emissions from petrochemical industry (Tan et al., 2018a). Lyu et al.**  
75 **(2016) reported the VOC-limited regime in Wuhan, central China. The VOC-limited regime has**  
76 **also been repeatedly confirmed for O<sub>3</sub> formation in Shanghai (Xue et al., 2014; Xing et al., 2017)**  
77 **and Nanjing (Ding et al., 2013), eastern China. In the Pearl River Delta of southern China, it was**  
78 **found that O<sub>3</sub> formation was generally limited by VOCs in the southwest, while limited by NO<sub>x</sub>**  
79 **in the northeast (Ye et al., 2016). In the NCP, both Han et al. (2018) and Xing et al. (2018)**  
80 **summarized that VOCs limited O<sub>3</sub> formation in most urban areas. However, in the suburban and**  
81 **rural areas, O<sub>3</sub> formation was generally in the transitional regime, e.g. Yucheng (Zong et al.,**  
82 **2018), or limited by NO<sub>x</sub>, e.g. Wangdu (Tan et al., 2018b). From a historical perspective, Jin et**  
83 **al. (2017) pointed out that the sensitivity of O<sub>3</sub> formation to VOCs increased in most Chinese**  
84 **cities, however decreased in some megacities (such as Beijing and Shanghai) due to the stringent**  
85 **control of NO<sub>x</sub> emissions in recent years. Different VOCs play non-equivalent roles in O<sub>3</sub>**  
86 **formation. Alkenes, aromatics and carbonyls can be readily oxidized by oxidative radicals (e.g.**  
87 **OH) or photolyzed (applicable for carbonyls), leading to O<sub>3</sub> formation (Cheng et al., 2010; Guo**

88 et al., 2013). Therefore, the sources with a bulk emission of these VOCs generally make  
89 considerable contributions to the photochemical production of ground-level O<sub>3</sub>. For example,  
90 Cheng et al. (2010) pointed out that carbonyls increased the peak O<sub>3</sub> production rates at a rural  
91 site and a suburban site in South China by 64% and 47%, respectively. Solvent based industry  
92 and paint solvent usage with high emissions of aromatics were responsible for more than half of  
93 O<sub>3</sub> formation potential in Shanghai (Cai et al., 2010). Carbonyls and alkenes accounted for 71-85%  
94 of the total OH reactivity of VOCs in Beijing (Shao et al., 2009).

95 In addition to the chemical processes, O<sub>3</sub> pollution is also closely associated with meteorological  
96 conditions, which influence the formation, transport and accumulation of O<sub>3</sub>. Studies (Chan and  
97 Chan, 2000; Huang et al., 2005) indicated that tropical cyclone (typhoon) and continental  
98 anticyclone are the most common synoptic systems conducive of O<sub>3</sub> pollution in coastal cities of  
99 southern China. Many O<sub>3</sub> episodes in eastern China occurred under the control of the west  
100 Pacific subtropical high pressure (He et al., 2012; Shu et al., 2016). In the NCP, the summertime  
101 O<sub>3</sub> pollution is generally accompanied with a weak high pressure system (Wang et al., 2010).  
102 Furthermore, the terrain also plays a role in O<sub>3</sub> pollution. For example, the mountains in north  
103 and west of Beijing lead to upslope winds (valley breeze) in daytime, transporting polluted air  
104 masses laden with O<sub>3</sub> from the NCP to Beijing (Lin et al., 2008). Overall, the causes of O<sub>3</sub>  
105 pollution are generally complicated and need to be analyzed case by case.

106 The NCP is the region with the largest emission amount of air pollutants in China (Gu et al.,  
107 2014; Li et al., 2017), partially accounting for the severe O<sub>3</sub> pollution there. In addition, O<sub>3</sub>  
108 pollution in the NCP is closely related to the synoptic systems and topographic features (Chen et  
109 al., 2009; Zhang et al., 2016). For example, the strong photochemical production of O<sub>3</sub> in urban  
110 plumes of Beijing was found by Wang et al. (2006), while the contribution of regional transport  
111 was revealed by the enhanced O<sub>3</sub> production at a rural site in the NCP under southerly winds  
112 (Lin et al., 2008). Through the review of synoptic systems in the NCP from 1980 to 2013, Zhang  
113 et al. (2016) concluded that the air quality was generally unhealthy under weak East Asian  
114 Monsoons. Moreover, a decadal statistical analysis indicated that meteorological factors  
115 explained ~50% of the O<sub>3</sub> variations in Beijing (Zhang et al., 2015). Despite many previous  
116 studies, the evolutions of the synoptic and photochemical processes in O<sub>3</sub> pollution events, and  
117 their contributions to the non-attainment of O<sub>3</sub> have been seldom looked into in the NCP.

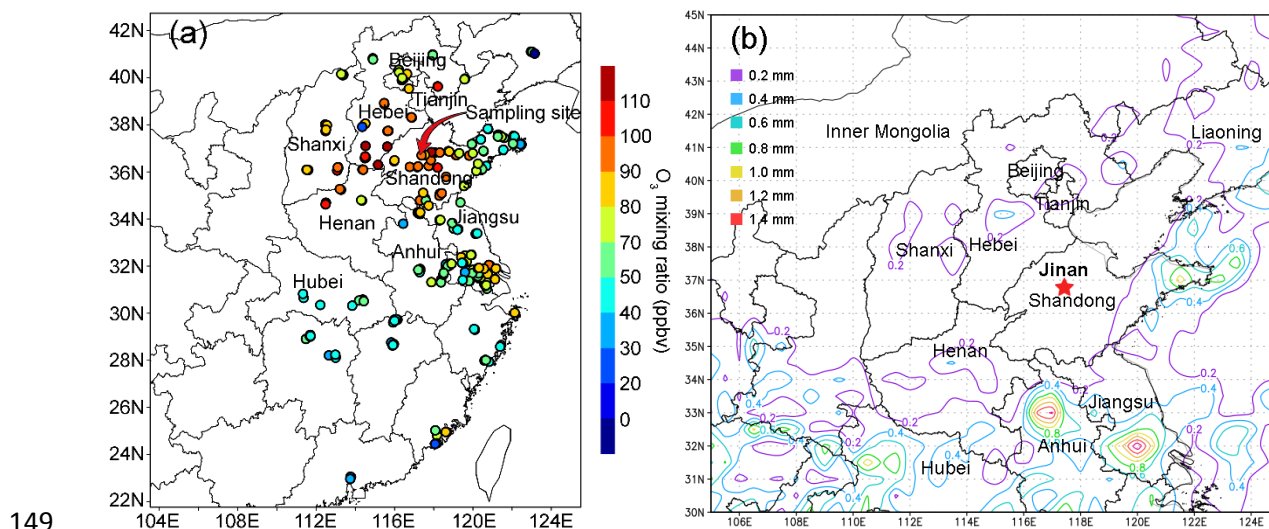
118 Besides, the local and regional contributions to the elevated O<sub>3</sub> in the NCP are not  
119 unambiguously quantified, limited by the deficiencies in model representation of either physical  
120 or local chemical processes. The situation was even much worse for Ji'nan, the capital of  
121 Shandong province. As early as 2000s, studies (Shan et al., 2008; Yin et al., 2009) reported the  
122 maximum hourly O<sub>3</sub> of 143.8 ppbv and 147.8 ppbv in June 2004 and 2005, respectively. Even  
123 higher O<sub>3</sub> (198 ppbv) was observed at a rural site downwind of Ji'nan in June 2013 (Zong et al.,  
124 2018). However, almost no study was carried out to explore the mechanisms responsible for high  
125 O<sub>3</sub> there, though it has been confirmed that air pollution in the NCP cities like Ji'nan influenced  
126 air quality in Beijing (Lin et al., 2008; Wang et al., 2010). To better understand O<sub>3</sub> pollution in  
127 the NCP, this study investigated the causes of an O<sub>3</sub> episode lasting for eight days in Ji'nan in the  
128 summer of 2017. The analyses presented here focus on the synoptic systems dominating  
129 Shandong Peninsula during this event; the chemical profiles of O<sub>3</sub> and O<sub>3</sub> precursors; and the  
130 simulation of factors contributing to O<sub>3</sub> in Ji'nan with the aid of a chemical transport model and  
131 a photochemical box model. In addition, we propose feasible O<sub>3</sub> control measures based on the  
132 source-resolved OH reactivity of VOCs and NO<sub>x</sub>.

## 133 **2 Methodology**

### 134 **2.1 Site description**

135 The air quality monitoring and sample collection were carried out on the rooftop of a 7-story  
136 building on the campus of Shandong University from July 15 to August 14, 2017. The campus is  
137 located in the urban area of Ji'nan, and the site is about 50 m from a main road (Shanda South  
138 Road) outside the campus. Figure 1 shows the locations of the sampling site (36.68 °N, 117.07 °E,  
139 22 m a.g.l.) and some surrounding urban air quality monitoring stations (AQMSs) set up by  
140 China National Environmental Monitoring Center (CNEMC). Also shown are the observed O<sub>3</sub>  
141 and monitored rainfall averaged over August 4-11, 2017 when O<sub>3</sub> episodes occurred in Ji'nan. It  
142 is noteworthy that the days with maximum hourly O<sub>3</sub> exceeding 100 ppbv (Grade II of National  
143 Ambient Air Quality Standard) were defined as O<sub>3</sub> episode days. O<sub>3</sub> data in hourly resolution at  
144 the AQMSs were obtained from the website of CNEMC (<http://www.cnemc.cn/>). The high O<sub>3</sub> at  
145 almost all the AQMSs in the NCP (Figure 1 (a)) indicated a regional O<sub>3</sub> pollution event in this  
146 period. The regional-wide homogeneity was to some extent represented by the observations at

147 the sampling site, in view of the comparable O<sub>3</sub> levels. This was confirmed by the strong  
148 influences of regional transport on O<sub>3</sub> variations at the site, as discussed in section 3.3.



149  
150 Figure 1 (a) Locations of the sampling site and the CNEMC AQMSs, and the average observed  
151 O<sub>3</sub> at 14:00 LT on August 4-11, 2017 (colored circles). The sampling site is overlapped with the  
152 nearest AQMS in Ji'nan. (b) Rainfall distribution, in millimeters (mm), averaged over August 4-  
153 11, 2017.

## 154 2.2 Air quality monitoring and sample collection

### 155 2.2.1 Continuous monitoring of air pollutants and meteorological parameters

156 O<sub>3</sub>, NO and NO<sub>2</sub> were continuously monitored at the sampling site between July 15 and August  
157 14, 2017. The air was drawn through a 4 m Teflon tube by the pumps in the trace gas analyzers  
158 with the total flow rate of 2 L/min (1.4 L/min for O<sub>3</sub> analyzer and 0.6 L/min for NO<sub>x</sub> analyzer).  
159 The inlet was located ~1 m above the rooftop of the 7-story building (~22 m a.g.l.). O<sub>3</sub> and  
160 NO/NO<sub>x</sub> were detected with a UV photometric based analyzer and a chemiluminescence NO-  
161 NO<sub>2</sub>-NO<sub>x</sub> analyzer, respectively (see Table S1 for the specifications). The lowest NO observed  
162 during the sampling period was 2.4 ppbv, 6 times (600% of) the lower detection of the NO<sub>x</sub>  
163 analyzer (0.4 ppbv). Taking the measurement accuracy of <15% into consideration, we believe  
164 that the NO measurements were basically reliable. NO<sub>2</sub> was calculated from the difference  
165 between NO and NO<sub>x</sub>. Studies indicated that NO<sub>2</sub> monitored with chemiluminescence was  
166 generally overestimated due to the conversion of the total odd nitrogen (NO<sub>y</sub>) to NO by

167 molybdenum oxide catalysts (McClenny et al., 2002; Dunlea et al., 2007; Xu et al., 2013). **The**  
168 **positive bias was more significant in more aged air masses, resulting from higher levels of NO<sub>z</sub>**  
169 **(NO<sub>z</sub> = NO<sub>y</sub> - NO<sub>x</sub>) (Dunlea et al., 2007).** The average overestimation of NO<sub>2</sub> was 22% in  
170 Mexico City, which even increased to 50% in the afternoon (Dunlea et al., 2007). Xu et al. (2013)  
171 suggested that the chemiluminescence monitors overestimated NO<sub>2</sub> by less than 10% in urban  
172 areas with fresh emission of NO<sub>x</sub>, **but the positive bias went up to 30-50% at the suburban sites.**  
173 As described in section 2.1, our sampling site was located in the urban area of Ji'nan and was  
174 only ~50 m to a main road. Therefore, we infer that NO<sub>2</sub> might not be significantly  
175 overestimated in this study. **However, the larger overestimations could be expected during O<sub>3</sub>**  
176 **episodes, because the stronger photochemical reactions enhanced the productions of many NO<sub>z</sub>**  
177 **species. We adopted 30% (minimum bias in suburban area) and 10% (maximum bias in urban**  
178 **area) as the maximum fraction of NO<sub>2</sub> overestimation during episodes and non-episodes at this**  
179 **urban site, respectively. The influences of the NO<sub>2</sub> measurement interferences on the results**  
180 **were discussed where necessary.**

181 The hourly concentrations of sulfur dioxide (SO<sub>2</sub>) and CO were acquired from a nearest AQMS  
182 of CNEMC which is ~1 km from our sampling site. Year-round monitoring of inorganic trace  
183 gases was conducted at this AQMS, where the air was drawn into the analytical instruments at a  
184 flow rate of 3 L/min through an inlet, ~1 m above the rooftop of a 5-story building (~ 16 m a.g.l.).  
185 **The specifications of the instruments deployed at the AQMS are also provided in Table S1.** The  
186 hourly concentrations of O<sub>3</sub> and NO<sub>2</sub> measured at our sampling site agreed well with those  
187 reported at the AQMS (NO data was not available on CNEMC website), with the slope of 1.04  
188 (R<sup>2</sup> = 0.82) and 1.13 (R<sup>2</sup> = 0.71) for O<sub>3</sub> and NO<sub>2</sub> in the linear least square regressions,  
189 respectively (Figure S1). Due to the instrumental differences and/or differences in sources and  
190 sinks of air pollutants at the two sites, the agreements were worse at low mixing ratios for both  
191 O<sub>3</sub> and NO<sub>2</sub>. Therefore, we only used SO<sub>2</sub> and CO monitored at the nearest AQMS in this study,  
192 which had lower photochemical reactivity than O<sub>3</sub> and NO<sub>2</sub>, and **were** more homogeneous at a  
193 larger scale.

194 In addition, the meteorological parameters, including wind speed, wind direction, pressure,  
195 temperature and relative humidity, were monitored **at the sampling site** by a widely used weather  
196 station (China Huayun group, Model CAWS600-B). The daily total solar radiation was obtained

197 from the observations at a meteorological station in Ji'nan (36.6 N, 117.05 E, 170.3 m a.s.l), 9  
198 km to our sampling site.

## 199 **2.2.2 Sample collection and chemical analysis**

200 **The** VOC and oxygenated VOC (OVOC) samples were collected on 9 selective days (*i.e.*, July  
201 20 and 30, August 1, 4-7 and 10-11), referred to as VOC sampling days hereafter. The days were  
202 selected to cover the periods with relatively high and low levels of O<sub>3</sub>. The high O<sub>3</sub> days were  
203 forecasted prior to sampling based on the numerical simulations of meteorological conditions  
204 and air quality. In total, 6 out of 9 VOC sampling days were O<sub>3</sub> episode days with the maximum  
205 hourly O<sub>3</sub> ranging from 100.4 to 154.1 ppbv. On each day (regardless of episode or non-episode),  
206 6 VOC/OVOC samples were collected between 08:00 and 18:00 **LT** every 2 hours with the  
207 duration of 1 hour for VOC and 2 hours for OVOC samples. VOC samples were collected with 2  
208 L stainless steel canisters which were cleaned and evacuated before sampling. A flow restrictor  
209 was connected to the inlet of the canister to guarantee 1 hour sampling. OVOC were sampled  
210 with the 2,4-dinitrophenylhydrazine (DNPH) cartridge, in front of which an O<sub>3</sub> scrubber was  
211 interfaced to remove O<sub>3</sub> in the air. A pump behind the DNPH cartridge drew the air at a flow of  
212 500 L/min. After sampling, all the DNPH cartridges were stored in a refrigerator at 4 °C until  
213 chemical analysis.

214 VOC samples were analyzed with a gas chromatograph-mass selective detector/flame ion  
215 detector/electron capture detector system (Colman et al., 2001). In total, 85 VOCs, including 59  
216 hydrocarbons, 19 halocarbons and 7 alkyl nitrates, were quantified. The overall ranges of the  
217 detection limit (DL), accuracy and precision for VOCs analysis were 1-154 pptv, 1.2-19.8% and  
218 0.1-17.9%, respectively. The analysis results given by this system have been compared with  
219 those analyzed by UCI and good agreements were achieved (Figure S2). OVOC samples were  
220 eluted with 5 mL acetonitrile, followed by analysis with the high performance liquid  
221 chromatography. The DL, accuracy and precision for all OVOCs analysis were within the range  
222 of 3-11 pptv, 0.32-0.98% and 0.01-1.03%, respectively.

## 223 **2.3 Model configuration**

### 224 **2.3.1 Chemical transport model**

225 To analyze the processes contributing to high O<sub>3</sub> in Ji'nan, a chemical transport model, the  
226 Weather Research Forecast-Community Multi-scale Air Quality (WRF-CMAQ), was utilized to  
227 simulate O<sub>3</sub> in this study. WRF v3.6.1 was run to provide the offline meteorological field for  
228 CMAQ v5.0.2. A two-nested domain was adopted with the resolution of 36 km (outer domain)  
229 and 12 km (inner domain), respectively. As shown in Figure S3, the outer domain covered the  
230 entire continental area of China aiming to provide sufficient boundary conditions for the inner  
231 domain, which specifically focused on eastern China.

232 We used the 2012-based Multi-resolution Emission Inventory for China (MEIC) to provide  
233 anthropogenic emissions of air pollutants, which was developed by Tsinghua University specific  
234 for China, with the grid resolution of 0.25 °×0.25 ° (Zhang et al., 2007; He, 2012). Five emission  
235 sectors, namely transportation, agriculture, power plant, industry and residence were included in  
236 MEIC. The emission inventory was linearly interpolated to the domains with consideration of the  
237 earth curvature effect. For grids outside China, the air pollutant emissions were derived from  
238 INTEX-B (Intercontinental Chemical Transport Experiment-Phase B) Asian emission inventory  
239 (Zhang et al., 2009). Consistent with many previous studies (Jiang et al., 2010; Wang et al.,  
240 2015b), the Model of Emissions of Gases and Aerosols from Nature (MEGAN) was used to  
241 calculate the **biogenic** emissions. The physical and chemical parameterizations for WRF-CMAQ  
242 were generally identical to those described in Wang et al. (2015b), with some improvements.  
243 Firstly, the carbon bond v5 with updated toluene chemistry (CB05-TU) was chosen as the gas  
244 phase chemical mechanism (Whitten et al., 2010). Secondly, a single-layer urban canopy model  
245 (Kusaka and Kimura, 2004) was used to model the urban surface-atmosphere interactions.  
246 Thirdly, the default 1990s U.S. Geological Survey data in WRF was replaced by adopting the  
247 2012-based moderate resolution imaging spectroradiometer (MODIS) land cover data for eastern  
248 China. The substitution was performed to update the simulation of boundary meteorological  
249 conditions (Wang et al., 2007).

250 An integrated process rate (IPR) module incorporated in CMAQ was used to analyze the  
251 processes influencing O<sub>3</sub> concentration. Through solving the mass continuity equation  
252 established between the overall change of O<sub>3</sub> concentration with time and the change of O<sub>3</sub>  
253 concentration caused by individual processes, including horizontal diffusion (HDIF), horizontal  
254 advection (HADV), vertical diffusion (VDIF), vertical advection (VADV), dry deposition



255 (DDEP), net effect of chemistry (CHEM) and cloud processes (CLD), the contributions of the  
256 processes to O<sub>3</sub> variation rate were determined. Note that the estimate of CHEM is influenced by  
257 the estimate of O<sub>3</sub> precursor emissions, the simulation of meteorological conditions and the  
258 chemical mechanism, all the three aspects should be taken into account wherever CHEM is  
259 discussed. The IPR analysis has been widely applied in process diagnosis of O<sub>3</sub> pollution (Huang  
260 et al., 2005; Wang et al., 2015b). **Since the field observations were conducted near the surface (~**  
261 **22 m a.g.l.), and the box model introduced below was constrained by the observations, the**  
262 **modeling results on the ground-level layer were extracted from WRF-CMAQ for analyses in this**  
263 **study.**

### 264 **2.3.2 Photochemical box model**

265 A Photochemical Box Model incorporating the Master Chemical Mechanism (PBM-MCM) was  
266 used to study the in situ O<sub>3</sub> chemistry, in view of the detailed (species-based) descriptions of  
267 VOC degradations in the MCM (Saunders et al., 2003; Lam et al., 2013). The PBM model was  
268 localized to be applicable in Ji'nan, with the settings of geographic coordinates, sunlight duration  
269 and photolysis rates. The photolysis rates were calculated by the TUV model (Madronich and  
270 Floke, 1997). Specifically, the geographical coordinates, date and time were input into the TUV  
271 model, initializing the calculation of solar radiation with the default aerosol optical depth (AOD),  
272 cloud optical depth (COD), surface albedo and other parameters. Then, COD was adjusted to  
273 make the calculated daily total solar radiation progressively closer to the observed value. When  
274 the difference between the calculated and observed solar radiation were less than 1%, the input  
275 parameters with the adjusted COD were accepted. Based on the settings, the hourly solar  
276 radiations and the photolysis rates of O<sub>3</sub> (J(O<sup>1</sup>D)) and NO<sub>2</sub> (JNO<sub>2</sub>) were calculated by the TUV  
277 model, and applied to PBM-MCM for O<sub>3</sub> chemistry modelling. Table S2 shows the daily  
278 maximum J(O<sup>1</sup>D) and JNO<sub>2</sub> on the VOC sampling days. The MCM v3.2  
279 (<http://mcm.leeds.ac.uk/MCM/>) used in the present model consists of 17,242 reactions among  
280 5,836 species. The measurements of O<sub>3</sub> and its precursors at 00:00 on each day were used as the  
281 initial conditions for each day's modelling. The initial O<sub>3</sub>, as the O<sub>3</sub> left over from the days  
282 before the modelling day, accounted for a part of the primary OH production. Hourly  
283 concentrations of 46 VOCs, 4 OVOCs and 4 trace gases (SO<sub>2</sub>, CO, NO and NO<sub>2</sub>), as well as  
284 hourly meteorological parameters (temperature and relative humidity) were input into the model,

285 so that the model was constrained to observations. The hourly observed O<sub>3</sub> were not input, as it  
286 was the species to be modeled. The Freon, cycloalkanes and methyl cycloalkanes with low O<sub>3</sub>  
287 formation potentials were not included in model input. Also omitted were the species whose  
288 concentrations were lower than the detection limits in more than 20% of the samples, such as the  
289 methyl hexane and methyl heptane isomers. For the hours when measurement data were not  
290 available, the concentrations were obtained with linear interpolation. Some secondary species,  
291 such as formaldehyde (HCHO), acetaldehyde and acetone, were input into the model to constrain  
292 the simulation. Since other secondary species, *e.g.*, PAN and HNO<sub>3</sub> were not observed in this  
293 study, their concentrations were calculated by the model. Dry deposition was considered for all  
294 the chemicals by setting the deposition velocities identical to those in Lam et al. (2013). Since  
295 NO and NO<sub>2</sub> were separately measured and input into the model, they experienced different  
296 reactions as described by the species-based chemical mechanisms.

297 The simulations were separately carried out on all the VOC sampling days. To spin-up the model,  
298 the concentrations of air pollutants and meteorological conditions which were the same as those  
299 on the day of interest were input into the model for 72-h simulation before the modelling on that  
300 day. The model treated the air pollutants to be well-mixed in the boundary layer, without  
301 consideration of dilution and transport. O<sub>3</sub> in the free troposphere was not considered either, due  
302 to the lack of O<sub>3</sub> observations above the boundary layer over Ji'nan. This might hinder the  
303 accurate reproduction of the observed O<sub>3</sub>, particularly on the days when advection and diffusion  
304 were strong. Since the model mainly described the in situ photochemistry, it was validated  
305 through comparison with the CHEM process simulated by WRF-CMAQ. The simulated O<sub>3</sub>  
306 production rates were output every hour, which were integrated values over every 3600 s (model  
307 resolution: 1 s). More details about the model configuration can be found in Lam et al. (2003)  
308 and Lyu et al. (2017).

### 309 **3. Results and discussion**

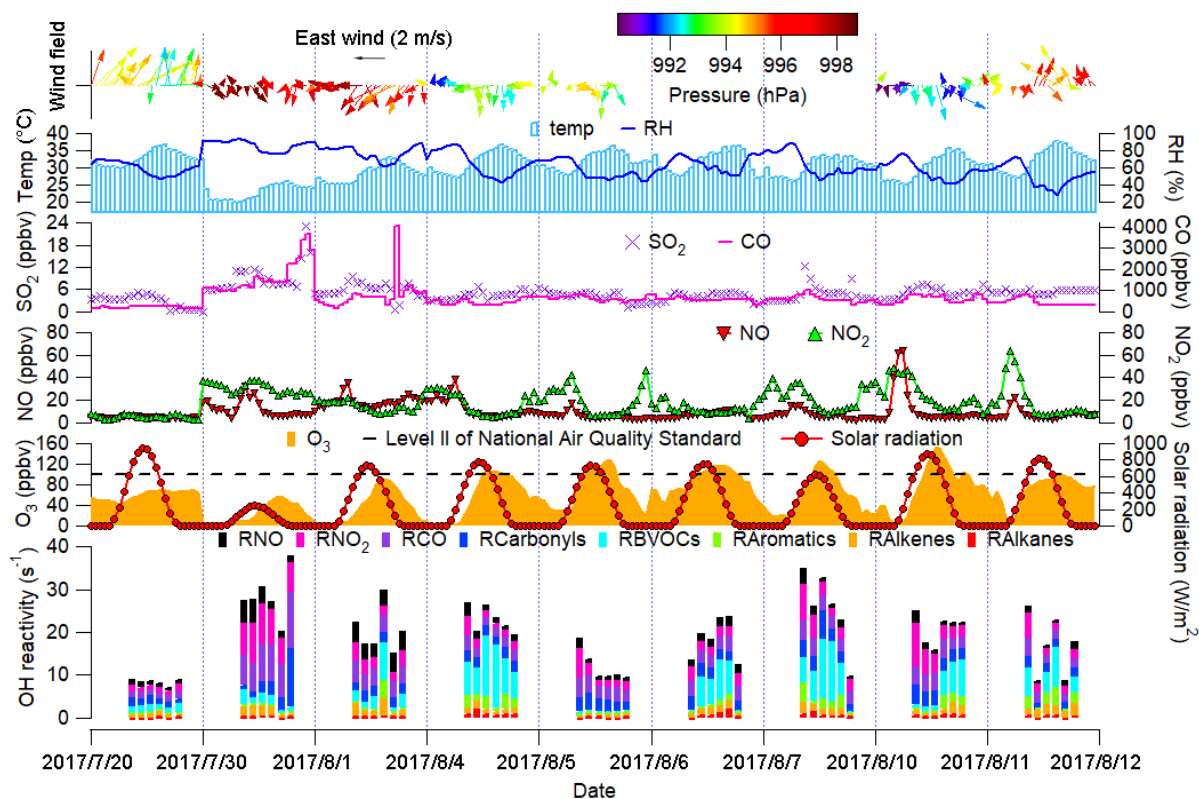
#### 310 **3.1 Overall characteristics of O<sub>3</sub> pollution in Ji'nan**

311 Figure 2 shows the time series of trace gases, the OH reactivity of VOCs, CO and NO<sub>x</sub>, and  
312 meteorological conditions on the VOC sampling days in Ji'nan (Trace gases in the whole  
313 sampling period are shown in Figure S4). All the OH reactivity values discussed in this study  
314 were calculated rather than observed. The OH reactivity values of VOCs are grouped into those

315 of carbonyls, biogenic VOCs (BVOCs), aromatics, alkenes and alkanes (Table S3 lists the VOCs  
316 included in **each group**). The reaction rate constants between O<sub>3</sub> precursors and OH in  
317 calculation of OH reactivity were adopted from the MCM v3.2 (<http://mcm.leeds.ac.uk/MCM/>).  
318 The average total OH reactivity on **all the** VOC sampling days ( $19.4 \pm 2.1 \text{ s}^{-1}$ ) was comparable to  
319 that reported in New York ( $19 \pm 3 \text{ s}^{-1}$ , Ren et al., 2003), Houston ( $9\text{-}22 \text{ s}^{-1}$ , Mao et al., 2010) and  
320 Beijing ( $15\text{-}27 \text{ s}^{-1}$ , Williams et al., 2016). Consistent with the previous studies in urban areas  
321 (Ren et al., 2003; Yang et al., 2016 and references therein), NO<sub>x</sub> was the largest contributor  
322 ( $28.9 \pm 1.9\%$ ) to the total OH reactivity. Noticeably,  $20.5 \pm 4.1\%$  of the total OH reactivity was  
323 attributable to BVOCs, which was much higher than the contributions in urban areas ( $<10\%$ )  
324 reviewed by Yang et al. (2016). The elevated isoprene levels ( **$2.2 \pm 0.6 \text{ ppbv}$  during episodes and  
325  $0.9 \pm 0.3 \text{ ppbv}$  during non-episodes**) under high temperature (mean:  $31 \text{ }^\circ\text{C}$ ) **explained** the  
326 considerable contribution of BVOCs to the total OH reactivity in this study.

327 **O<sub>3</sub> episodes were captured on 6 out of the 9 VOC sampling days**, with the highest O<sub>3</sub> of 154.1  
328 ppbv at 13:00 LT on August 10. It was found that the total OH reactivity of VOCs and CO  
329 ( $OH \text{ reactivity}_{VOCs+CO}$ ) was comparable between O<sub>3</sub> episodes ( $14.8 \pm 2.0 \text{ s}^{-1}$ ) and non-episodes  
330 ( $12.2 \pm 3.0 \text{ s}^{-1}$ ), so was the OH reactivity of NO<sub>x</sub> ( $4.7 \pm 0.8 \text{ s}^{-1}$  and  $6.9 \pm 1.9 \text{ s}^{-1}$  during episodes and  
331 non-episodes, respectively). **Taking the positive biases of NO<sub>2</sub> measurement into account**  
332 **(section 2.2.1), we found that the OH reactivity of NO<sub>x</sub> was overestimated by the maximum of**  
333  **$17.5 \pm 1.1\%$  and  $5.4 \pm 0.7\%$  during O<sub>3</sub> episodes and non-episodes, respectively. In the case of**  
334 **maximum overestimations, the actual OH reactivity of NO<sub>x</sub> during episodes ( $4.0 \pm 0.7 \text{ s}^{-1}$ ) might**  
335 **be lower ( $p < 0.05$ ) than that during non-episodes ( $6.6 \pm 1.9 \text{ s}^{-1}$ ). The high OH reactivity during**  
336 **non-episodes mainly occurred on July 30 and August 1, due to the high pressure, weak solar**  
337 **radiation and low temperature. Despite the comparable OH reactivity, we found that the ratio of**  
338  $\frac{OH \text{ reactivity}_{VOCs+CO}}{OH \text{ reactivity}_{NOx}}$  during O<sub>3</sub> episodes ( $3.7 \pm 0.7 \text{ s}^{-1}/\text{s}^{-1}$ ) was higher ( $p < 0.05$ ) than during non-  
339 episodes ( $2.0 \pm 0.4 \text{ s}^{-1}/\text{s}^{-1}$ ). **It was likely that the difference was even larger, due to the more**  
340 **significant overestimation of NO<sub>2</sub> during episodes. This indicated that O<sub>3</sub> formation was more**  
341 **limited by VOCs during non-episodes than during episodes. In fact, O<sub>3</sub> formation in Ji'nan**  
342 **switched to the transitional regime during episodes from the VOC-limited regime during non-**  
343 **episodes (see section 3.4.2). This partially explained the building-up of O<sub>3</sub> on episode days, as**  
344 **O<sub>3</sub> productions were generally the highest in the transitional regime.**

345 From the perspective of meteorological conditions, O<sub>3</sub> episodes had relatively stronger solar  
346 radiation, higher temperature, lower relative humidity and weaker winds ( $p<0.05$ ). This is  
347 reasonable as O<sub>3</sub> formation and accumulation are generally enhanced under these weather  
348 conditions. As aforementioned, the solar radiation on July 30 was much weaker than those  
349 during O<sub>3</sub> episodes, which was probably the most critical factor leading to low O<sub>3</sub> on this day.  
350 Figure S5 shows the COD retrieved from the terra/MODIS ([https://ladsweb.modaps.eosdis.nasa.gov/search/imageViewer/1/MOD06\\_L2--61/2017-08-06/DB/Site:142/2873994172--](https://ladsweb.modaps.eosdis.nasa.gov/search/imageViewer/1/MOD06_L2--61/2017-08-06/DB/Site:142/2873994172--3)  
351 [3](https://ladsweb.modaps.eosdis.nasa.gov/search/imageViewer/1/MOD06_L2--61/2017-08-06/DB/Site:142/2873994172--3)) at 10:00 – 12:00 **LT** of the VOC sampling days. The terra/MODIS image revealed thick cloud  
352 cover with high COD over Ji'nan on July 30, explaining the weak solar radiation. In fact,  
353 obvious anti-correlation existed between solar radiation and the COD. The influences of cloud  
354 cover/ COD and solar radiation on O<sub>3</sub> pollution during the study period in Ji'nan are discussed in  
355 section 3.2. Unlike many previous findings that O<sub>3</sub> pollution was aggravated by high pressure  
356 (Chan and Chan, 2000; Zhao et al., 2009), the sea-level pressure during O<sub>3</sub> episodes ( $993.4\pm0.2$   
357 hPa) was significantly lower than during non-episodes ( $996.1\pm0.4$  hPa) in this study ( $p<0.05$ ).  
358 When O<sub>3</sub> reached its hourly maximum on August 10 (154.1 ppbv), the pressure was at its lowest  
359 value (990.2 hPa). The continuously severe O<sub>3</sub> pollution event under low pressure is further  
360 investigated below.  
361



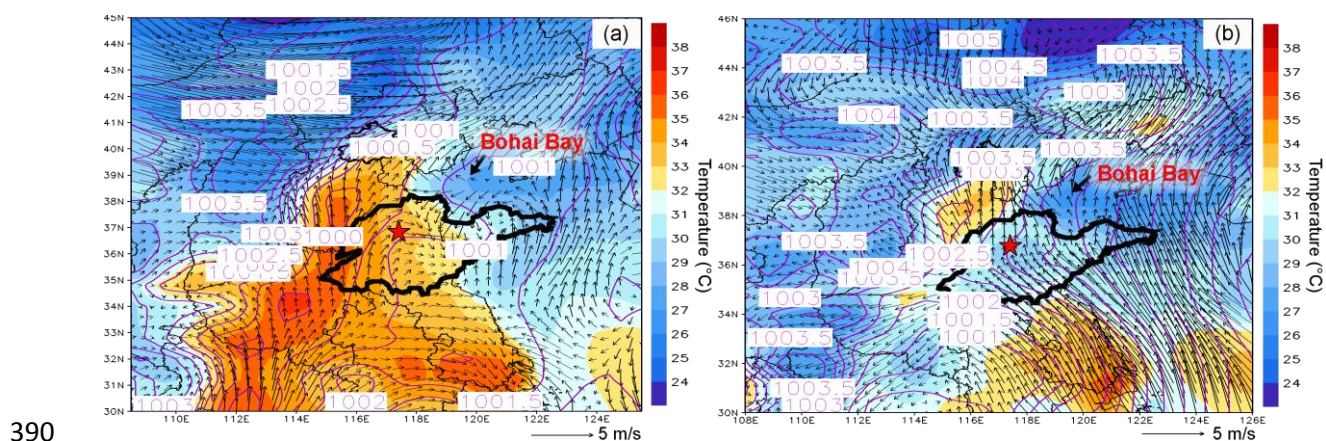
362

363 Figure 2 Time series of trace gases, OH reactivity of O<sub>3</sub> precursors and meteorological  
 364 parameters. Wind speed and wind direction were not monitored from 17:00 LT on August 5 to  
 365 23:00 LT on August 7 due to malfunction of the weather station. RX in the bottom panel is the  
 366 OH reactivity of species/group X.

### 367 3.2 Synoptic processes and relationship with O<sub>3</sub> pollution

368 Obviously, this O<sub>3</sub> pollution event was accompanied by unique weather conditions (e.g. low  
 369 pressure on high O<sub>3</sub> days), which needed to be further studied. Figure 3 displays the average  
 370 weather charts at 14:00 LT during O<sub>3</sub> episodes and non-episodes (weather charts on individual  
 371 VOC sampling days are shown in Figure S6). Clearly, the temperature over Shandong Peninsula  
 372 was much higher during O<sub>3</sub> episodes than non-episodes, which favored O<sub>3</sub> formation on episode  
 373 days. Additionally, southerly and southwesterly winds originating from the inland areas (Hubei,  
 374 Henan, and Anhui provinces) prevailed in central and western Shandong province during O<sub>3</sub>  
 375 episodes. In contrast, the winds were generally from the sea or coastal region in Jiangsu province  
 376 during non-episodes. O<sub>3</sub> and O<sub>3</sub> precursors might be transported to Ji'nan in the former cases.  
 377 Though the winds were from the relatively clean sea and coastal regions during non-episodes,

378 the concentrations of O<sub>3</sub> precursors on July 30 and August 1 were still high, which were mainly  
 379 caused by weather conditions (high pressure, low temperature and low solar radiation), as  
 380 discussed in section 3.1. Further, we also noted that the winds changed direction from southwest  
 381 to northwest around Ji'nan during O<sub>3</sub> episodes. This meant that there might be a local circulation  
 382 hampering the dispersion of air pollutants during episodes. It seems that the turning-round of the  
 383 winds around Ji'nan was associated with the sea breeze from Bohai Bay. **This was very similar**  
 384 **to** the convergence of continental air and sea breeze (from South China Sea) in Pearl River Delta  
 385 (Fung et al., 2005; Lo et al., 2006). Overall, the wind fields were more favorable for regional  
 386 transport and accumulation of air pollutants in Ji'nan during O<sub>3</sub> episodes. In addition, Shandong  
 387 Peninsula was under a uniform pressure field with the sea-level pressure of 1000-1001 hPa  
 388 during O<sub>3</sub> episodes, implying the relatively stagnant weather conditions unfavorable for the  
 389 dispersion of air pollutants.



391 Figure 3 Weather chart at 14:00 LT averaged over (a) O<sub>3</sub> episodes and (b) non-episodes. The red  
 392 star represents Ji'nan. The dark black line is the boundary of Shandong province. Bohai Bay is  
 393 located to the northeast of Shandong province. Numbers in the figure are sea-level pressures in  
 394 unit of hPa.

395 To better understand the relationship between O<sub>3</sub> pollution and the synoptic systems, Table 1  
 396 summarizes the synoptic systems, weather conditions and air mass origins on **all the** VOC  
 397 sampling days. The weather charts at surface level and 500 hPa on August 1, 4, 7, 10 and 13 are  
 398 presented in Figures **S7-S8**, **showing** the evolution of **the** synoptic systems. To identify the  
 399 origins of air masses, the 48 hour backward trajectories of air masses are shown in Figure 4. The  
 400 trajectories were computed using the Hybrid Single Particle Lagrangian Integrated Trajectory

401 (HYSPLIT) Model v 4.9. Each trajectory was calculated for 48 hours and the calculation was  
402 done every 6 hours (4 trajectories each day). Our sampling site (36.68 °N, 117.07 °E) was set as  
403 the starting point of the backward trajectories with the height of 500 m a.s.l. The discrepancy  
404 between the wind direction and origin of air masses, *e.g.* on August 1 and 11, was likely due to  
405 the air recirculation at the ground level.

406 It was found that Ji'nan was under the control of the Western Pacific Subtropical High (WPSH)  
407 on July 20 (weather chart on 500 hPa is not shown here), and the air masses arriving in Ji'nan  
408 originated from South China 48 hours prior (Figure 4). As anticipated, the WPSH caused high  
409 temperatures and the intensive solar radiation during the study period (maximum: 943 W/m<sup>2</sup>) in  
410 Ji'nan (Figure 2), which was conducive to O<sub>3</sub> formation. However, the winds on July 20 were the  
411 strongest in the entire VOC sampling period, with the highest hourly wind speed of 3.9 m/s. The  
412 strong winds facilitated the transport and dispersion of O<sub>3</sub> precursors and locally formed O<sub>3</sub> on  
413 July 20 (refer to the low levels of O<sub>3</sub>, O<sub>3</sub> precursors and OH reactivity in Figure 2). The WPSH  
414 moved southward on the following days and Ji'nan was under a uniform pressure field, which  
415 was formed in the peripheries of two low pressure systems (two rain belts as shown in Figure 1),  
416 *i.e.* one over Central China and another over North China (Figure S7). Thus, the pressure in  
417 Ji'nan was relatively high (997.1±0.3 hPa), compared to the south and north regions. This  
418 synoptic system lasted for several days until August 7, covering 2 non-episode days and 4 O<sub>3</sub>  
419 episode days. The low O<sub>3</sub> values on July 30 and August 1 were mainly attributable to the weak  
420 solar radiation and low temperature as discussed above.

421 In contrast, continuously strong solar radiation with low COD (Figure 2 and Figure S5), high  
422 temperature and continental air masses (Figure 4) were observed on August 4-7. This, in addition  
423 to the shift of O<sub>3</sub> formation mechanism (see sections 3.1 and 3.4.2), explained the prolonged O<sub>3</sub>  
424 pollution event. On August 10, the rain belt over North China moved southward, forming a deep  
425 low pressure trough over the NCP and Ji'nan was behind the trough (Figure S8 (d)). The low  
426 pressure trough is a typical synoptic system conducive of O<sub>3</sub> pollution, resulting from the  
427 intrusion of O<sub>3</sub> in the stratosphere and/or the upper troposphere (Chan and Chan, 2000).  
428 Moreover, there was nearly no cloud cover over the entire NCP on August 10 (Figure S5).  
429 Consequently, the highest O<sub>3</sub> (154.1 ppbv) in this sampling campaign was observed on August  
430 10. On August 11, the low pressure system continued to extend to the Yellow Sea. O<sub>3</sub> decreased

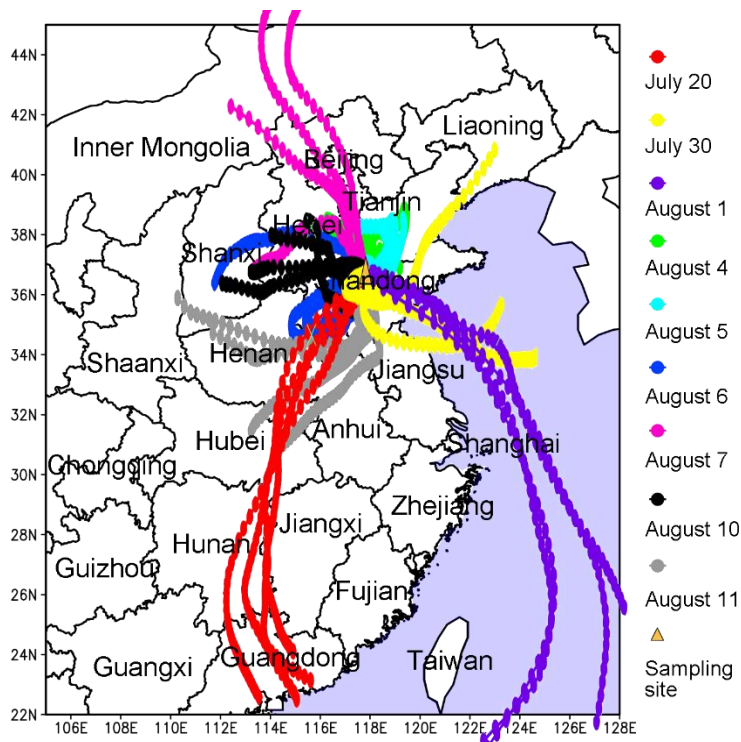
431 substantially on this day with the disappearance of the low pressure trough and the weakening of  
 432 solar radiation, though the hourly maximum O<sub>3</sub> still reached 100.4 ppbv. On the following days,  
 433 **the precipitations relieved the O<sub>3</sub> pollution in Ji'nan.**

434 Table 1 Summary of the synoptic systems, weather conditions and air mass origins on VOC  
 435 sampling days.

Date	O <sub>3</sub> maximum (ppbv)	Episode/non-episode	Synoptic system Weather condition	Air mass origin
July 20	71.0	Non-episode	WPSH, strong southwesterly winds	Continental air masses from South China
July 30	57.6		Uniform pressure field (weak high pressure), rain, fog, calm winds	Marine air masses
August 1	90.6		Uniform pressure field (weak high pressure), northeasterly winds	
August 4	107.5	Episode	Uniform pressure field (weak high pressure), northeasterly winds	Continental air masses from Shandong province
August 5	128.2		Uniform pressure field (weak high pressure), calm winds	
August 6	116.9		Uniform pressure field (weak high pressure), southwesterly winds	
August 7	126.9		Uniform pressure field (weak high pressure), calm winds	Continental air masses from the north
August 10	154.1		Low-pressure trough, calm winds	Continental air masses from the west
August 11	100.4		Subtropical high, southeasterly winds	Continental air masses from the southwest

436



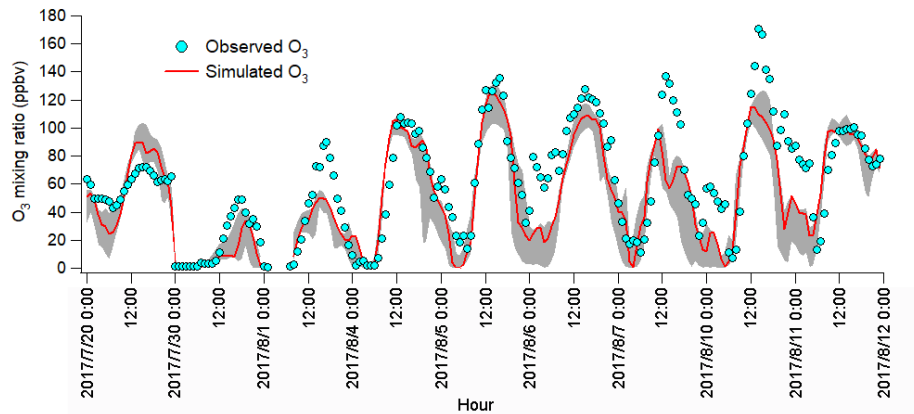


437

438 Figure 4 Forty eight hour backward trajectories calculated every 6 hours, with Ji'nan (36.68 N,  
 439 117.07 E, 500 m a.g.l.) as the starting point. The trajectories are simulated by HYSPLIT v4.9.  
 440 The water areas are highlighted in blue.

### 441 3.3 O<sub>3</sub> simulation and process analysis

442 The observations indicated the likely different regimes controlling local O<sub>3</sub> formation and the  
 443 potential impacts of regional transport. To understand the atmospheric chemistry and dynamics,  
 444 as well as their roles in this O<sub>3</sub> pollution event, the WRF-CMAQ was applied. Figure 5 shows  
 445 the hourly average simulated and observed O<sub>3</sub> on the VOC sampling days in Ji'nan. Overall, the  
 446 model well reproduced the magnitudes and diurnal patterns of the observed O<sub>3</sub>, except for the  
 447 higher simulated O<sub>3</sub> on July 20 and the under-prediction of O<sub>3</sub> on August 1, 7 and 10.  
 448 Discussions on the discrepancies and the detailed model validation are provided in Text S1,  
 449 Figures S9-S11 and Table S4.



450

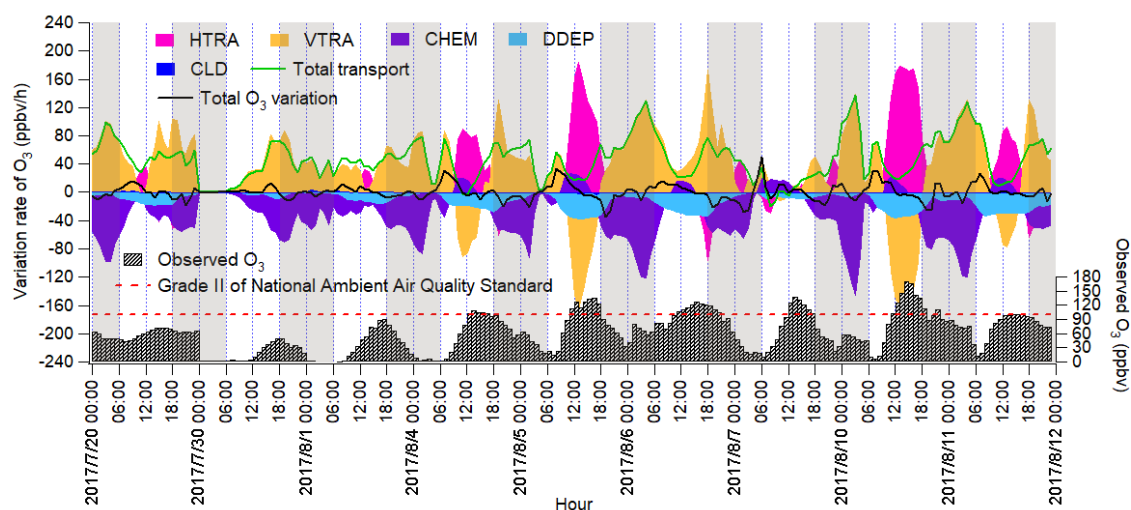
451 Figure 5 Hourly average mixing ratios of the WRF-CMAQ simulated and observed O<sub>3</sub> in Ji'nan.  
 452 The grey area shows the minimum and maximum simulated O<sub>3</sub> at the sampling site and 8  
 453 adjoining grids (12×12 km<sup>2</sup> for each grid).

454 The IPR analysis quantifies the contributions of different processes to the O<sub>3</sub> production rate, as  
 455 shown in Figure 6. HDIF and HADV were summed as horizontal transport (HTRA), and the  
 456 vertical transport (VTTRA) was a total representative of VDIF and VADV. It was found that  
 457 chemical reactions generally led to O<sub>3</sub> decrease during non-episodes. The negative contributions  
 458 of chemical reactions on July 20 coincided with the very low concentrations of O<sub>3</sub> precursors and  
 459 the flat diurnal cycle of O<sub>3</sub> (Figure 2). The chemical destruction of O<sub>3</sub> on July 30 and August 1  
 460 **was most likely** related to the relatively weak solar radiation and low temperature, which  
 461 inhibited the in situ photochemical reactions. In fact, the negative chemical effect should be  
 462 considered as the titration of NO to regionally-transported and/or background O<sub>3</sub> and the  
 463 **depletion** of O<sub>3</sub> by the **freshly** emitted NO **near the sources** (Beck and Grennfelt, 1994; Sillman,  
 464 1999). Conversely, the combined effect of horizontal and vertical transport was to increase O<sub>3</sub>.

465 During O<sub>3</sub> episodes, chemical reactions made positive contributions to O<sub>3</sub> production between  
 466 09:00 LT and 15:00 LT, with the average hourly O<sub>3</sub> production rate of 14.0±2.3 ppbv/hr. At the  
 467 same time, O<sub>3</sub> was also elevated by transport at an average rate of 18.7±4.0 ppbv/hr, **as a**  
 468 **combined effect of vertical transport (-40.8±20.2 ppbv/hr) and horizontal transport (59.5±19.8**  
 469 **ppbv/hr)**. The negative contribution of vertical transport to O<sub>3</sub> in these hours might be caused by  
 470 the updraft with the increase of temperature in the city. The O<sub>3</sub> enhancement by horizontal  
 471 transport could be explained by the westerly to northerly airflows and the high O<sub>3</sub> in the **NCP**  
 472 where the airflows originated or passed (**Figure 4 and Figure S10**). **The much higher O<sub>3</sub> over the**

473 **NCP than in the surrounding regions indicated that the NCP was an O<sub>3</sub> source in this case.** In fact,  
474 the transport of O<sub>3</sub> from the lower troposphere over the NCP to the free troposphere and further  
475 to northeast China was **also presented** by Ding et al. (2009).

476 During 16:00-08:00 LT on O<sub>3</sub> episode days, O<sub>3</sub> was titrated and chemically consumed at the rate  
477 of 49.4±6.3 ppbv/hr. This was reasonable in view of the fresh vehicular emissions (particularly  
478 NO<sub>x</sub>) in the morning and evening rush hours, when the titration of O<sub>3</sub> by NO produced NO<sub>2</sub>. The  
479 NO<sub>2</sub> was carried over to the other places by air circulation, and/or oxidized to NO<sub>3</sub> and N<sub>2</sub>O<sub>5</sub>,  
480 which could further react with aerosol to form HNO<sub>3</sub> and ClNO<sub>2</sub> in the evening. Horizontal and  
481 vertical transport dominated O<sub>3</sub> sources, with the average positive contribution of 5.7±7.0 and  
482 54.5±9.6 ppbv/hr during 16:00-08:00 LT on August 4-11, respectively. The strong vertical  
483 transport coincided with the downward winds in the evening, which **brought** the high-altitude O<sub>3</sub>  
484 to the ground, as indicated **in** Figure S9. However, the sources of O<sub>3</sub> in the upper atmosphere  
485 were beyond the scope of this study.



486  
487 **Figure 6** Time series of O<sub>3</sub> variation rate in Ji'nan induced by individual processes calculated  
488 based on the change of O<sub>3</sub> per hour. Total transport is the sum of HTRA and VTRA, and the sum  
489 of O<sub>3</sub> variation rates attributable to all the processes is represented by total O<sub>3</sub> variation rate. The  
490 nighttime (18:00 – 06:00 LT) has been highlighted in grey.

### 491 **3.4 Local O<sub>3</sub> formation and control**

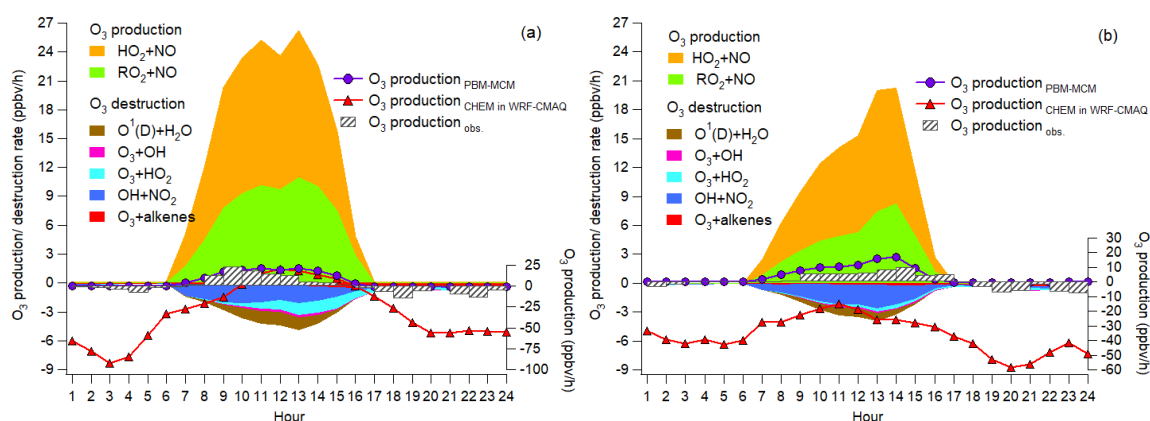
#### 492 **3.4.1 Pathway and source contributions to O<sub>3</sub> production**

493 The IPR analyses showed that chemical reactions served as an important source of O<sub>3</sub> on episode  
494 days in Ji'nan, particularly during 09:00-15:00 LT when O<sub>3</sub> was at high levels. This process was  
495 further studied through the simulation of the in-situ photochemistry by PBM-MCM. It should be  
496 noted that the simulations were based on the observed concentrations of O<sub>3</sub> precursors, which  
497 could be influenced by both local and regional air. It required cautions to extend the results to all  
498 the situations in Ji'nan, because the regional effect was not always consistent. Table S5 lists the  
499 production and destruction pathways of O<sub>3</sub> (Thornton et al., 2002; Monks, 2005; Kanaya et al.,  
500 2009). Briefly, the oxidation of NO by HO<sub>2</sub> and RO<sub>2</sub> produced NO<sub>2</sub>, which led to O<sub>3</sub> formation  
501 following NO<sub>2</sub> photolysis (R2 and R4-R5 in introduction). Therefore, the reactions between NO  
502 and HO<sub>2</sub>/RO<sub>2</sub> were considered as the production pathways of O<sub>3</sub>. To account for O<sub>3</sub> destruction,  
503 reaction between O<sup>1</sup>(D) and H<sub>2</sub>O denoted the photolysis of O<sub>3</sub>, and reactions of O<sub>3</sub> with OH,  
504 HO<sub>2</sub> and alkenes were also included. Furthermore, since HNO<sub>3</sub> was an important sink of NO<sub>2</sub>,  
505 the reaction between OH and NO<sub>2</sub> was treated to be destructive to O<sub>3</sub>. The titration of O<sub>3</sub> by NO  
506 was not included in O<sub>3</sub> destruction, because NO<sub>2</sub> produced in this reaction was either not  
507 considered as a source of O<sub>3</sub>.

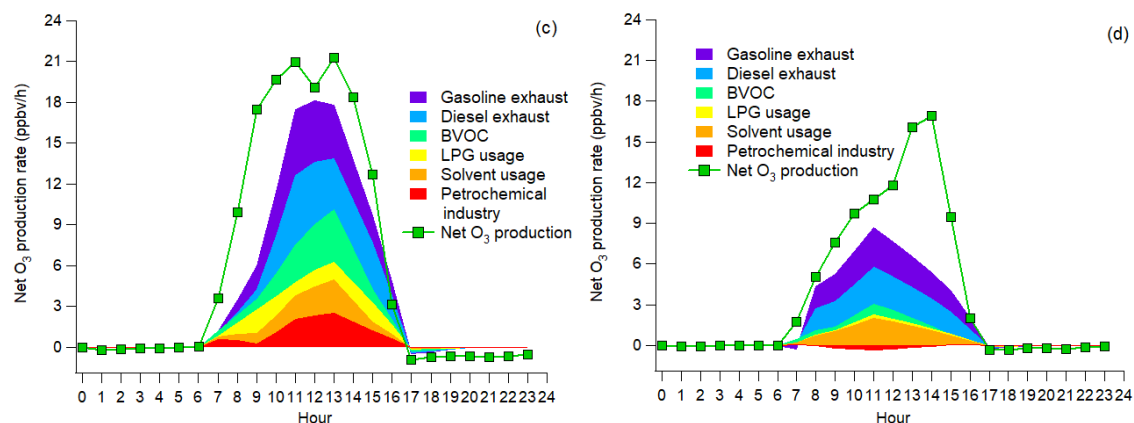
508 Figure 7 (a) and (b) show the 24 hour average simulated pathway contributions to O<sub>3</sub> production  
509 rate for the 6 O<sub>3</sub> episode days and 3 non-episode days. Also shown are the O<sub>3</sub> production rates  
510 simulated by PBM-MCM (O<sub>3</sub> production<sub>PBM-MCM</sub>), those simulated by WRF-CMAQ simulation  
511 (O<sub>3</sub> production<sub>CHEM</sub>), and those calculated from the observed hourly O<sub>3</sub> (O<sub>3</sub> production<sub>obs.</sub>).  
512 Overall, O<sub>3</sub> production<sub>PBM-MCM</sub> and O<sub>3</sub> production<sub>obs.</sub> were on the same magnitudes, especially  
513 during O<sub>3</sub> episodes with more stagnant weather conditions. This indicated that the PBM-MCM  
514 model reasonably reproduced the in situ O<sub>3</sub> photochemistry. Though obvious discrepancies  
515 existed between O<sub>3</sub> production<sub>CHEM</sub> and O<sub>3</sub> production<sub>PBM-MCM</sub>, they agreed well with each other  
516 during 10:00-15:00 LT on episode days, consistent with the finding that chemical reactions made  
517 great contributions to O<sub>3</sub> in this period (Figure 6). The lower or even negative O<sub>3</sub> production<sub>CHEM</sub>  
518 resulted from the titration of the regionally transported and/or local background O<sub>3</sub> by NO  
519 and the following depletion of NO<sub>2</sub> through reacting with OH and/or transport. Differently,  
520 PBM-MCM did not consider the transport of O<sub>3</sub>, though the transport effect was partially  
521 represented by constraining the model to the observed concentrations of O<sub>3</sub> precursors. In  
522 addition, the PBM-MCM was constructed by the observed air pollutants, which were already  
523 subject to chemical reactions before being detected by the analytical instruments. This meant that

524 the reaction between NO and O<sub>3</sub> from the emission to the detection of NO<sub>x</sub> was not considered in  
 525 PBM-MCM. However, as an emission-based model, WRF-CMAQ performed better in  
 526 describing the reactions immediately after the emissions of air pollutants. Therefore, the  
 527 chemical destructions of O<sub>3</sub> in the vicinity of NO<sub>x</sub> sources also accounted for the aforementioned  
 528 discrepancy. The obviously higher reaction rate between NO and O<sub>3</sub> simulated by WRF-CMAQ  
 529 (Figure S12) confirmed our inferences.

530 During both O<sub>3</sub> episodes and non-episodes, the reaction between HO<sub>2</sub> and NO dominated over  
 531 “RO<sub>2</sub>+NO” in O<sub>3</sub> production, while the O<sub>3</sub> destruction was mainly attributable to the formation  
 532 of HNO<sub>3</sub>, the reaction between O<sub>3</sub> and HO<sub>2</sub> and photolysis of O<sub>3</sub>. The net O<sub>3</sub> production rate  
 533 during O<sub>3</sub> episodes (maximum: 21.3 ppbv/hr) was much ( $p < 0.05$ ) higher than during non-  
 534 episodes (maximum: 16.9 ppbv/hr), which partially explained the higher O<sub>3</sub> on episode days. In  
 535 general, “OH+NO<sub>2</sub>” serves as the chain terminating reaction in VOC-limited regime of O<sub>3</sub>  
 536 formation, while the radical-radical reactions take over the role in NO<sub>x</sub>-limited regime  
 537 (Finlayson-Pitts and Pitts, 1993; Kleinman, 2005). Here, we found that the ratio of total reaction  
 538 rates between “HO<sub>2</sub>+RO<sub>2</sub>” and “OH+NO<sub>2</sub>” substantially increased from 0.2±0.1 during non-  
 539 episodes to 1.0±0.3 during O<sub>3</sub> episodes ( $p < 0.05$ ). This suggested that O<sub>3</sub> formation during non-  
 540 episodes was limited by VOCs, while it switched to be co-limited by VOCs and NO<sub>x</sub> during O<sub>3</sub>  
 541 episodes in view of the equivalent role of “HO<sub>2</sub>+RO<sub>2</sub>” and “OH+NO<sub>2</sub>” in terminating the chain  
 542 reactions.



543



544  
 545 Figure 7 Pathway contributions to O<sub>3</sub> production and destruction rate during episodes (a) and  
 546 non-episodes (b). Contributions of O<sub>3</sub> precursor sources to net O<sub>3</sub> production rate during  
 547 episodes (c) and non-episodes (d).

548 Further, the 24 hour average contributions to net O<sub>3</sub> production rate of different sources of O<sub>3</sub>  
 549 precursors were identified for the 6 episode days and 3 non-episode days, as presented in Figure  
 550 7 (c) and (d). Text S2 and Figure S13 illustrate the source apportionment of O<sub>3</sub> precursors and  
 551 the simulations of the source-specific contributions to O<sub>3</sub> production rates. The results are  
 552 presented in Table 2. Since the source apportionment was performed for the ambient O<sub>3</sub>  
 553 precursors which were already subject to atmospheric processes, such as dispersion, deposition  
 554 and chemical reactions, the results represented the source contributions to the steady – state  
 555 concentrations of O<sub>3</sub> precursors and the corresponding O<sub>3</sub> productions. It was found that gasoline  
 556 exhaust and diesel exhaust were the largest contributors to O<sub>3</sub> production regardless of O<sub>3</sub>  
 557 episodes or non-episodes. Specifically, the net O<sub>3</sub> production rate was  $1.0 \pm 0.3$  ppbv/hr for both  
 558 gasoline and diesel exhaust during non-episodes, which however increased to  $1.8 \pm 0.6$  ppbv/hr  
 559 for gasoline exhaust and  $1.7 \pm 0.4$  ppbv/hr for diesel exhaust during O<sub>3</sub> episodes. This suggested  
 560 that vehicular emissions played critical roles in building up ground-level O<sub>3</sub> in Ji'nan. If  
 561 carbonyls were taken into account, the contributions of vehicular emissions to O<sub>3</sub> production rate  
 562 were even higher than the currently simulated values, due to the dominance of vehicular exhausts  
 563 in the sources of carbonyls in urban areas (Grosjean et al., 1990; Granby et al., 1997). In addition,  
 564 the contributions of the other sources to O<sub>3</sub> production rates all increased during O<sub>3</sub> episodes  
 565 except for solvent usage ( $p > 0.05$ ), as listed in Table 2. It is not surprising to see the coincident  
 566 increases, in view of the higher simulated and observed overall O<sub>3</sub> production rate during  
 567 episodes.

568 Further insight into the percentage contributions (not shown here) found that the contributions of  
 569 BVOC, LPG usage and petrochemical industry relative to the sum of the O<sub>3</sub> production rates of  
 570 the 6 sources increased substantially from 9.9±4.2%, 4.3±1.4% and -2.8±1.9% during non-  
 571 episodes to 19.2±4.3%, 9.1±3.4% and 12.1±3.1% during O<sub>3</sub> episodes, respectively. The  
 572 increased O<sub>3</sub> production rates by BVOCs could be explained by the increase of isoprene  
 573 (episodes: 2.2±0.6 ppbv; non-episodes: 0.9±0.3 ppbv), under higher temperature and stronger  
 574 solar radiation during O<sub>3</sub> episodes. The enhanced O<sub>3</sub> formation from petrochemical industry on  
 575 episode days was likely associated with the dominance of continental air (Figure 4) and the  
 576 extensive petrochemical industries in the NCP. For example, the mixing ratio of styrene  
 577 increased from 54.7±22.0 pptv during non-episodes to 162.3±44.7 pptv during O<sub>3</sub> episodes. The  
 578 reason for elevated O<sub>3</sub> production rate by LPG usage during episodes was unknown. It is worth  
 579 noting that the source contributions to O<sub>3</sub> production might have some uncertainty due to the  
 580 limited number of samples (54 samples) and O<sub>3</sub> precursors (31 VOCs, CO, NO and NO<sub>2</sub>) for  
 581 source apportionment.

582 Table 2 Contributions to VOCs, CO, NO, NO<sub>2</sub> and O<sub>3</sub> production rate by the sources of O<sub>3</sub>  
 583 precursors averaged on the VOC sampling days in Ji'nan (Unit: % unless otherwise specified).

Source	VOCs*	CO	NO	NO <sub>2</sub>	O <sub>3</sub> production rate (ppbv/hr)	
					O <sub>3</sub> episodes	Non-episodes
GE <sup>1</sup>	25.7±3.6	29.9±2.1	30.9±2.4	22.2±2.4	1.8±0.6	1.0±0.3
DE <sup>2</sup>	17.6±2.4	57.3±5.2	52.0±5.8	54.4±5.8	1.7±0.4	1.0±0.3
BVOC	6.1±2.6	0.0±1.7	0.0±2.8	0.0±2.3	1.2±0.5	0.2±0.1
LPG <sup>3</sup>	14.7±2.0	2.2±1.1	9.1±1.6	4.7±0.9	0.8±0.5	0.1±0.1
Solvent <sup>4</sup>	17.1±3.9	3.1±1.8	5.1±3.8	7.8±3.1	0.8±0.5	0.7±0.3
PI <sup>5</sup>	18.8±3.1	7.4±1.9	2.9±1.8	10.9±2.5	1.0±0.3	-0.1±0.1

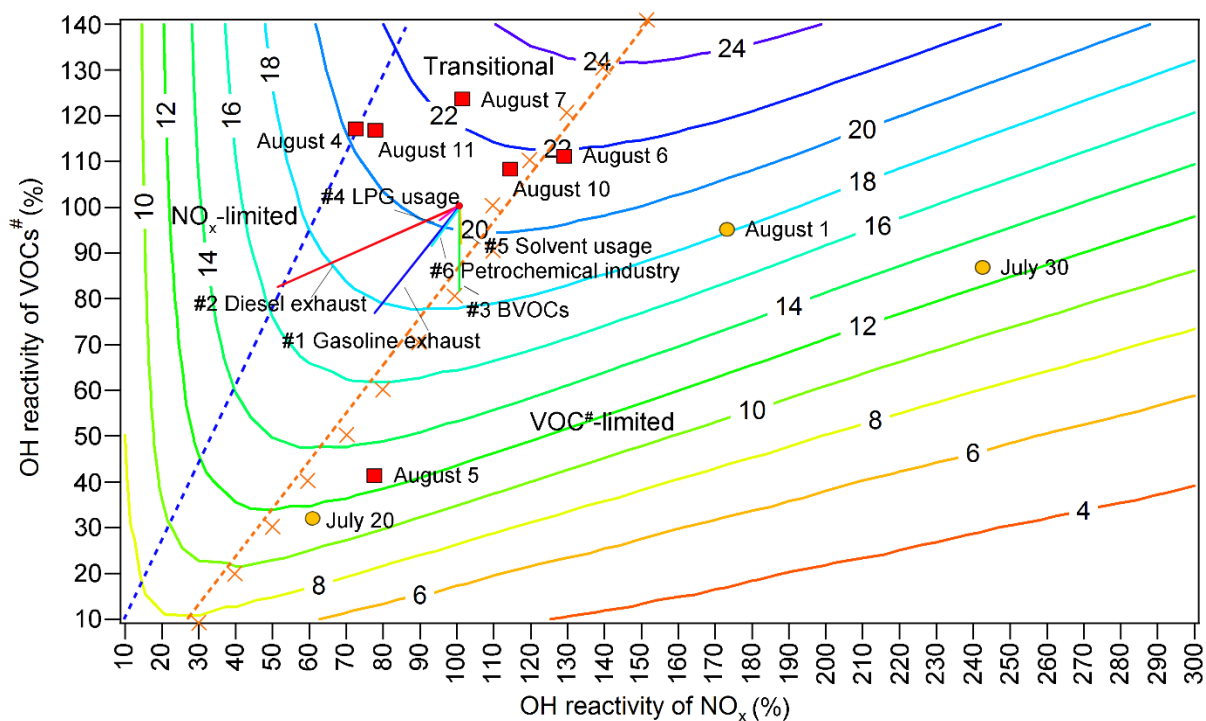
584 VOCs\*: VOCs applied in source apportionment (see Text S2).

585 <sup>1</sup> gasoline exhaust, <sup>2</sup> diesel exhaust, <sup>3</sup> LPG usage, <sup>4</sup> solvent usage and <sup>5</sup> petrochemical industry.

### 586 3.4.2 O<sub>3</sub> control measures

587 Both WRF-CMAQ and PBM-MCM revealed the significant local O<sub>3</sub> production in the O<sub>3</sub>  
 588 pollution event. The relationships between O<sub>3</sub> and its precursors need to be clarified, so that the  
 589 science-based control measures can be taken. Throughout the VOC sampling period, the OH

590 reactivity of VOCs ( $OH\ reactivity_{VOCs}$ ) were within the range of 33-123% of the average  
 591  $OH\ reactivity_{VOCs}$  during  $O_3$  episodes. For  $OH\ reactivity\ of\ NO_x$  ( $OH\ reactivity_{NO_x}$ ), the  
 592 range was 61-242%. The  $O_3$  production rates were simulated in a set of assumed scenarios with  
 593 different  $OH\ reactivity_{VOCs}$  and  $OH\ reactivity_{NO_x}$ . To include the OH reactivity of VOCs and  
 594  $NO_x$  on all the VOC sampling days, factors from 10% to 140% with the step of 10% were  
 595 applied to the average diurnal profiles of VOCs and CO during  $O_3$  episodes, while the factors  
 596 ranged from 10% to 300% with the step of 10% for  $NO_x$ . The initial concentrations of all the air  
 597 pollutants were also scaled by the factors and the model was constrained to these scaled  
 598 concentrations every hour, except for  $O_3$ . It should be noted that the factors applied to CO were  
 599 exactly the same as those applied to VOCs, therefore we use  $VOCs^\#$  to represent the sum of  
 600 VOCs and CO hereafter. The 14 gradients of  $OH\ reactivity_{VOCs^\#}$  and 30 gradients of  
 601  $OH\ reactivity_{NO_x}$  made up 420 scenarios. Meteorological conditions were exactly the same for  
 602 all the scenarios and the clear sky was hypothesized. According to the simulations, the  
 603 maximums of the  $O_3$  production rates occurred at 12:00 LT. Thus, the simulated  $O_3$  production  
 604 rates at 12:00 LT, as a function of  $OH\ reactivity_{VOCs}$  and  $OH\ reactivity_{NO_x}$ , are plotted in  
 605 Figure 8. Text S3 describes the methods to define the regimes controlling  $O_3$  formation.



606



607 Figure 8 Isopleths of the net O<sub>3</sub> production rate (ppbv/hr) at 12:00 LT as a function of  
608  $OH\ reactivity_{VOCs^\#}$  and  $OH\ reactivity_{NO_x}$ . The red blocks and orange circles denote the  
609 calculated  $OH\ reactivity_{VOCs^\#}$  and  $OH\ reactivity_{NO_x}$  at 12:00 LT on O<sub>3</sub> episode and non-  
610 episode days, respectively. Each orange cross represents the  $OH\ reactivity_{VOCs^\#}$  and  
611  $OH\ reactivity_{NO_x}$  at 12:00 LT in the scenario with highest O<sub>3</sub> production rate at a given  
612  $OH\ reactivity_{VOCs^\#}$ . The orange dashed line and blue dashed line divide O<sub>3</sub> formation into the  
613 VOC-limited regime, **transitional regime**, and NO<sub>x</sub>-limited regime.

614 It was found that O<sub>3</sub> formation was mainly limited by VOCs<sup>#</sup> during non-episodes. However, it  
615 switched to be co-limited by VOCs<sup>#</sup> and NO<sub>x</sub> (**transitional regime**) on episode days with the net  
616 O<sub>3</sub> production rate among the highest, except for August 5 when the strong sea breeze **diluted** air  
617 pollutants in Ji'nan and/or intercept the transport of air pollutants from Central China to Ji'nan  
618 (Figure S6). **In reality, the sensitivity of O<sub>3</sub> formation to NO<sub>x</sub> might be underemphasized due to**  
619 **the positive biases of NO<sub>2</sub> measurement (Lu et al., 2010). This effect was expected to be more**  
620 **significant during episodes when the overestimates of NO<sub>2</sub> were higher.** However, O<sub>3</sub> formation  
621 was not likely only limited by NO<sub>x</sub> **even during O<sub>3</sub> episodes**, which should be still sensitive to  
622 VOCs, as NO<sub>2</sub> could not be much overestimated in the urban areas (see section 2.2.1). Therefore,  
623 O<sub>3</sub> formation was considered to be in the **transitional regime** during episodes. This partially  
624 **explained** the increased O<sub>3</sub> during episodes in Ji'nan, given the higher O<sub>3</sub> production rates in  
625 **transitional regime** (Figure 8). **Noticeably, the change of regimes controlling O<sub>3</sub> formation is**  
626 **consistent with that predicted by the  $\frac{OH\ reactivity_{VOCs^\#}}{OH\ reactivity_{NO_x}}$  ratio and the ratio of the reaction rates**  
627 **between “HO<sub>2</sub>+RO<sub>2</sub>” and “OH+NO<sub>2</sub>”.**

628 The source apportionment of O<sub>3</sub> precursors enabled us to calculate the source-specific  
629  $OH\ reactivity_{VOCs^\#}$  and  $OH\ reactivity_{NO_x}$ . Accordingly, the variations of O<sub>3</sub> production rates  
630 **induced by the reductions in source emissions are presented in Figure 8** (straight solid lines #1-  
631 #6). The start point of the straight lines corresponded to 100% of **the total average**  
632  $OH\ reactivity_{VOCs^\#}$  and  $OH\ reactivity_{NO_x}$  during O<sub>3</sub> episodes. The end points, however,  
633 denoted **the  $OH\ reactivity_{VOCs^\#}$  and  $OH\ reactivity_{NO_x}$  with the complete elimination of**  
634 **emissions from the individual sources.** Therefore, the differences of the O<sub>3</sub> production rate  
635 **between the start point and end points were the source contributions to the O<sub>3</sub> production rate,**

636 while the lengths of the lines reflected the contributions to the OH reactivity. Further, the  
637 simulated O<sub>3</sub> production rates on the lines #1-#6, as a response of reductions in source emissions,  
638 are extracted and plotted in Figure S14. Obviously, the highest efficiencies of O<sub>3</sub> reduction could  
639 be achieved by cutting diesel exhaust (0.58 ppbv hr<sup>-1</sup>/10% emission reduction) and gasoline  
640 exhaust (0.47 ppbv hr<sup>-1</sup>/10% emission reduction). In fact, the sensitivity of O<sub>3</sub> production rate to  
641 the vehicle exhausts might be somewhat underestimated, due to the exclusion of carbonyls in the  
642 source apportionment. However, the reductions of O<sub>3</sub> production rate by cutting 10% of vehicle  
643 exhausts were still insignificant, compared to the overall maximum O<sub>3</sub> production rate of 21.3  
644 ppbv/hr during O<sub>3</sub> episodes. This indicated that by only restraining emissions from one to two  
645 sources, high percentages of emission reductions were required to sufficiently reduce the O<sub>3</sub>  
646 production rate. Otherwise, the combined efforts should be made to control the emissions of O<sub>3</sub>  
647 precursors from the diverse sources. In particular, it is essential to get rid of the transitional  
648 regime featuring high O<sub>3</sub> production rates and low sensitivities of O<sub>3</sub> production to the precursors.

#### 649 **4 Implications**

650 This study investigates the causes of a severe O<sub>3</sub> pollution event lasting for eight consecutive  
651 days in the NCP, one of the most densely populated regions in the world. Photochemical O<sub>3</sub>  
652 formation in the lower troposphere of the NCP is demonstrated as the main source, under the  
653 synoptic conditions of weak high pressure or low pressure trough. Though NO<sub>x</sub>, as an important  
654 precursor of O<sub>3</sub>, has been significantly reduced in emissions in China since 2013 (Duncan et al.,  
655 2016; Liu et al., 2017), O<sub>3</sub> pollution is still severe or even becoming worse in the NCP, as  
656 revealed in the present and also previous studies (Zhang et al., 2014; Sun et al., 2016). The  
657 finding that O<sub>3</sub> formation shifted from VOC-limited regime on relatively low O<sub>3</sub> days to the  
658 transitional regime on O<sub>3</sub> non-attainment days may elucidate the cause of the increase in O<sub>3</sub>,  
659 because O<sub>3</sub> productions in the transitional regime are even higher, despite decreases in NO<sub>x</sub>  
660 emissions. It is unrealistic to expect a continuously linear reduction in NO<sub>x</sub> emissions in the NCP,  
661 after the substantial decreases of NO<sub>x</sub> emissions from power plants and industries in recent years.  
662 In other words, restraining on VOC emissions is urgent for O<sub>3</sub> abatement in the NCP. Another  
663 important finding in this study was that the NCP served as an O<sub>3</sub> source. This was ever proposed  
664 by Ding et al. (2009), based on the aircraft measurement and simulation of atmospheric  
665 dynamics. We confirmed it through the ground-level observation and the simulation of in-situ

666 **photochemistry**. It can be expected that organic nitrates are also intensively formed **in the NCP**  
667 as byproducts in the photochemical cycles of O<sub>3</sub> formation. In combination with the fact that the  
668 NCP locates within the mid-latitude band of Northern Hemisphere under the dominance of  
669 westerlies, O<sub>3</sub> and organic nitrates formed in this region can be transported over a long distance  
670 following uplift processes, which has been confirmed to partially account for the enhancement of  
671 background O<sub>3</sub> in North America and even Europe (Derwent et al., 2015; Lin et al., 2017).  
672 **Therefore, the recent air pollution control measures taken in China (including China's Clean Air**  
673 **Act Plan in force in 2013) are still inadequate** to ease the global O<sub>3</sub> burden in a short period.  
674 More **effective Action Plans should be implemented** to achieve an O<sub>3</sub> benefit, with  
675 comprehensive thinking of atmospheric dynamics and chemistry.

676 **Acknowledgements:** This study was supported by the National Key R&D Program of China  
677 (2017YFC0212001), the Research Grants Council of the Hong Kong Special Administrative  
678 Region via grants PolyU5154/13E, PolyU152052/14E, PolyU152052/16E, CRF/C5004-15E and  
679 CRF/C5022-14G, the Collaborative Research program between The Beijing University of  
680 Technology and The Hong Kong Polytechnic University (PolyU) (4-ZZFW), the Hong Kong  
681 Polytechnic University PhD scholarships (project RTUP), and the National Natural Science  
682 Foundation of China (No. 41675118). This study is partly supported by the Hong Kong PolyU  
683 internal grant (G-YBUQ, 1-ZVJT and 1-BBW4). The data are accessible at  
684 [https://drive.google.com/open?id=1\\_KeOxOuVsLY83xL74RtcRORSiiyIR\\_8FZ](https://drive.google.com/open?id=1_KeOxOuVsLY83xL74RtcRORSiiyIR_8FZ).

## 685 **References**

- 686 Atkinson, R.: Atmospheric chemistry of VOCs and NO<sub>x</sub>, *Atmos. Environ.*, 34, 2063-2101, **2000**.
- 687 Beck, J.P. and Grennfelt, P.: Estimate of ozone production and destruction over northwestern  
688 Europe, *Atmos. Environ.*, 28, 129-140, **1994**.
- 689 Cai, C., Geng, F., Tie, X., Yu, Q., and An, J.: Characteristics and source apportionment of VOCs  
690 measured in Shanghai, China, *Atmos. Environ.*, 44, 5005-5014, **2010**.
- 691 Carter, W.P.: Development of ozone reactivity scales for volatile organic compounds, *Air &*  
692 *Waste Manage. Assoc.*, 44, 881-899, **1994**.

693 Carter, W.P., Pierce, J.A., Luo, D., and Malkina, I.L.: Environmental chamber study of  
694 maximum incremental reactivities of volatile organic compounds, *Atmos. Environ.*, 29(18),  
695 2499-2511, **1995**.

696 Chameides, W. and Walker, J.C.: A photochemical theory of tropospheric ozone, *J. Geophys.*  
697 *Res.*, 78(36), 8751-8760, **1973**.

698 Chan, C.Y. and Chan, L.Y.: Effect of meteorology and air pollutant transport on ozone episodes  
699 at a subtropical coastal Asian city, Hong Kong, *J. Geophys. Res. – Atmos.*, 105(D16), 20707-  
700 20724, **2000**.

701 Chen, Y., Zhao, C., Zhang, Q., Deng, Z., Huang, M., and Ma, X.: Aircraft study of mountain  
702 chimney effect of Beijing, China, *J. Geophys. Res. – Atmos.*, 114(D8),  
703 doi:10.1029/2008JD010610, **2009**.

704 Cheng, H., Guo, H., Wang, X., Saunders, S.M., Lam, S.H.M., Jiang, F., Wang, T., Ding, A., Lee,  
705 S., and Ho, K.F.: On the relationship between ozone and its precursors in the Pearl River Delta:  
706 application of an observation-based model (OBM), *Environ. Sci. Pollut. Res.*, 17(3), 547-560,  
707 **2010**.

708 Colman, J.J., Swanson, A.L., Meinardi, S., Sive, B.C., Blake, D.R., and Rowland, F.S.:  
709 Description of the analysis of a wide range of volatile organic compounds in whole air samples  
710 collected during PEM-Tropics A and B, *Anal. Chem.*, 73(15), 3723-3731, **2001**.

711 Cooper, O.R., Stohl, A., Hübler, G., Hsie, E.Y., Parrish, D.D., Tuck, A.F., Kiladis, G.N.,  
712 Oltmans, S.J., Johnson, B.J., Shapiro, M., and Moody, J.L.: Direct transport of midlatitude  
713 stratospheric ozone into the lower troposphere and marine boundary layer of the tropical Pacific  
714 Ocean, *J. Geophys. Res.: Atmos.*, 110(D23), **2005**.

715 Crutzen, P.: A discussion of the chemistry of some minor constituents in the stratosphere and  
716 troposphere, *Pure Appl. Geophys.*, 106(1), 1385-1399, **1973**.

717 Derwent, R.G., Utembe, S.R., Jenkin, M.E., and Shallcross, D.E.: Tropospheric ozone  
718 production regions and the intercontinental origins of surface ozone over Europe, *Atmos.*  
719 *Environ.*, 112, 216-224, **2015**.

720 Ding, A.J., Fu, C.B., Yang, X.Q., Sun, J.N., Zheng, L.F., Xie, Y.N., Herrmann, E., Nie, W.,  
721 Petaja, T., Kerminen, V.M., and Kulmala, M.: Ozone and fine particle in the western Yangtze  
722 River Delta: an overview of 1 yr data at the SORPES station, *Atmos. Chem. Phys.*, 13(11):5813-  
723 30, **2013**.

724 Ding, A., Wang, T., Xue, L., Gao, J., Stohl, A., Lei, H., Jin, D., Ren, Y., Wang, X., Wei, X., and  
725 Qi, Y.: Transport of north China air pollution by midlatitude cyclones: Case study of aircraft  
726 measurements in summer 2007, *J. Geophys. Res.: Atmos.*, 114(D8), **2009**.

727 Duncan, B.N., Lamsal, L.N., Thompson, A.M., Yoshida, Y., Lu, Z., Streets, D.G., Hurwitz,  
728 M.M., and Pickering, K.E.: A space-based, high-resolution view of notable changes in urban  
729 NO<sub>x</sub> pollution around the world (2005-2014), *J. Geophys. Res.: Atmos.*, 121(2), 976-996, **2016**.

730 Dunlea, E.J., Herndon, S.C., Nelson, D.D., Volkamer, R.M., San Martini, F., Sheehy, P.M.,  
731 Zahniser, M.S., Shorter, J.H., Wormhoudt, J.C., Lamb, B.K., and Allwine, E.J.: Evaluation of  
732 nitrogen dioxide chemiluminescence monitors in a polluted urban environment, *Atmos. Chem.*  
733 *Phys.*, 7(10), 2691-2704, **2007**.

734 Finlayson-Pitts, B.J., and Pitts Jr, J.N.: Atmospheric chemistry of tropospheric ozone formation:  
735 scientific and regulatory implications, *Air & Waste Manage. Assoc.*, 43(8), 1091-1100, **1993**.

736 Fung, J.C.H., Lau, A.K.H., Lam, J.S.L., and Yuan, Z.: Observational and modeling analysis of a  
737 severe air pollution episode in western Hong Kong, *J. Geophys. Res. – Atmos.*, 110(D9), **2005**.

738 Gao, J., Wang, T., Ding, A., and Liu, C.: Observational study of ozone and carbon monoxide at  
739 the summit of mount Tai (1534m asl) in central-eastern China, *Atmos. Environ.*, 39(26), 4779-  
740 4791, **2005**.

741 Granby, K., Christensen, C.S., and Lohse, C.: Urban and semi-rural observations of carboxylic  
742 acids and carbonyls, *Atmos. Environ.*, 31(10), 1403-1415, **1997**.

743 Grosjean, D., Miguel, A.H., and Tavares, T.M.: Urban air pollution in Brazil: Acetaldehyde and  
744 other carbonyls, *Atmos. Environ.*, 24(1), 101-106, **1990**.

745 Gu, D., Wang, Y., Smeltzer, C., and Boersma, K.F.: Anthropogenic emissions of NO<sub>x</sub> over  
746 China: Reconciling the difference of inverse modeling results using GOME-2 and OMI  
747 measurements. *J. Geophys. Res.: Atmos.*, 119(12):7732-40, **2014**.

748 Guo, H., Ling, Z.H., Cheung, K., Jiang, F., Wang, D.W., Simpson, I.J., Barletta, B., Meinardi, S.,  
749 Wang, T.J., Wang, X.M., Saunders, S.M., and Blake, D.R.: Characterization of photochemical  
750 pollution at different elevations in mountainous areas in Hong Kong, *Atmos. Chem. Phys.*, 13(8),  
751 3881-3898, **2013**.

752 Han, X., Zhu, L., Wang, S., Meng, X., Zhang, M., and Hu, J.: Modeling study of impacts on  
753 surface ozone of regional transport and emissions reductions over North China Plain in summer  
754 2015, *Atmos. Chem. Phys.*, 18(16):12207-21, **2018**.

755 He, J., Wang, Y., Hao, J., Shen, L., and Wang, L.: Variations of surface O<sub>3</sub> in August at a rural  
756 site near Shanghai: influences from the West Pacific subtropical high and anthropogenic  
757 emissions, *Environ. Sci. Pollut. Res.*, 19(9), 4016-4029, **2012**.

758 He, K.: Multi-resolution Emission Inventory for China (MEIC): model framework and 1990-  
759 2010 anthropogenic emissions, In AGU Fall Meeting Abstracts, December, **2012**.

760 Huang, J.P., Fung, J.C., Lau, A.K., and Qin, Y.: Numerical simulation and process analysis of  
761 typhoon-related ozone episodes in Hong Kong, *J. Geophys. Res. – Atmos.*, 110(D5), **2005**.

762 Jenkin, M.E. and Clemitshaw, K.C.: Ozone and other secondary photochemical pollutants:  
763 chemical processes governing their formation in the planetary boundary layer, *Atmos. Environ.*,  
764 34(16), 2499-2527, **2000**.

765 Jenkin, M.E., Saunders, S.M., and Pilling, M.J.: The tropospheric degradation of volatile organic  
766 compounds: a protocol for mechanism development, *Atmos. Environ.*, 31(1), 81-104, **1997**.

767 Jiang, F., Guo, H., Wang, T.J., Cheng, H.R., Wang, X.M., Simpson, I.J., Ding, A.J., Saunders,  
768 S.M., Lam, S.H.M., and Blake, D.R.: An ozone episode in the Pearl River Delta: Field  
769 observation and model simulation, *J. Geophys. Res. – Atmos.*, 115(D22), **2010**.

770 Jin, X., Fiore, A.M., Murray, L.T., Valin, L.C., Lamsal, L.N., Duncan, B., Folkert Boersma, K.,  
771 De Smedt, I., Abad, G.G., Chance, K., and Tonnesen, G.S.: Evaluating a Space-Based Indicator  
772 of Surface Ozone-NO<sub>x</sub>-VOC Sensitivity Over Midlatitude Source Regions and Application to  
773 Decadal Trends, *J. Geophys. Res.: Atmos.*, 122(19), **2017**.

774 Kanaya, Y., Pochanart, P., Liu, Y., Li, J., Tanimoto, H., Kato, S., Suthawaree, J., Inomata, S.,  
775 Taketani, F., Okuzawa, K., and Kawamura, K.: Rates and regimes of photochemical ozone

776 production over Central East China in June 2006: a box model analysis using comprehensive  
777 measurements of ozone precursors, *Atmos. Chem. Phys.*, 9(20), 7711-7723, **2009**.

778 Kleinman, L.I.: The dependence of tropospheric ozone production rate on ozone precursors,  
779 *Atmos. Environ.*, (3), 575-586, **2005**.

780 Kusaka, H. and Kimura, F.: Coupling a single-layer urban canopy model with a simple  
781 atmospheric model: Impact on urban heat island simulation for an idealized case, *J. Meteorol. Soc.*  
782 *Japan: Ser. II*, 82(1), 67-80, **2004**.

783 Lam, S.H.M., Saunders, S.M., Guo, H., Ling, Z.H., Jiang, F., Wang, X.M., and Wang, T.J.:  
784 Modelling VOC source impacts on high ozone episode days observed at a mountain summit in  
785 Hong Kong under the influence of mountain-valley breezes, *Atmos. Environ.*, 81, 166-176, **2013**.

786 Lang, J., Zhang, Y., Zhou, Y., Cheng, S., Chen, D., Guo, X., Chen, S., Li, X., Xing, X., and  
787 Wang, H.: Trends of PM<sub>2.5</sub> and chemical composition in Beijing, 2000–2015, *Aerosol Air Qual.*  
788 *Res.*, 17, 412-425, **2017**.

789 Li, M., Zhang, Q., Kurokawa, J.I., Woo, J.H., He, K., Lu, Z., Ohara, T., Song, Y., Streets, D.G.,  
790 Carmichael, G.R., and Cheng, Y.: MIX: a mosaic Asian anthropogenic emission inventory under  
791 the international collaboration framework of the MICS-Asia and HTAP, *Atmos. Chem. Phys.*,  
792 17(2), **2017**.

793 Lin, M., Fiore, A.M., Horowitz, L.W., Langford, A.O., Oltmans, S.J., Tarasick, D., and Rieder,  
794 H.E.: Climate variability modulates western US ozone air quality in spring via deep stratospheric  
795 intrusions, *Nat. Commun.*, 6:7105, **2015**.

796 Lin, M., Horowitz, L.W., Payton, R., Fiore, A.M., and Tonnesen, G.: US surface ozone trends  
797 and extremes from 1980 to 2014: quantifying the roles of rising Asian emissions, domestic  
798 controls, wildfires, and climate, *Atmos. Chem. Phys.*, 17(4), 2943-2970, **2017**.

799 Lin, W., Xu, X., Zhang, X., and Tang, J.: Contributions of pollutants from North China Plain to  
800 surface ozone at the Shangdianzi GAW Station, *Atmos. Chem. Phys.*, 8(19), 5889-5898, **2008**.

801 Liu, F., Beirle, S., Zhang, Q., Zheng, B., Tong, D., and He, K.: NO<sub>x</sub> emission trends over  
802 Chinese cities estimated from OMI observations during 2005 to 2015, *Atmospheric chemistry*  
803 *and physics*, 17(15), 9261-9275, **2017**.

804 Liu, X.H., Zhang, Y., Xing, J., Zhang, Q., Wang, K., Streets, D.G., Jang, C., Wang, W.X., and  
805 Hao, J.M.: Understanding of regional air pollution over China using CMAQ, part II. Process  
806 analysis and sensitivity of ozone and particulate matter to precursor emissions, *Atmos. Environ.*,  
807 44(30), 3719-3727, **2010**.

808 Lo, J.C., Lau, A.K., Fung, J.C., and Chen, F.: Investigation of enhanced cross-city transport and  
809 trapping of air pollutants by coastal and urban land-sea breeze circulations, *J. Geophys. Res. –*  
810 *Atmos.*, 111(D14), **2006**.

811 *Lyu, X.P., Chen, N., Guo, H., Zhang, W.H., Wang, N., Wang, Y., and Liu, M.: Ambient volatile*  
812 *organic compounds and their effect on ozone production in Wuhan, central China, Sci. Total*  
813 *Environ.*, 541:200-9, **2016**.

814 Lyu, X.P., Guo, H., Wang, N., Simpson, I.J., Cheng, H.R., Zeng, L.W., Saunders, S.M., Lam, S.  
815 H.M., Meinardi, S., and Blake, D.R.: Modeling C<sub>1</sub>-C<sub>4</sub> alkyl nitrate photochemistry and their  
816 impacts on O<sub>3</sub> production in urban and suburban environments of Hong Kong, *J. Geophys. Res.*  
817 *– Atmos.*, 122(19), **2017**.

818 *Lu, K., Zhang, Y., Su, H., Brauers, T., Chou, C.C., Hofzumahaus, A., Liu, S.C., Kita, K., Kondo,*  
819 *Y., Shao, M., and Wahner, A.: Oxidant (O<sub>3</sub> + NO<sub>2</sub>) production processes and formation regimes*  
820 *in Beijing, J. Geophys. Res.: Atmos.*, 115(D7), **2010**.

821 Madronich, S. and Flocke, S.: Theoretical estimation of biologically effective UV radiation at the  
822 Earth's surface, In *Solar Ultraviolet Radiation* (pp. 23-48), Springer, Berlin, Heidelberg, **1997**.

823 Mao, J., Ren, X., Chen, S., Brune, W.H., Chen, Z., Martinez, M., Harder, H., Lefer, B.,  
824 Rappenglueck, B., Flynn, J., and Leuchner, M.: Atmospheric oxidation capacity in the summer  
825 of Houston 2006: Comparison with summer measurements in other metropolitan studies, *Atmos.*  
826 *Environ.*, 44(33), 4107-4115, **2010**.

827 McClenny, W.A., Williams, E.J., Cohen, R.C., and Stutz, J.: Preparing to measure the effects of  
828 the NO<sub>x</sub> SIP Call—methods for ambient air monitoring of NO, NO<sub>2</sub>, NO<sub>y</sub>, and individual NO<sub>z</sub>  
829 species, *Air & Waste Manage. Assoc.*, 52(5), 542-562, **2002**.

830 Monks, P. S.: Gas-phase radical chemistry in the troposphere, *Chem. Soc. Reviews*, 34(5), 376-  
831 395, **2005**.



832 Ren, X., Harder, H., Martinez, M., Leshner, R.L., Oligier, A., Simpas, J.B., Brune, W.H., Schwab,  
833 J.J., Demerjian, K.L., He, Y., and Zhou, X.: OH and HO<sub>2</sub> chemistry in the urban atmosphere of  
834 New York City, *Atmos. Environ.*, 37(26), 3639-3651, **2003**.

835 Saunders, S.M. Jenkin, M.E., Derwent, R.G., and Pilling, M.J.: Protocol for the development of  
836 the Master Chemical Mechanism, MCM v3 (Part A): tropospheric degradation of non-aromatic  
837 volatile organic compounds, *Atmos. Chem. Phys.*, 3(1), 161-180, **2003**.

838 Shan, W., Yin, Y., Zhang, J., and Ding, Y.: Observational study of surface ozone at an urban site  
839 in East China, *Atmos. Res.*, 89(3), 252-261, **2008**.

840 Shao, M., Lu, S., Liu, Y., Xie, X., Chang, C., Huang, S., and Chen, Z.: Volatile organic  
841 compounds measured in summer in Beijing and their role in ground-level ozone formation, *J.*  
842 *Geophys. Res. – Atmos.*, 114(D2), doi.org/10.1029/2008JD010863, **2009b**.

843 Shu, L., Xie, M., Wang, T., Gao, D., Chen, P., Han, Y., Li, S., Zhuang, B., and Li, M.: Integrated  
844 studies of a regional ozone pollution synthetically affected by subtropical high and typhoon  
845 system in the Yangtze River Delta region, China, *Atmos. Chem. Phys.*, 16(24), 15801-15819,  
846 **2016**.

847 Sillman, S.: The relation between ozone, NO<sub>x</sub> and hydrocarbons in urban and polluted rural  
848 environments, *Atmos. Environ.*, 33(12), 1821-1845, **1999**.

849 Sun, L., Xue, L., Wang, T., Gao, J., Ding, A., Cooper, O.R., Lin, M., Xu, P., Wang, Z., Wang, X.,  
850 Wen, L., Zhu, Y., Chen, T., Yang, L., Wang, Y., Chen, J., and Wang, W.: Significant increase of  
851 summertime ozone at Mount Tai in Central Eastern China, *Atmos. Chem. Phys.*, 16(16), 10637-  
852 10650, **2016**.

853 Tan, Z., Lu, K., Dong, H., Hu, M., Li, X., Liu, Y., Lu, S., Shao, M., Su, R., Wang, H., and Wu,  
854 Y.: Explicit diagnosis of the local ozone production rate and the ozone-NO<sub>x</sub>-VOC sensitivities,  
855 *Sci. Bull.*, 63(16):1067-76, **2018**.

856 Tan, Z., Lu, K., Jiang, M., Su, R., Dong, H., Zeng, L., Xie, S., Tan, Q., and Zhang, Y.: Exploring  
857 ozone pollution in Chengdu, southwestern China: A case study from radical chemistry to O<sub>3</sub>-  
858 VOC-NO<sub>x</sub> sensitivity, *Sci. Total Environ.*, 636:775-86, **2018**.

859 Thornton, J.A., Wooldridge, P.J., Cohen, R.C., Martinez, M., Harder, H., Brune, W.H., Williams,  
860 E.J., Roberts, J.M., Fehsenfeld, F.C., Hall, S.R., and Shetter, R.E.: Ozone production rates as a

861 function of NO<sub>x</sub> abundances and HO<sub>x</sub> production rates in the Nashville urban plume, *J. Geophys.*  
862 *Res. – Atmos.*, 107(D12), doi.org/10.1029/2001JD000932, **2002**.

863 Wang, N., Guo, H., Jiang, F., Ling, Z. H., and Wang, T.: Simulation of ozone formation at  
864 different elevations in mountainous area of Hong Kong using WRF-CMAQ model, *Sci. Total*  
865 *Environ.*, 505, 939-951, **2015b**.

866 Wang, T., Ding, A., Gao, J., and Wu, W.S.: Strong ozone production in urban plumes from  
867 Beijing, China, *Geophys. Res. Lett.*, 33(21), **2006**.

868 Wang, T., Nie, W., Gao, J., Xue, L.K., Gao, X.M., Wang, X.F., Qiu, J., Poon, C.N., Meinardi, S.,  
869 Blake, D., Wang, S.L., Ding, A.J., Chai, F.H., Zhang, Q.Z., and Wang, W.X.: Air quality during  
870 the 2008 Beijing Olympics: secondary pollutants and regional impact, *Atmos. Chem. Phys.*,  
871 10(16), 7603-7615, **2010**.

872 Wang, X.M., Lin, W.S., Yang, L.M., Deng, R.R., and Lin, H.: A numerical study of influences  
873 of urban land - use change on ozone distribution over the Pearl River Delta region, China, *Tellus*  
874 *B*, 59(3), 633-641, **2007**.

875 Wang, Z., Li, Y., Chen, T., Zhang, D., Sun, F., Wei, Q., Dong, X., Sun, R., Huan, N., and Pan, L.:  
876 Ground-level ozone in urban Beijing over a 1-year period: Temporal variations and relationship  
877 to atmospheric oxidation, *Atmos. Res.*, 164, 110-117, **2015a**.

878 Whitten, G.Z., Heo, G., Kimura, Y., McDonald-Buller, E., Allen, D.T., Carter, W.P., and  
879 Yarwood, G.: A new condensed toluene mechanism for Carbon Bond: CB05-TU, *Atmos.*  
880 *Environ.*, 44(40), 5346-5355, **2010**.

881 Williams, J., Keßel, S.U., Nölscher, A.C., Yang, Y., Lee, Y., Yáñez-Serrano, A.M., Wolff, S.,  
882 Kesselmeier, J., Klüpfel, T., Lelieveld, J., and Shao, M.: Opposite OH reactivity and ozone  
883 cycles in the Amazon rainforest and megacity Beijing: Subversion of biospheric oxidant control  
884 by anthropogenic emissions, *Atmos. Environ.*, 125, 112-118, **2016**.

885 Xing, C., Liu, C., Wang, S., Chan, K.L., Gao, Y., Huang, X., Su, W., Zhang, C., Dong, Y., Fan,  
886 G., and Zhang, T.: Observations of the vertical distributions of summertime atmospheric  
887 pollutants and the corresponding ozone production in Shanghai, China, *Atmos. Chem. Phys.*,  
888 17(23), **2017**.

889 Xing, J., Ding, D., Wang, S., Zhao, B., Jang, C., Wu, W., Zhang, F., Zhu, Y., and Hao, J.:  
890 Quantification of the enhanced effectiveness of NO<sub>x</sub> control from simultaneous reductions of  
891 VOC and NH<sub>3</sub> for reducing air pollution in the Beijing–Tianjin–Hebei region, China, *Atmos.*  
892 *Chem. Phys.*, 18(11):7799-814, **2018**.

893 Xu, Z., Wang, T., Xue, L.K., Louie, P.K., Luk, C.W., Gao, J., Wang, S.L., Chai, F.H., and Wang,  
894 W.X.: Evaluating the uncertainties of thermal catalytic conversion in measuring atmospheric  
895 nitrogen dioxide at four differently polluted sites in China, *Atmos. Environ.*, 76, 221-226, **2013**.

896 Xue, L.K., Wang, T., Gao, J., Ding, A.J., Zhou, X.H., Blake, D.R., Wang, X.F., Saunders, S.M.,  
897 Fan, S.J., Zuo, H.C., Zhang, Q.Z. and Wang, W.X.: Ground-level ozone in four Chinese cities:  
898 precursors, regional transport and heterogeneous processes, *Atmos. Chem. Phys.*, 14(23), 13175-  
899 13188, **2014**.

900 Yang, Y., Shao, M., Wang, X., Nolscher, A.C., Kessel, S., Guenther, A., and Williams, J.:  
901 Towards a quantitative understanding of total OH reactivity: A review, *Atmos. Environ.*,  
902 134:147-161, **2016**.

903 Ye, L., Wang, X., Fan, S., Chen, W., Chang, M., Zhou, S., Wu, Z., and Fan, Q.: Photochemical  
904 indicators of ozone sensitivity: application in the Pearl River Delta, China, *Front. Env. Sci. Eng.*  
905 *10(6):15*, **2016**.

906 Yin, Y., Lu, H., Shan, W., and Zheng, Y.: Analysis of observed ozone episode in urban Jinan,  
907 China, *Bulletin Environ. Contamination & toxico.*, 83(2), 159-163, **2009**.

908 Zhang, Q., Streets, D.G., Carmichael, G.R., He, K.B., Huo, H., Kannari, A., Klimont, Z., Park,  
909 I.S., Reddy, S., Fu, J.S., Chen, D., Duan, L., Lei, Y., Wang, L.T., and Yao, Z.L.: Asian  
910 emissions in 2006 for the NASA INTEX-B mission, *Atmos. Chem. Phys.*, 9(14), 5131-5153,  
911 **2009**.

912 Zhang, Q., Streets, D.G., He, K., Wang, Y., Richter, A., Burrows, J.P., Uno, I., Jang, C.J., Chen,  
913 D., Yao, Z., and Lei, Y.: NO<sub>x</sub> emission trends for China, 1995-2004: The view from the ground  
914 and the view from space, *J. Geophys. Res. – Atmos.*, 112(D22), **2007**.

915 Zhang, Q., Yuan, B., Shao, M., Wang, X., Lu, S., Lu, K., Wang, M., Chen, L., Chang, C.C., and  
916 Liu, S.C.: Variations of ground-level O<sub>3</sub> and its precursors in Beijing in summertime between  
917 2005 and 2011, *Atmos. Chem. Phys.*, 14(12), 6089-6101, **2014**.

918 Zhang, Y., Ding, A., Mao, H., Nie, W., Zhou, D., Liu, L., Huang, X., and Fu, C.: Impact of  
919 synoptic weather patterns and inter-decadal climate variability on air quality in the North China  
920 Plain during 1980-2013, *Atmos. Environ.*, 124, 119-128, **2016**.

921 Zhang, Z., Zhang, X., Gong, D., Quan, W., Zhao, X., Ma, Z., and Kim, S.J.: Evolution of surface  
922 O<sub>3</sub> and PM<sub>2.5</sub> concentrations and their relationships with meteorological conditions over the last  
923 decade in Beijing, *Atmos. Environ.*, 108, 67-75, **2015**.

924 Zhao, C., Wang, Y., and Zeng, T.: East China plains: A “basin” of ozone pollution, *Environ. Sci.*  
925 *Technol.*, 43(6), 1911-1915, **2009**.

926 Zong, R., Yang, X., Wen, L., Xu, C., Zhu, Y., Chen, T., Yao, L., Wang, L., Zhang, J., Yang, L.,  
927 Wang, X., Shao, M., Zhu, T., Xue, L., and Wang, W.: Strong ozone production at a rural site in  
928 the North China Plain: Mixed effects of urban plumes and biogenic emissions, *J. Environ. Sci.*,  
929 [doi.org/10.1016/j.jes.2018.05.003](https://doi.org/10.1016/j.jes.2018.05.003), **2018**.

## Supporting Information for “Causes of a continuous summertime O<sub>3</sub> pollution event in Ji’nan, a central city in the North China Plain”

Xiaopu Lyu<sup>1</sup>, Nan Wang<sup>2</sup>, Hai Guo<sup>1\*</sup>, Likun Xue<sup>3</sup>, Fei Jiang<sup>4</sup>, Yangzong Zeren<sup>1</sup>, Hairong Cheng<sup>5</sup>, Zhe Cai<sup>4</sup>, Lihui Han<sup>6</sup> and Ying Zhou<sup>6</sup>

<sup>1</sup> Department of Civil and Environmental Engineering, The Hong Kong Polytechnic University, Hong Kong, China

<sup>2</sup> Division of Environmental Meteorology, Institute of Tropical and Marine Meteorology, China Meteorology Administration, Guangzhou, China

<sup>3</sup> Environment Research Institute, Shandong University, Ji’nan, China

<sup>4</sup> Jiangsu Provincial Key Laboratory of Geographic Information Science and Technology, International Institute for Earth System Science, Nanjing University, Nanjing, China

<sup>5</sup> Department of Environmental Engineering, School of Resource and Environmental Sciences, Wuhan University, Wuhan, China

<sup>6</sup> Department of Environmental Science, College of Environmental and Energy Engineering, Beijing University of Technology, Beijing, China

### Text S1 Validation of the WRF-CMAQ modeling

Due to inevitable uncertainties inherent in the chemical transport models, such as the uncertainties in emission inventory, meteorological simulation and chemical mechanisms (Hu et al., 2016), it is difficult to deduce the reasons for the discrepancies between the simulation and observation. However, the observation data revealed extremely high levels of some VOCs on the three days when O<sub>3</sub> was under-predicted. Specifically, 13.5 ppbv of ethene was observed at 14:00 LT on August 1. On August 7, 5.6 ppbv of isoprene, 16.2 ppbv of HCHO and 2.3 ppbv of hexanal were measured during 12:00 – 14:00 LT. On August 10, 22.7 ppbv of propene and 12.7 ppbv of i-butane were recorded at 08:00 and 16:00 LT, respectively. It is noteworthy that these mixing ratios were 5 – 10 times higher than their averages. Further, most of these VOCs are highly reactive in O<sub>3</sub> photochemistry and may make great contributions to local O<sub>3</sub> production. With the setting of constant emissions of O<sub>3</sub> precursors, WRF-CMAQ did not reproduce these extremely high levels of VOCs, which was a plausible reason for the under-prediction of O<sub>3</sub> on August 1, 7 and 10. Ji’nan was behind a low pressure trough on August 9 – 10. However, vertical transport was simulated to make negative contributions to O<sub>3</sub> between 10:00 LT and 18:00 LT on August 10, according to the process analysis. In addition, the simulated O<sub>3</sub> in the upper atmosphere on August 10 was relatively

low compared to that on August 5, 6 and 9 (Figure S9). Namely, the model might fail to reproduce the O<sub>3</sub> enhancement driven by the low pressure trough on August 10.

The process analysis indicated that horizontal and vertical transport dominated the sources of O<sub>3</sub> at noon (10:00-12:00 LT) and the other times of July 20, respectively. While vertical transport explained the high O<sub>3</sub> at night (Figure 2), it was not likely that horizontal transport built up O<sub>3</sub> at noon, because the southwesterly airflow originated from South China and passed central China (Figure 4) where O<sub>3</sub> values were relatively low on that day (high O<sub>3</sub> occurred in Hebei province in the northwest). Therefore, the overestimate of the transport effect led to the higher simulated O<sub>3</sub> on July 20.

Despite these discrepancies, overall the observed O<sub>3</sub> at the sampling site was well reproduced. In addition, the spatial distribution of the simulated O<sub>3</sub> was highly consistent with the observed O<sub>3</sub> distribution, as shown in Figure S10. The average concentrations of the simulated VOCs were also compared with the observations (Figure S11). While the day-to-day and diurnal variations of the observed VOCs were not well reproduced (not shown), which is a proverbial drawback of the WRF-CMAQ, the model reasonably simulated the magnitudes of VOCs. Moreover, the averages of the observations (Avg. Obs.) and simulations (Avg. Sim.), difference between Avg. Obs. and Avg. Sim. (Diff.), root mean square error (RMSE), normalized mean bias (NMB), normalized mean error (NME) and index of agreement (IOA) were calculated to reflect the agreements between the simulated and observed temperature (Temp.), relative humidity (R.H.), wind speed (W.S.), pressure (Press.), NO<sub>2</sub> and O<sub>3</sub>, as listed in Table S4. Generally, the lower Diff., RMSE, NMB and NME, but higher IOA indicate better agreement between the simulated and observed values (Willmott et al., 1985). The validation of the simulations of air pollutants was carried out at 8 AQMSs of CNEMC in and around Ji'nan, and at the sampling site, while the meteorological parameters monitored at 6 airports in eastern and northern China and at the sampling site were used to validate the simulated meteorological conditions. The statistics calculated in this study were well within the ranges of those reported in previous studies involving WRF-CMAQ simulations (Table S4) (Jiang et al., 2010; Wang et al., 2015), suggesting good performance of the model in reproducing the meteorological conditions and air pollutants. Thus, the simulated results were accepted for further analyses.

## **Text S2** Source apportionment of O<sub>3</sub> precursors

The positive matrix factorization (PMF) model was employed to identify the sources of O<sub>3</sub> precursors. Details about the operation principles of PMF can be found in Paatero and Tapper (1994). Briefly, the model treats the matrix of input concentrations as the product of two matrixes (*i.e.*, factor contribution and factor profile). Here, hourly concentrations of 31 VOCs, CO, NO and NO<sub>2</sub> in 54 samples were input into the model. The VOCs, which were common tracers of specific sources (*e.g.*, isoprene for biogenic emissions), and had relatively high concentrations (detectable in at least 80% samples), were selected for source apportionment (termed as VOCs\* hereafter). On average, VOCs\* accounted for 79.5±11.7% of the total quantified VOCs (mean ± 95% confidence interval of the hourly values in the statistical period, same for all the other “a ± b” expressions elsewhere unless otherwise specified). The uncertainties of the input concentrations of O<sub>3</sub> precursors were set as  $\frac{5}{6} \times DL$  and  $\sqrt{(10\% \times concentration)^2 + (0.5 \times DL)^2}$  for the concentrations lower than and higher than DL, respectively.

The model was run for 20 times with a random seed and the best resolution automatically given by the model was accepted. A total of 6 sources of O<sub>3</sub> precursors were resolved by PMF in this study. The number of sources was chosen based on the criteria that the tracers indicating different sources were not allocated in the same source, and all the sources were interpretable according to the tracers. The Bootstrap method integrated in PMF was used to estimate the uncertainties of the modelling results.

Figure S13 shows the profiles of the six sources of O<sub>3</sub> precursors extracted from PMF. The first source contained high levels of *n/i*-pentanes and aromatics, likely representing gasoline exhaust (Ho et al., 2009; Ling and Guo, 2014). The heavy (C<sub>8</sub>-C<sub>10</sub>) hydrocarbons dominated in the second source accompanied by great abundances of the combustion tracers, such as C<sub>2</sub>-C<sub>3</sub> hydrocarbons, CO, NO and NO<sub>2</sub>, in line with the features of diesel exhaust (Liu et al., 2008). The third source was assigned as BVOC, due to the exclusively high loading of isoprene (Guenther, 2006). The fourth source was rich in C<sub>4</sub> hydrocarbons, including *n/i*-butanes and 1,3-butadiene. It was defined as liquefied petroleum gas (LPG) usage, since butanes and butenes are present in large quantities in China's LPG (Song et al., 2008 and references therein). Solvent usage was represented by the fifth source, in view of the high loadings of hexane isomers (2,3-dimethylbutane, 2-methylpentane and 3-methylpentane) and moderate loadings of *n*-hexane, toluene, ethylbenzene and xylenes (Guo et al., 2011). At last, most of styrene, benzene, toluene, ethylbenzene and xylenes are allocated to the sixth source, which also contained

moderate levels of light (C<sub>2</sub>-C<sub>5</sub>) hydrocarbons. Since styrene is a common petrochemical product (Jobson et al., 2004; Liu et al., 2008), this source was designated as petrochemical industry.

The source contributions to the O<sub>3</sub> production rates were obtained from the differences in simulated O<sub>3</sub> production rates between a base run and a constrained run. In the base run, the O<sub>3</sub> production rate was simulated with the observed concentrations of air pollutants except for the carbonyls, while the concentrations of air pollutants attributable to a specific source were deducted from the observed concentrations in the input of the constrained run. To account for the influence of primary hydrocarbons on the formation of carbonyls, and the subsequent impact on O<sub>3</sub> production, carbonyls were not constrained to observations in either the base run or the constrained runs. However, the source-specific primary emissions of carbonyls and their contributions to O<sub>3</sub> production were not considered in this approach. Therefore, the source-specific contributions to net O<sub>3</sub> production rates were expected to be underestimated, as carbonyls are generally of high O<sub>3</sub> formation potentials (Cheng et al., 2010; Dong et al., 2014). The method was applied to each of the six sources, derived from the PMF analysis, thereby acquiring the contribution to O<sub>3</sub> production rates of each source.

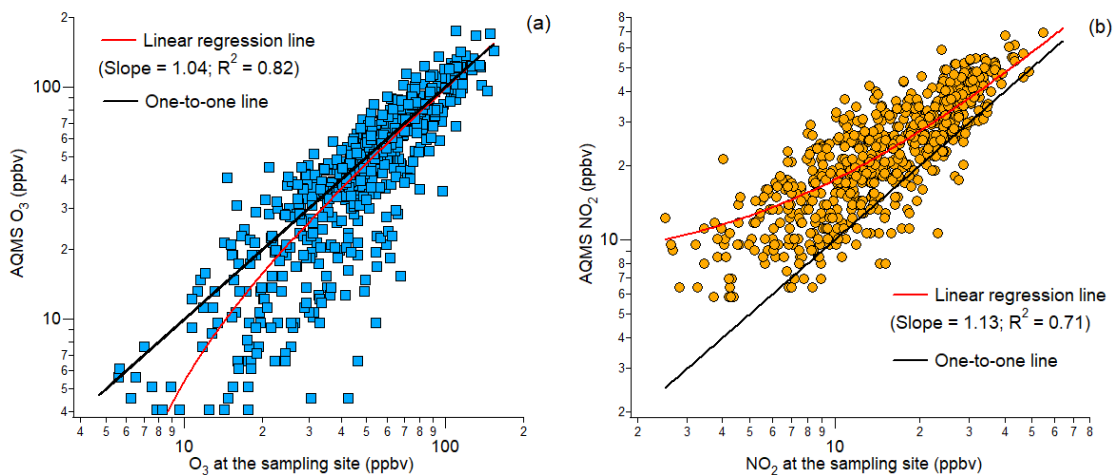
### **Text S3** Definitions of the O<sub>3</sub> formation regimes

As shown in Figure 8, O<sub>3</sub> formation can be divided into VOC<sup>#</sup>-limited regime and NO<sub>x</sub>-limited regime with the method used in Lyu et al. (2017). Briefly, at a given *OH reactivity*<sub>VOCs<sup>#</sup></sub>, O<sub>3</sub> production rate generally reached the maximum at a specific *OH reactivity*<sub>NO<sub>x</sub></sub> due to the dual role of NO<sub>x</sub> in O<sub>3</sub> formation. The scenario with this specific *OH reactivity*<sub>NO<sub>x</sub></sub> was treated as dividing point between NO<sub>x</sub>-limited regime and VOC<sup>#</sup>-limited regime. Since 14 gradients of *OH reactivity*<sub>VOCs<sup>#</sup></sub> (10% - 140% with the step of 10%) were set for all the scenarios, 14 pairs of *OH reactivity*<sub>NO<sub>x</sub></sub> and *OH reactivity*<sub>VOCs<sup>#</sup></sub> were obtained, as shown by the orange crosses in Figure 8. A dividing line was acquired from the linear regression between *OH reactivity*<sub>VOCs<sup>#</sup></sub> and *OH reactivity*<sub>NO<sub>x</sub></sub> in these scenarios (orange dashed line in Figure 8). O<sub>3</sub> formation was limited by VOCs<sup>#</sup> and NO<sub>x</sub> in the lower right and upper left of the dividing line, respectively. Since the horizontal and vertical coordinates were percentages relative to the average *OH reactivity*<sub>VOCs<sup>#</sup></sub> and *OH reactivity*<sub>NO<sub>x</sub></sub> during O<sub>3</sub> episodes, rather than the actual values of OH reactivity, we did not present the dividing ratio of  $\frac{OH\ reactivity_{VOCs^{\#}}}{OH\ reactivity_{NO_x}}$  here.

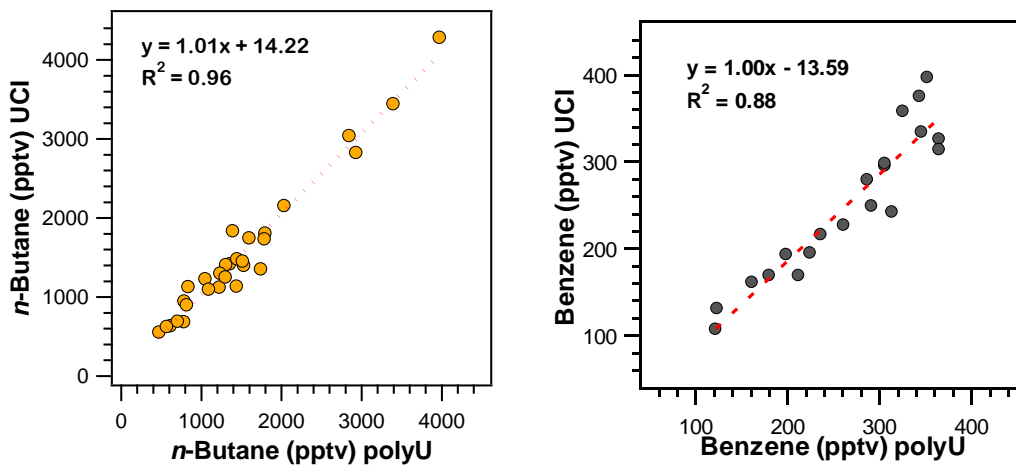
Further, it was found that O<sub>3</sub> production rate was also enhanced with the increase of

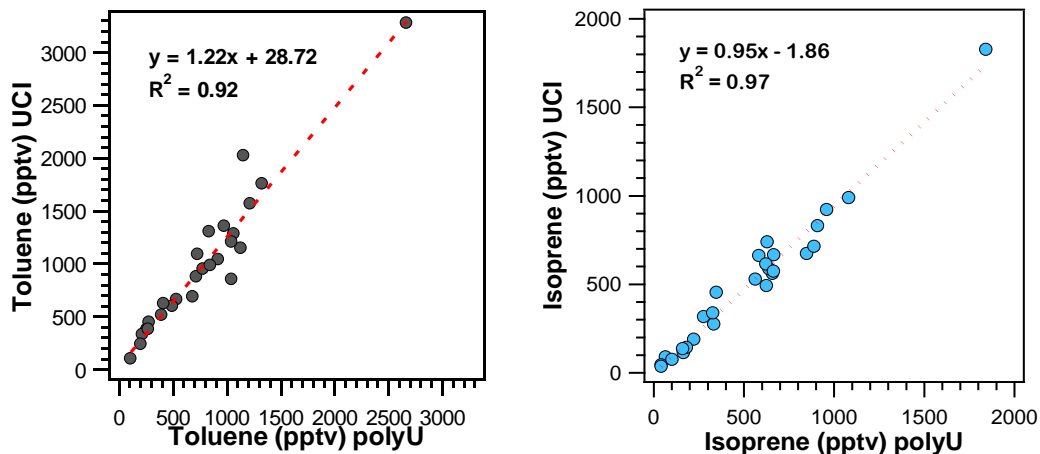


$OH$  reactivity $_{VOCs^\#}$  in the upper left area close to the dividing line. We defined it as a transitional regime where the  $O_3$  production rate was comparably sensitive to  $VOCs^\#$  and  $NO_x$ . Beyond the transition area in the upper left of the dividing line, the sensitivity of  $O_3$  production rate to  $NO_x$  was generally ten times higher than to  $VOCs^\#$ , which was designated as  $NO_x$ -limited regime. The transitional regime and the  $NO_x$ -limited regime are divided by the blue dashed line in Figure 8.

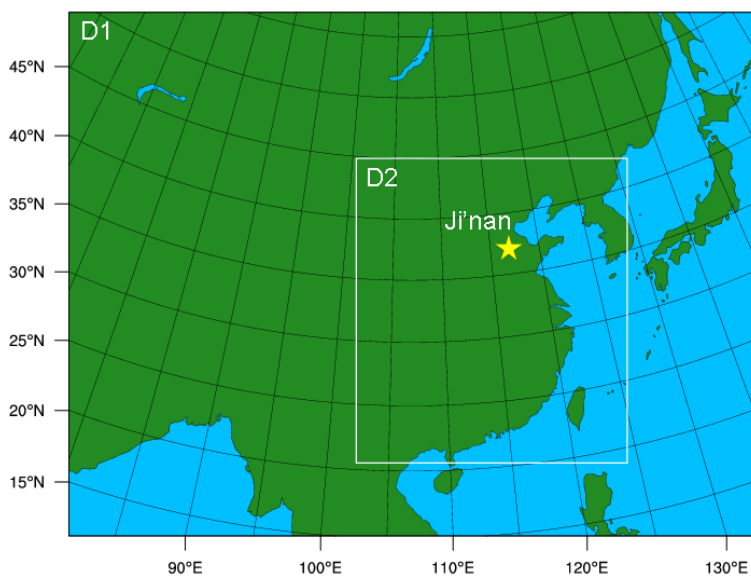


**Figure S1.** Agreement of the hourly (a)  $O_3$  and (b)  $NO_2$  between our observations on the campus of Shandong University and those monitored at the nearest AQMS by CNEMC.

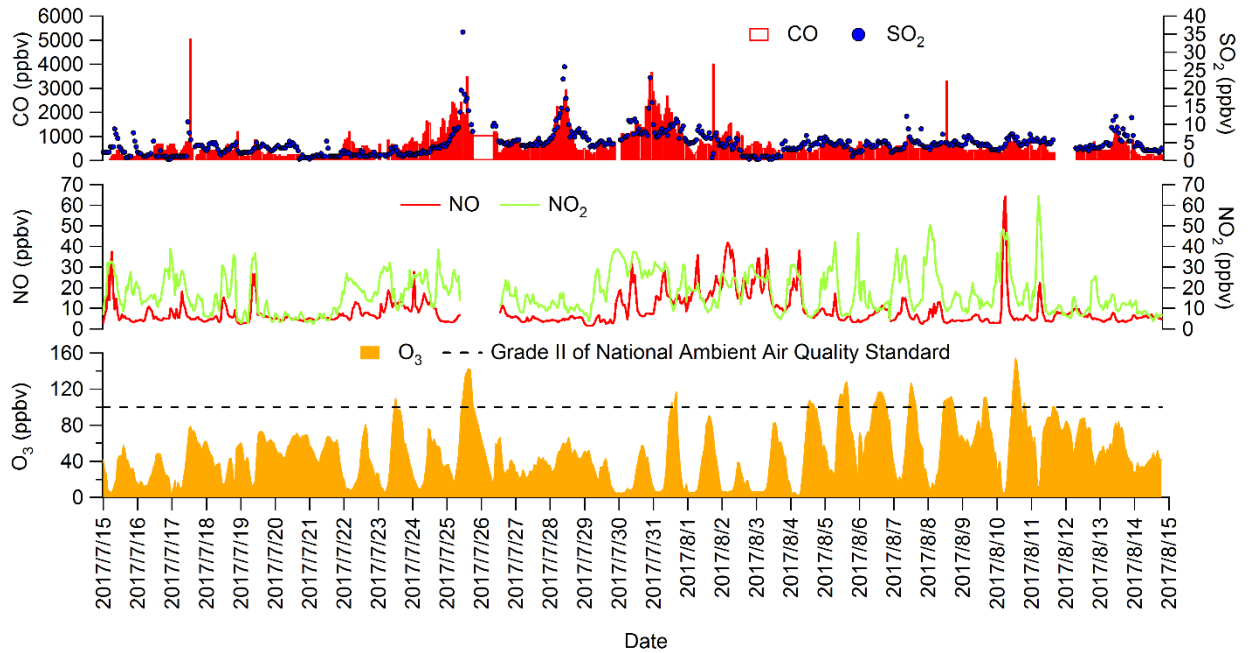




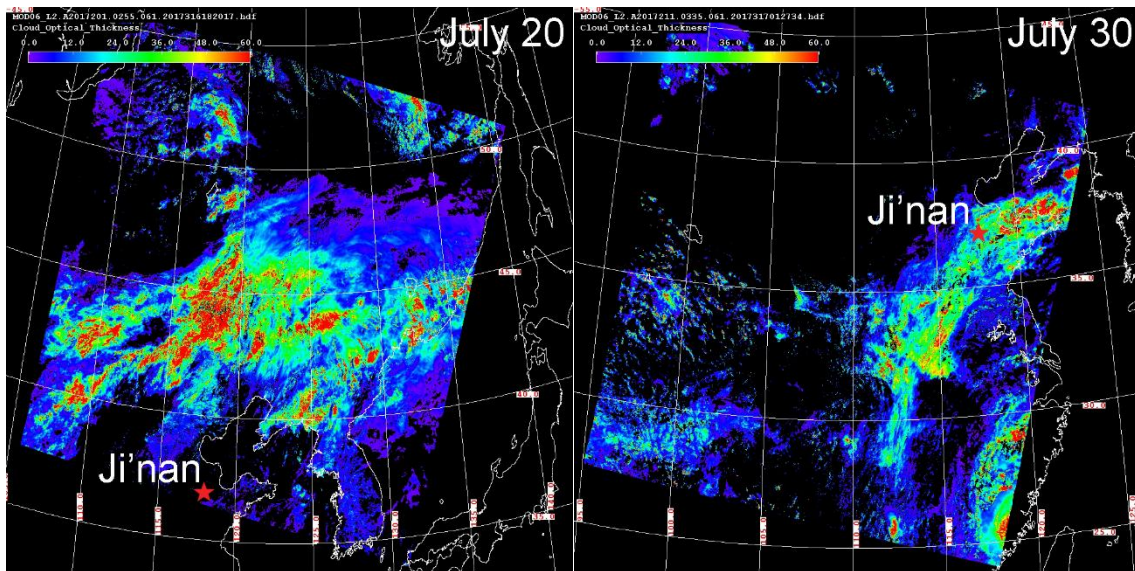
**Figure S2.** Inter-comparison of VOC analysis results between our laboratory (x axis) and Prof. Donald Blake's group (y axis). *n*-butane, benzene, toluene and isoprene are selected as examples. The red dashed line represents the linear regression between VOCs analyzed in two laboratories.

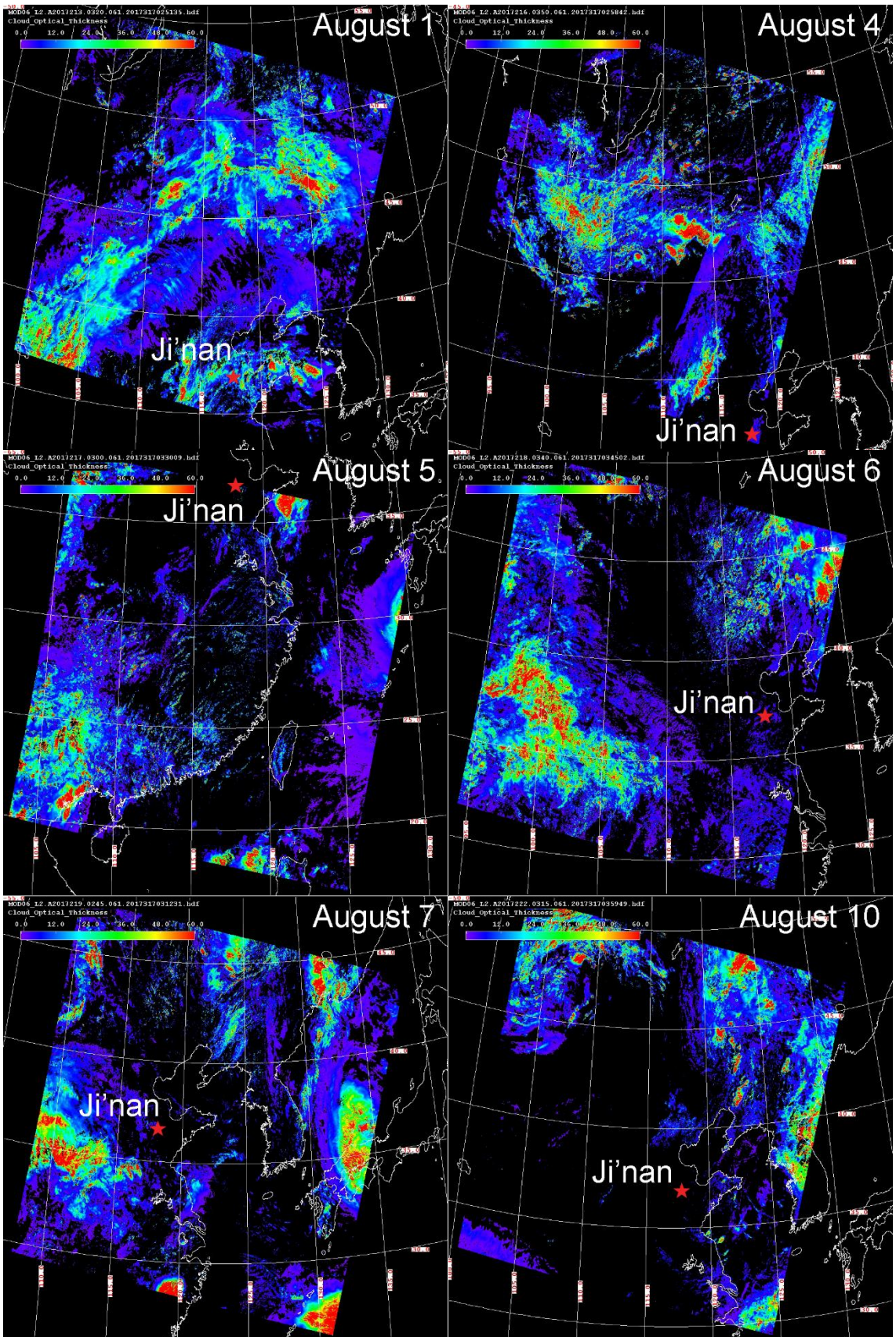


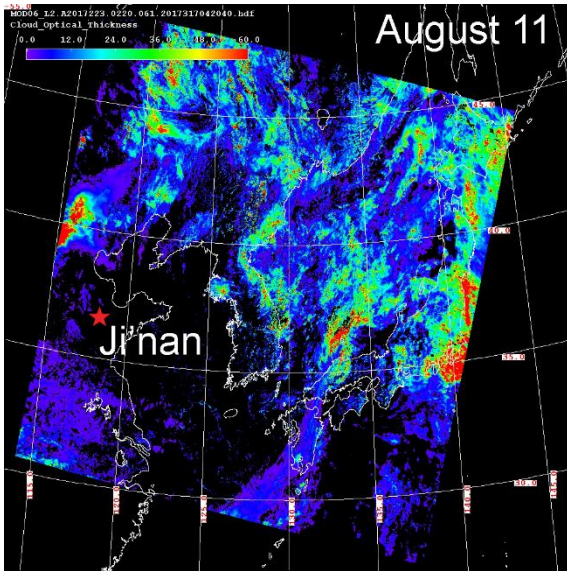
**Figure S3.** Settings of the two-nested domains for the WRF-CMAQ model. D1 and D2 are the outer and inner domain, covering the entire continental area of China and eastern China, respectively. The yellow star represents Ji'nan.



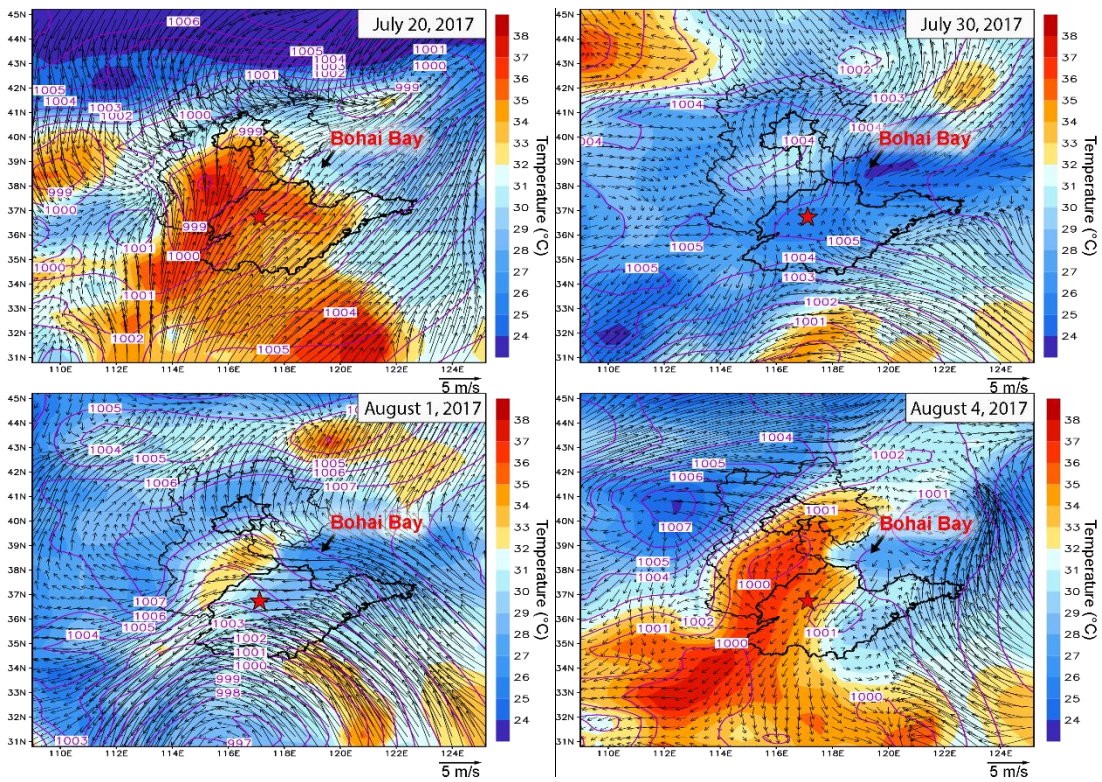
**Figure S4.** Hourly variations of trace gases monitored at the sampling site (O<sub>3</sub>, NO and NO<sub>2</sub>) and at the nearest AQMS (CO and SO<sub>2</sub>) during July 15-August 14, 2017.

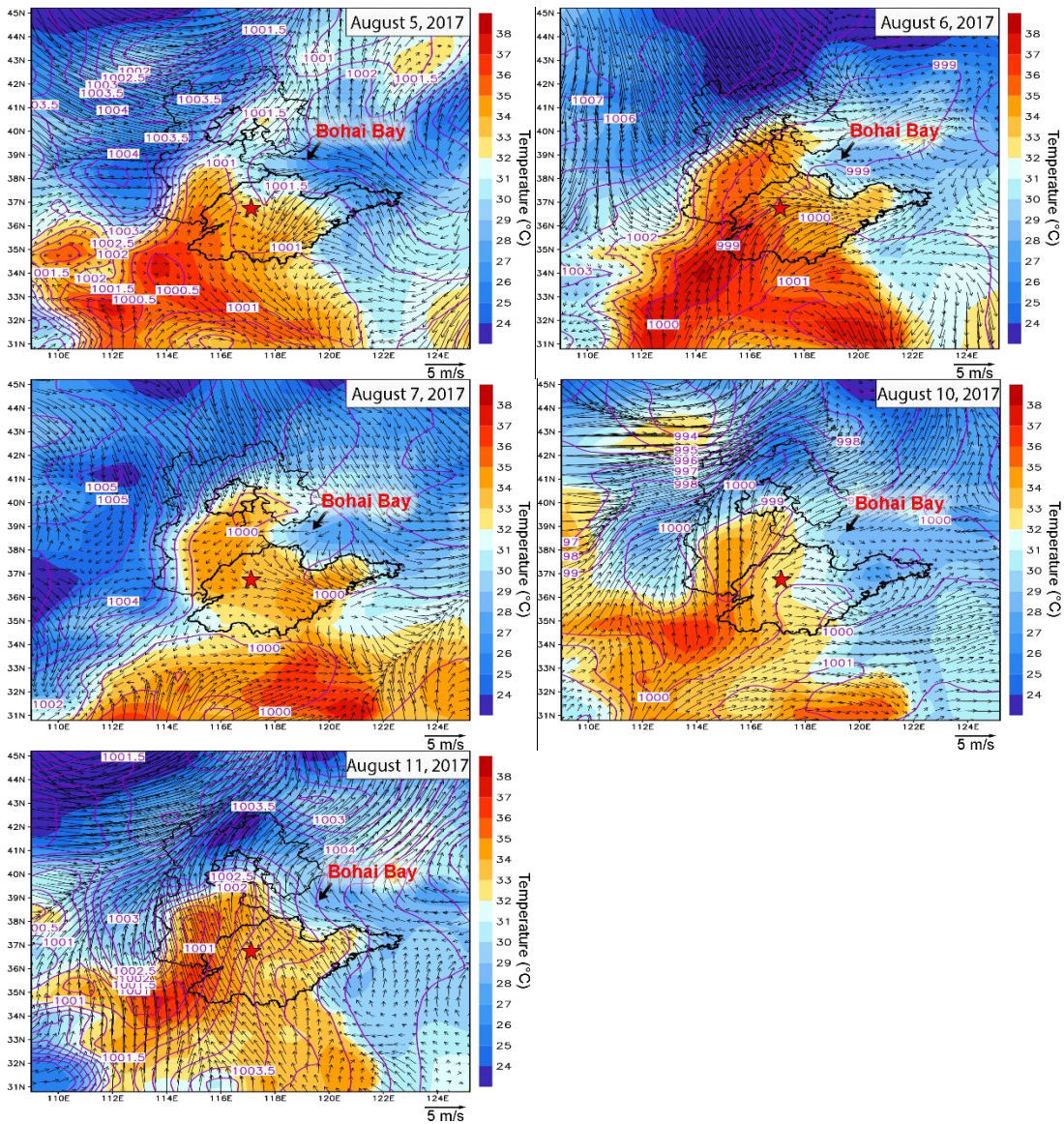




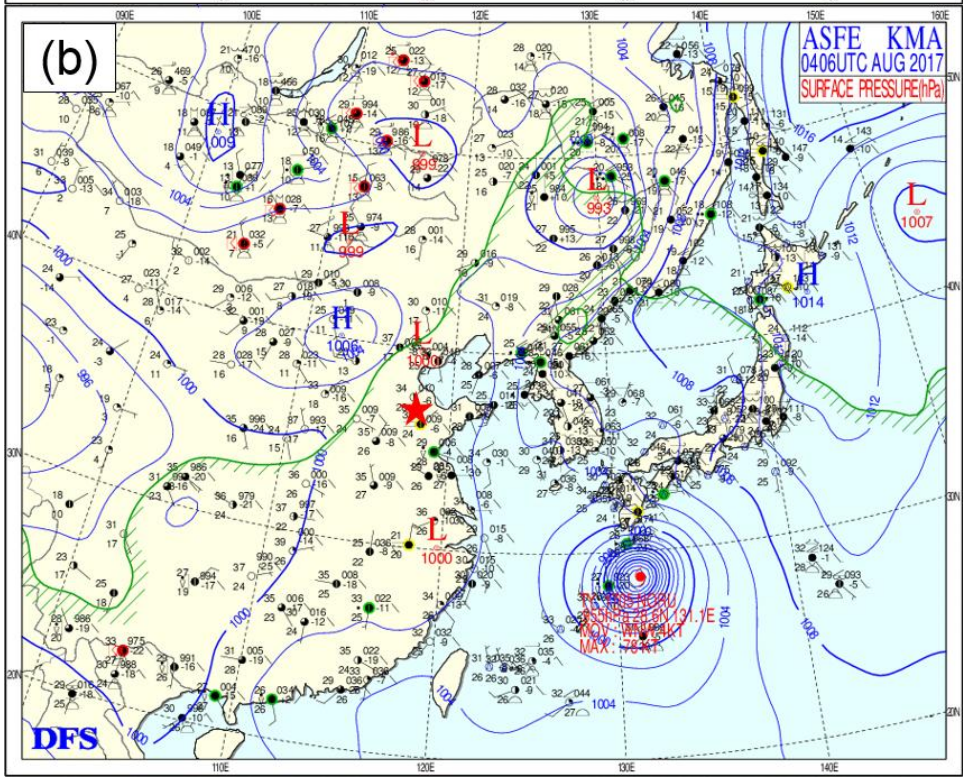
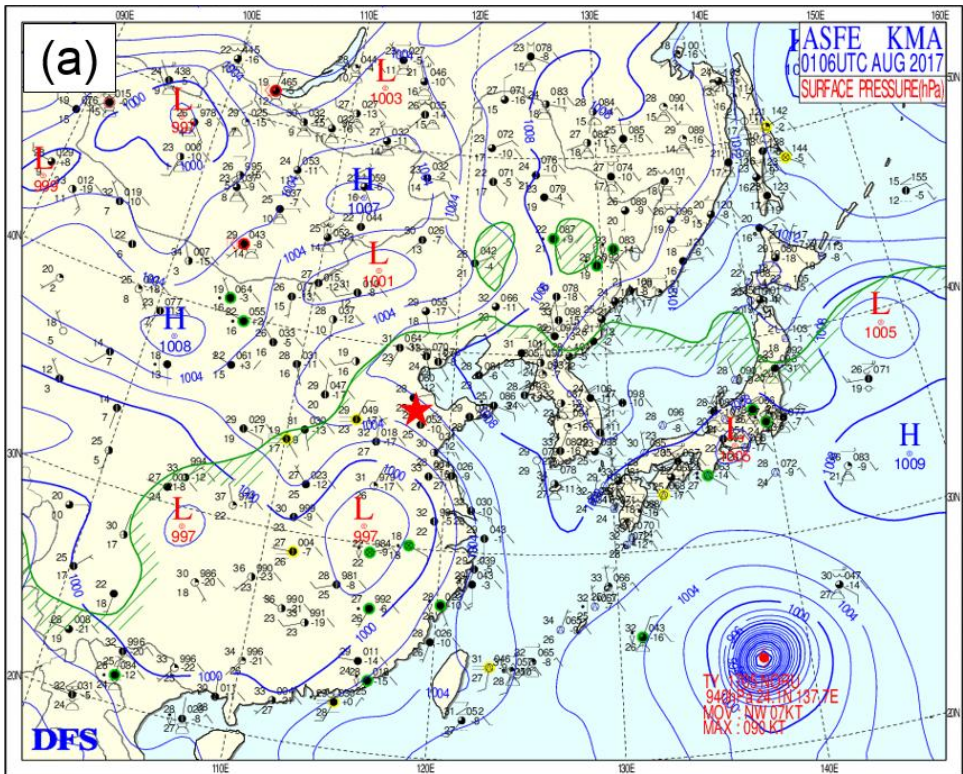


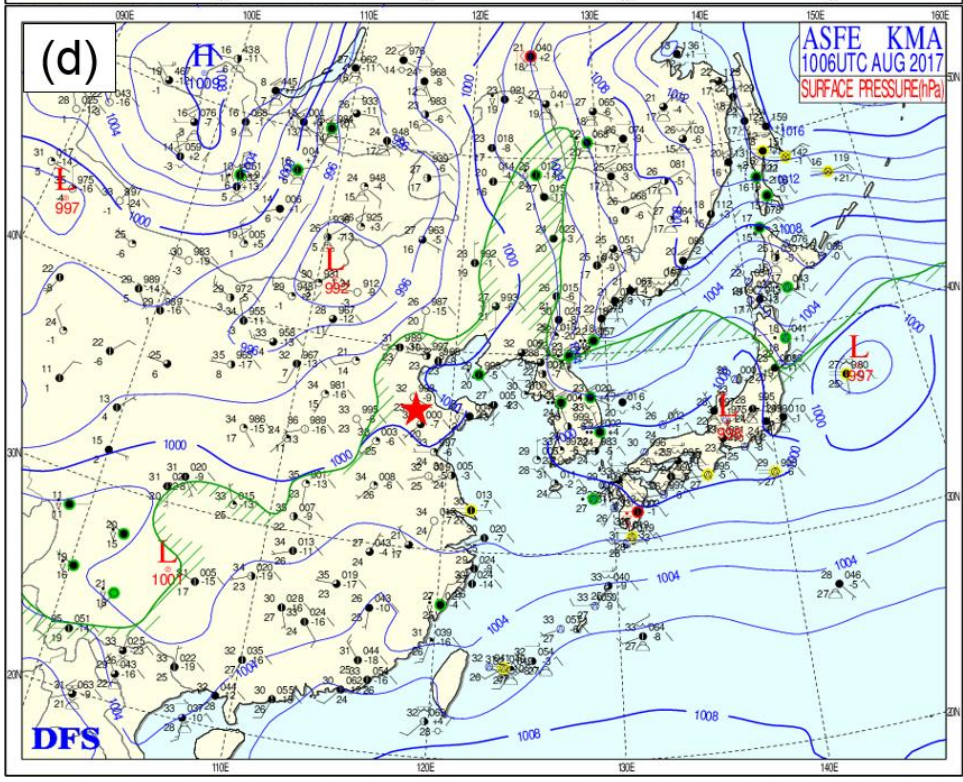
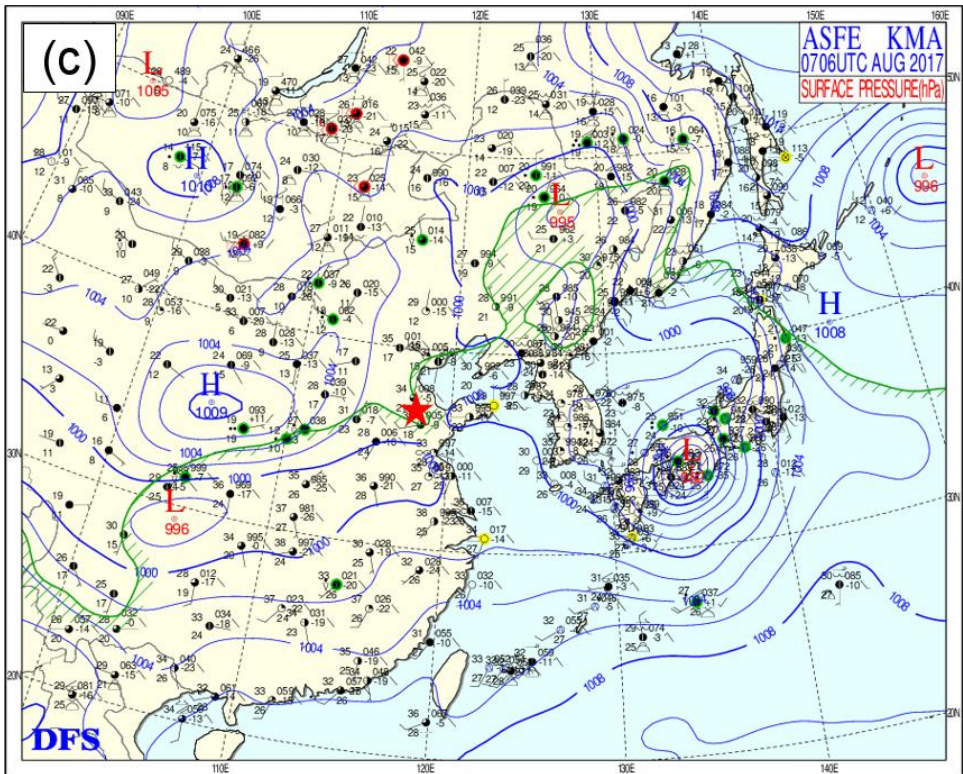
**Figure S5.** Cloud optical depth (COD) retrieved from terra/MODIS at noon (10:30 – 12:00 LT) of the canister sampling days. The color scale denotes for the COD within the range of 0 (purple) to 60 (red). The red star denotes Ji'nan.



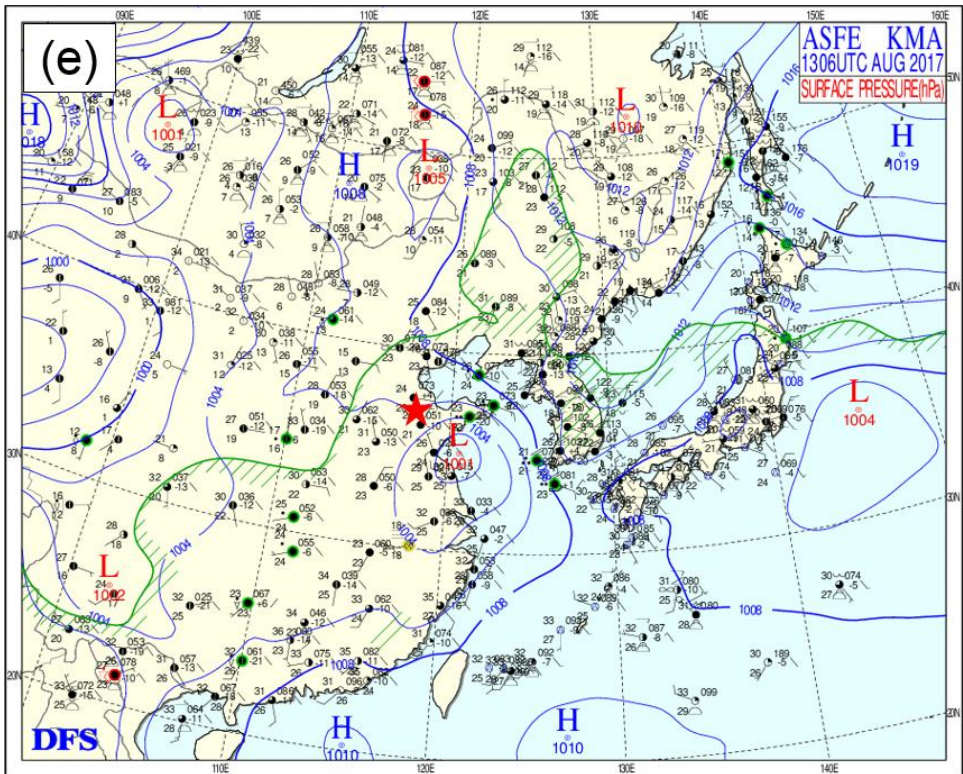


**Figure S6.** Weather charts at 14:00 LT on individual VOC sampling days. The red star denotes for Ji'nan. The dark black line is the boundary of Shandong province. Bohai Bay is located to the northeast of Shandong province. Numbers in the figure are sea-level pressures in unit of hPa.

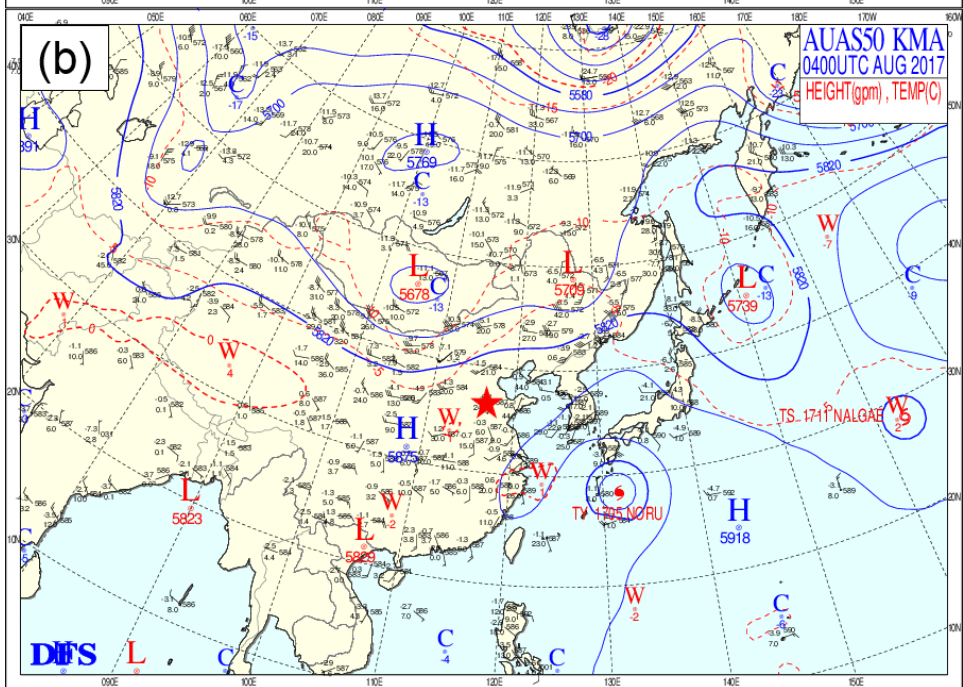
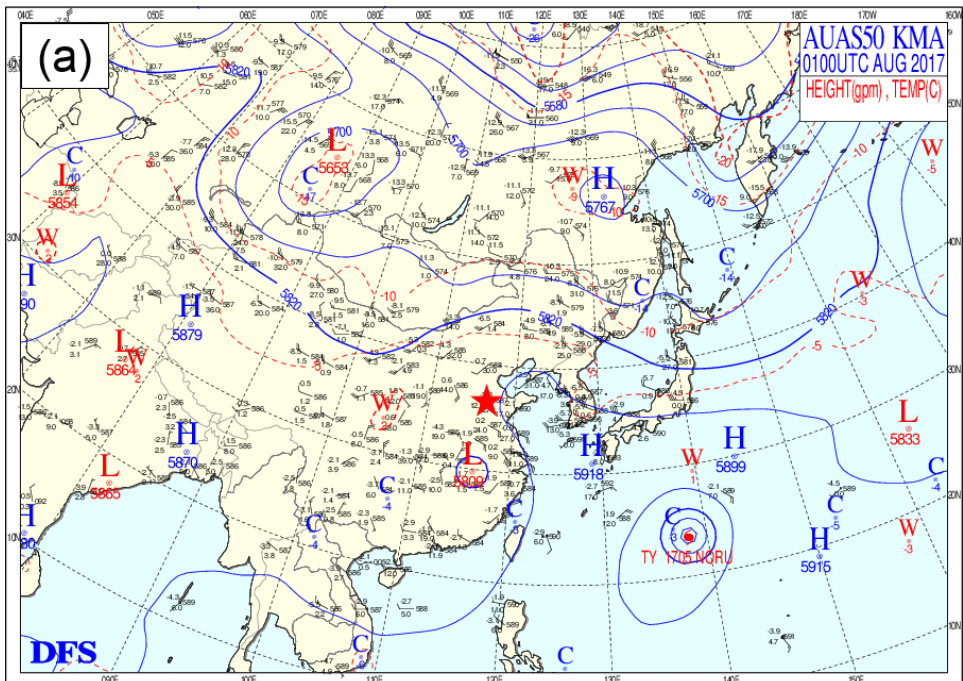


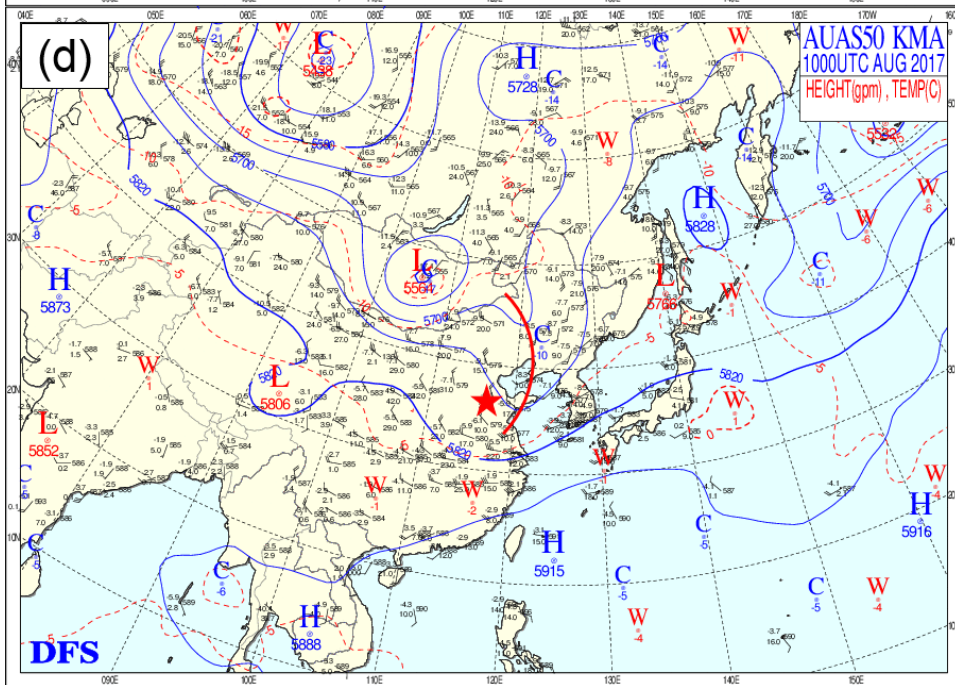
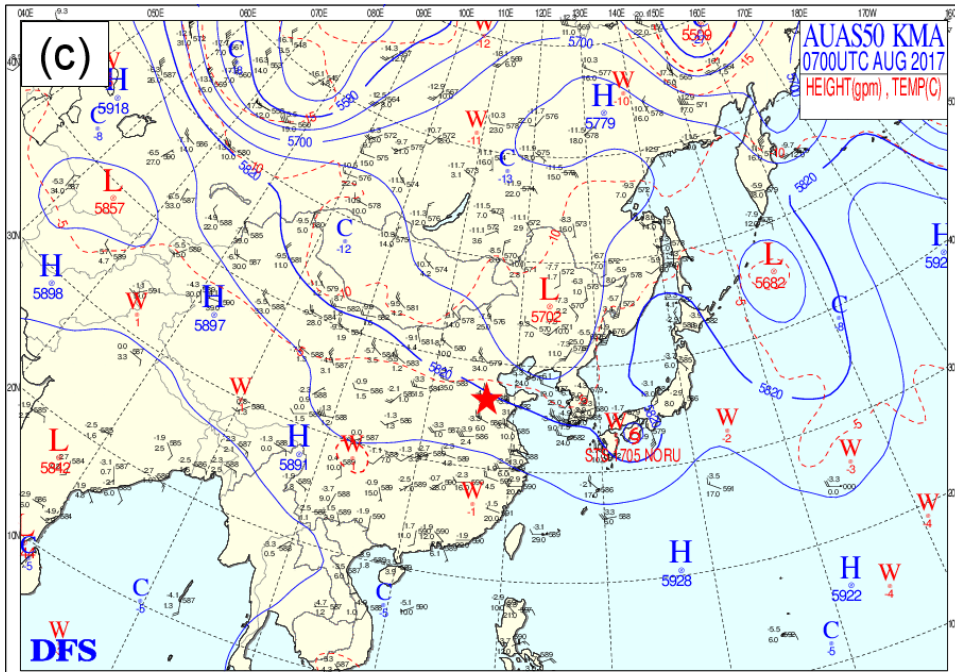






**Figure S7.** Weather chart over the Northeast Asia on (a) August 01, (b) August 04, (c) August 07, (d) August 10 and (e) August 13 at 06:00 UTC (14:00 LT) at surface level. The red star denotes Ji'nan city. The capital letter "H" and "L" represents high pressure center and low pressure center, respectively. Blue lines are the sea level isobars. Green line is the isometric humidity line with the specific humidity of  $\geq 15\text{g/kg}$  on the grid side. All the charts can be accessed through the link: <http://222.195.136.24/forecast.html>.





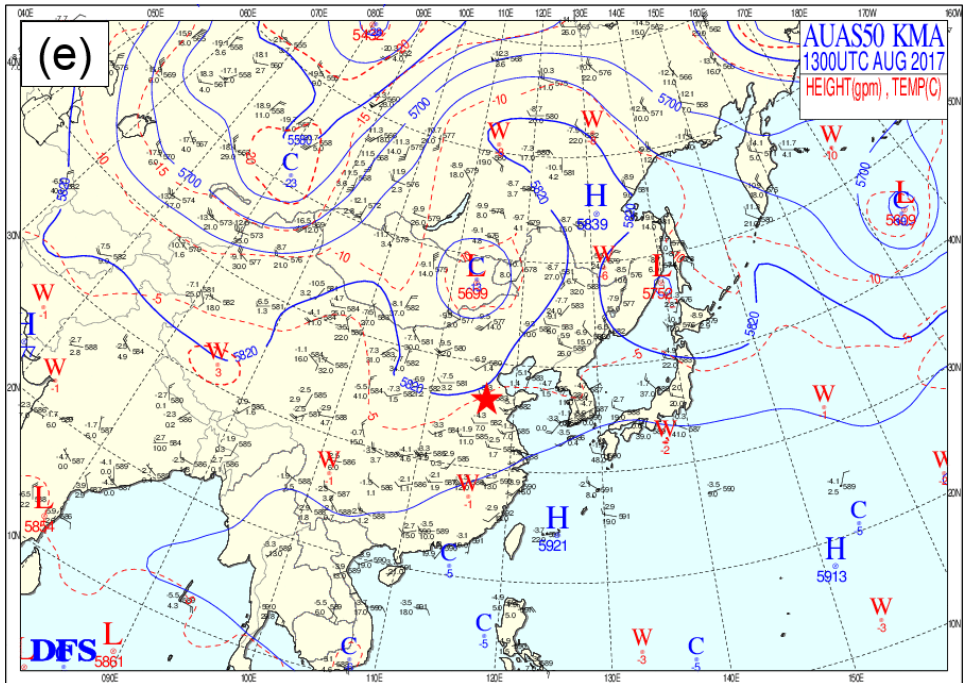


**Figure S8.** Weather chart over the Northeast Asia on (a) August 01, (b) August 04, (c) August 07, (d) August 10 and (e) August 13 at 00:00 UTC (08:00 LT) at altitude of 500 hPa. The red star denotes Ji'nan city. The capital letter "H" and "L" represents high pressure center and low pressure center, respectively. Blue lines are the 500 hPa geopotential height (gpm) lines. The red curve in panel (d) demonstrates the low pressure trough. All the charts can be accessed through the link: <http://222.195.136.24/forecast.html>.

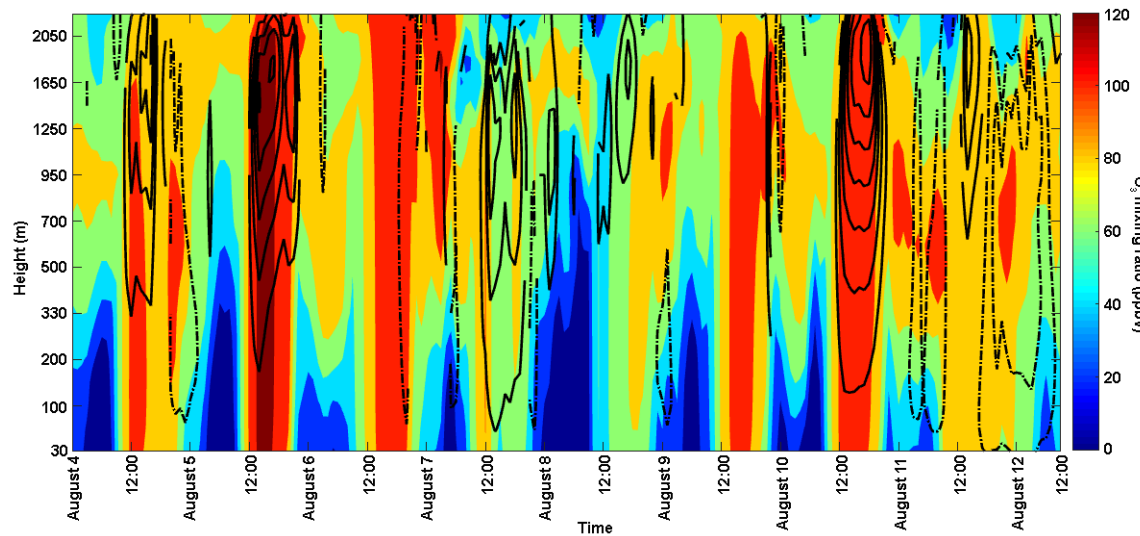


**Figure S9.** Vertical profile of the simulated  $O_3$  over Ji'nan during August 4-11. The black solid and dotted lines represent the updraft and downdraft simulated by WRF-CMAQ, respectively. The areas with no line indicate that there were no simulated winds in vertical direction.

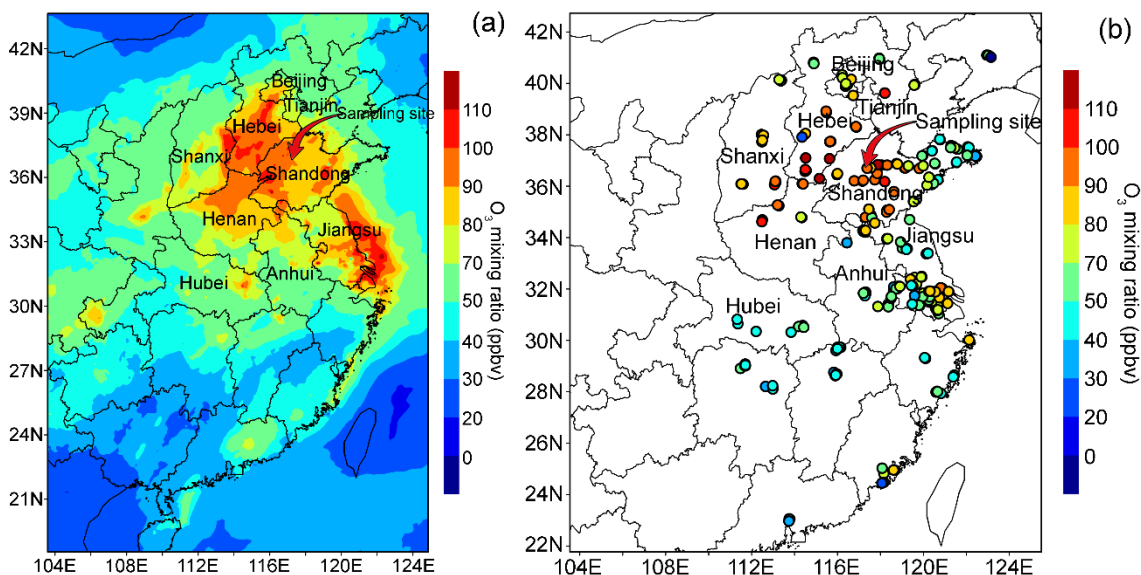


**Figure S10.** Comparison between the spatial distributions of (a) the WRF-CMAQ simulated O<sub>3</sub> and (b) the observed O<sub>3</sub> at 14:00 LT averaged over August 4-11. The observed O<sub>3</sub> was acquired from the AQMSs of CNEMC.

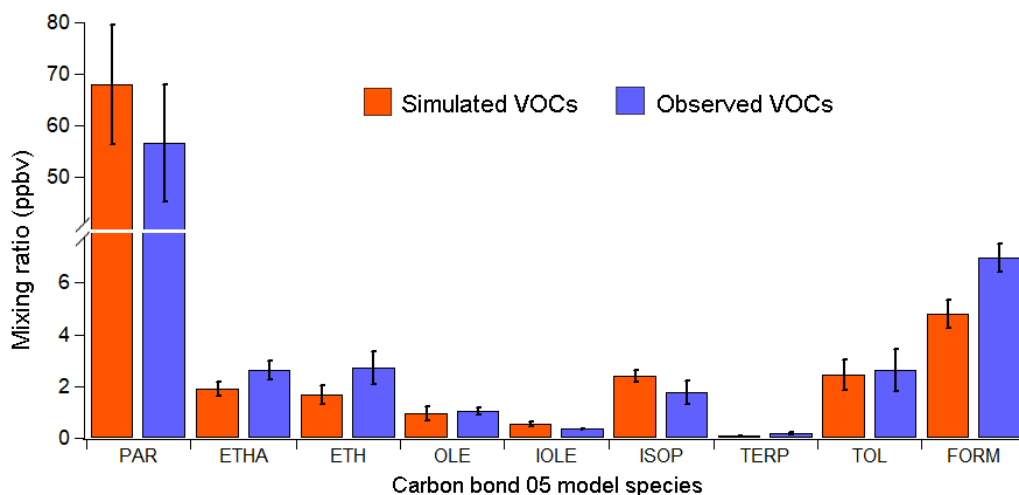


**Figure S11.** Comparison between the averages of the hourly observed and WRF-CMAQ simulated VOCs. PAR: paraffin carbon bond; ETHA: ethane; ETH: ethene; OLE: terminal olefin carbon bond; IOLE: internal olefin carbon bond; ISOP: isoprene; TERP: terpene; TOL: toluene and other monoalkyl aromatics; FORM: formaldehyde. The matrix of assignments from real compounds to carbon bond 05 model species can be found in Yarwood et al. (2005).

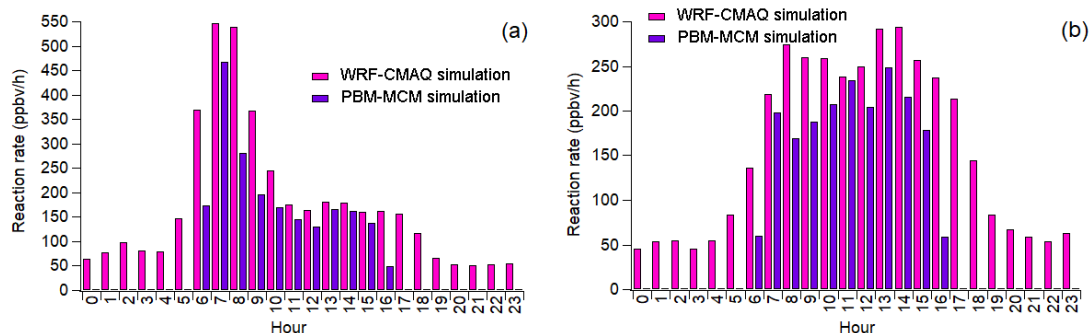


**Figure S12.** Average diurnal cycle of “NO+O<sub>3</sub>” reaction rates simulated by WRF-CMAQ and PBM-MCM during (a) O<sub>3</sub> episodes and (b) non-episodes.

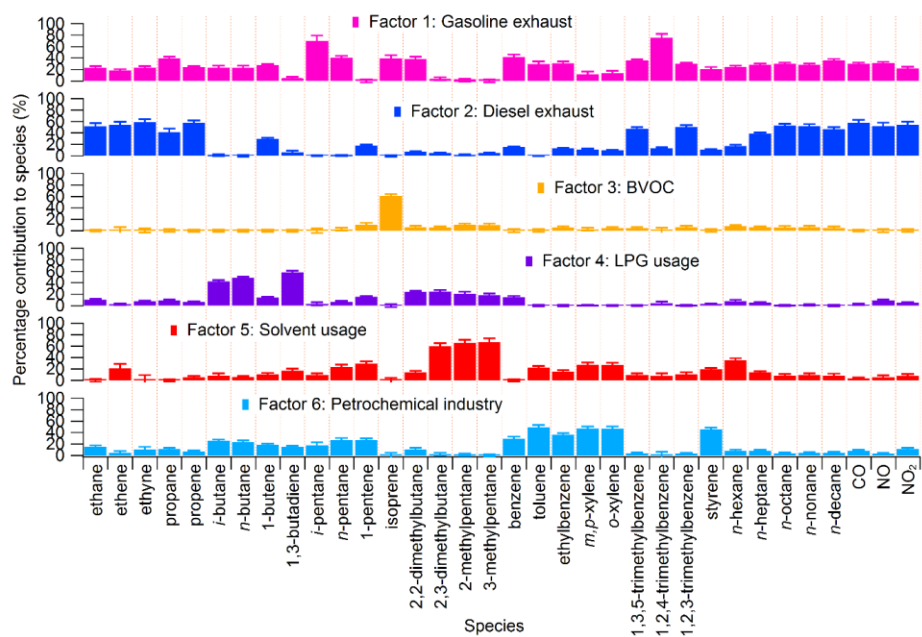


**Figure S13.** Profiles of the six sources of O<sub>3</sub> precursors identified for the samples collected in daytime of the VOC sampling days in Ji’nan.

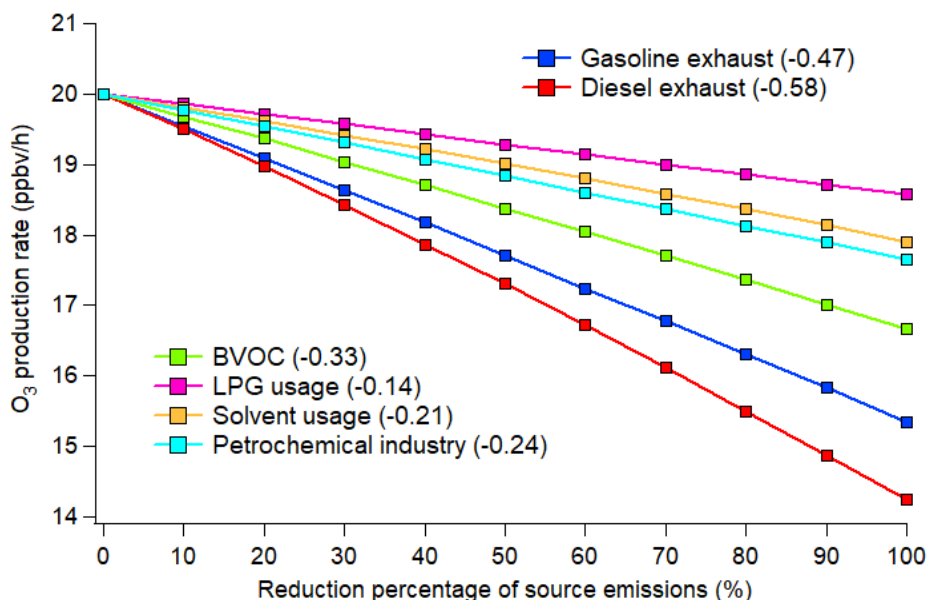


**Figure S14.** Average O<sub>3</sub> production rate at 12:00 LT during O<sub>3</sub> episodes as a response of the reduction percentages of source emissions. Numbers in the brackets are the average O<sub>3</sub> reduction efficiencies (ppbv/10% reduction in source emissions).

Species	Site	Instrument	Resolution	Accuracy	Precision	Detection limit
SO <sub>2</sub>	AQMS*	API, Model 100 E	20 sec	<20%	0.5% of reading above 50 ppbv	0.4 ppbv
CO	AQMS	API, Model 300 E	10 sec	<20%	0.5% of reading	40 ppbv
NO-NO <sub>2</sub> -NO <sub>x</sub>	AQMS	API, Model 200E	20 sec	<20%	0.5% of reading	0.4 ppbv
	Campus site #	Thermo, Model 42C	1 min	<15%	0.4 ppbv	0.4 ppbv
O <sub>3</sub>	AQMS	API, Model 400E	10 sec	<20%	<0.5% of reading	0.6 ppbv
	Campus site	Thermo, Model 49C	20 sec	<15%	1.0 ppbv	1.0 ppbv

\* An air quality monitoring station of China National Environmental Monitoring Center closest to our sampling site in the campus of Shandong University; # Our sampling site on the campus of Shandong University.

**Table S1.** Descriptions of the trace gas analyzers used in this study.

Date	Episode/Non-episode	J(O <sup>1</sup> D) (s <sup>-1</sup> )	JNO <sub>2</sub> (s <sup>-1</sup> )
July 20	Non-episode	$3.40 \times 10^{-5}$	$9.27 \times 10^{-3}$
July 30	Non-episode	$1.02 \times 10^{-5}$	$2.73 \times 10^{-3}$

August 1	Non-episode	$2.71 \times 10^{-5}$	$7.50 \times 10^{-3}$
August 4	Episode	$2.85 \times 10^{-5}$	$7.95 \times 10^{-3}$
August 5	Episode	$2.69 \times 10^{-5}$	$7.50 \times 10^{-3}$
August 6	Episode	$2.75 \times 10^{-5}$	$7.70 \times 10^{-3}$
August 7	Episode	$2.34 \times 10^{-5}$	$6.52 \times 10^{-3}$
August 10	Episode	$3.07 \times 10^{-5}$	$8.72 \times 10^{-3}$
August 11	Episode	$2.90 \times 10^{-5}$	$8.25 \times 10^{-3}$

**Table S2.** Daily maximum photolysis rates of O<sub>3</sub> and NO<sub>2</sub> on VOC sampling days in Ji'nan.

OH reactivity of species X	Full name of species/VOC groups	Species included
RNO	Nitric oxide	Nitric oxide
RNO <sub>2</sub>	Nitrogen dioxide	Nitrogen dioxide
RCO	Carbon monoxide	Carbon monoxide
RCarbonyls	Carbonyls	Formaldehyde, acetaldehyde, acetone, hexanal
RBVOCs	Biogenic VOCs	Isoprene, <i>α</i> -pinene, <i>β</i> -pinene
RAromatics	Aromatics	Benzene, toluene, ethylbenzene, <i>m/p</i> -xylenes, <i>o</i> -xylene
RAkenes	Alkenes	Ethene, ethyne, propene, 1- <i>i</i> -butene, 1,3-butadiene, <i>trans</i> -2-butene, <i>cis</i> -2-butene, 1-pentene
RAkanes	Alkanes	Ethane, propane, <i>n/i</i> -butanes, <i>n/i</i> -pentanes

**Table S3.** Full name of inorganic trace gases and VOC species for the calculation of OH reactivity.

Meteorological parameter/Air pollutant	Avg. Obs.	Avg. Sim.	Diff.	RMSE	NMB	NME	IOA
Temp. (°C)	30.0	30.7	0.7	2.4	0.02	0.06	0.89
R.H. (%)	72.7	67.5	-5.2	14.4	-0.06	0.15	0.82
W.S. (m/s)	2.8	3.3	0.5	1.5	0.38	0.56	0.74
Press. (hPa)	1000.5	998.8	-1.7	4.0	-0.002	0.003	0.56
NO <sub>2</sub> (ppbv)	26.7	28.4	1.7	16.7	0.18	0.58	0.73
O <sub>3</sub> (ppbv)	62.8	52.4	-10.4	24.0	-0.07	0.48	0.89

**Table S4.** Statistical comparisons of the WRF-CMAQ simulated and observed meteorological parameters, O<sub>3</sub> and NO<sub>2</sub>. The comparisons are made for the hourly data in 24 hours on all the VOC sampling days.



O <sub>3</sub> production pathway	O <sub>3</sub> destruction pathway
HO <sub>2</sub> + NO	OH + NO <sub>2</sub>
RO <sub>2</sub> + NO	O <sup>1</sup> (D) + H <sub>2</sub> O
	O <sub>3</sub> + OH
	O <sub>3</sub> + HO <sub>2</sub>
	O <sub>3</sub> + alkenes

**Table S5.** Production and destruction pathways of O<sub>3</sub>.

**References:**

- Dong, D., Shao, M., Li, Y., Lu, S., Wang, Y., Ji, Z., and Tang, D.: Carbonyl emissions from heavy-duty diesel vehicle exhaust in China and the contribution to ozone formation potential, *J. Environ. Sci.*, 26(1), 122-128, **2014**.
- Guenther, A., Karl, T., Harley, P., Wiedinmyer, C., Palmer, P.I., and Geron, C.: Estimates of global terrestrial isoprene emissions using MEGAN (Model of Emissions of Gases and Aerosols from Nature), *Atmos. Chem. Phys.*, 6(11), 3181-3210, **2006**.
- Guo, H., Cheng, H.R., Ling, Z.H., Louie, P.K., and Ayoko, G.A.: Which emission sources are responsible for the volatile organic compounds in the atmosphere of Pearl River Delta?, *J. Hazard. Mat.*, 188(1-3), 116-124, **2011**.
- Ho, K.F., Lee, S.C., Ho, W.K., Blake, D.R., Cheng, Y., Li, Y.S., Ho, S.S., Fung, K., Louie, P.K., and Park, D.: Vehicular emission of volatile organic compounds (VOCs) from a tunnel study in Hong Kong, *Atmos. Chem. Phys.*, 9(19), 7491-7504, **2009**.
- Hu, J., Chen, J., Ying, Q., and Zhang, H.: One-year simulation of ozone and particulate matter in China using WRF/CMAQ modeling system, *Atmos. Chem. Phys.*, 16(16), 10333–10350, **2016**.
- Jiang, F., Guo, H., Wang, T.J., Cheng, H.R., Wang, X.M., Simpson, I.J., Ding, A.J., Saunders, S.M., Lam, S.H.M., and Blake, D.R.: An ozone episode in the Pearl River Delta: Field observation and model simulation, *J. Geophys. Res. – Atmos.*, 115(D22), **2010**.
- Jobson, B.T., Berkowitz, C.M., Kuster, W.C., Goldan, P.D., Williams, E.J., Fesenfeld, F.C., Apel, E.C., Karl, T., Lonneman, W.A., and Riemer, D.: Hydrocarbon source signatures in Houston, Texas: Influence of the petrochemical industry, *J. Geophys. Res. – Atmos.*, 109(D24), doi.org/10.1029/2004JD004887, **2004**.
- Ling, Z.H. and Guo, H.: Contribution of VOC sources to photochemical ozone formation and its control policy implication in Hong Kong, *Environ. Sci. Policy*, 38, 180-191, **2014**.
- Liu, Y., Shao, M., Fu, L., Lu, S., Zeng, L., and Tang, D.: Source profiles of volatile organic compounds (VOCs) measured in China: Part I, *Atmos. Environ.*, 42(25), 6247-6260, **2008**.

Lyu, X.P., Guo, H., Wang, N., Simpson, I.J., Cheng, H.R., Zeng, L.W., Saunders, S.M., Lam, S. H.M., Meinardi, S., and Blake, D.R.: Modeling C1-C4 alkyl nitrate photochemistry and their impacts on O<sub>3</sub> production in urban and suburban environments of Hong Kong, *J. Geophys. Res. – Atmos.*, 122(19), **2017**.

Paatero, P. and Tapper, U.: Positive matrix factorization: A non-negative factor model with optimal utilization of error estimates of data values, *Environmetrics*, 5(2), 111-126, **1994**.

Song, Y., Dai, W., Shao, M., Liu, Y., Lu, S., Kuster, W., and Goldan, P.: Comparison of receptor models for source apportionment of volatile organic compounds in Beijing, China, *Environ. Pollut.*, 156(1), 174-183, **2008**.

Wang, N., Guo, H., Jiang, F., Ling, Z.H., and Wang, T.: Simulation of ozone formation at different elevations in mountainous area of Hong Kong using WRF-CMAQ model, *Sci. Total Environ.*, 505, 939-951, **2015**.

Willmott, C.J., Ackleson, S.G., Davis, R.E., Feddema, J.J., Klink, K.M., Legates, D.R., O'Donnell, J., and Rowe, C.M.: Statistics for the evaluation and comparison of models, *J. Geophys. Res. - Oceans*, 90(C5), 8995-9005, **1985**.